

**COLOR FACE RECOGNITION USING QUATERNION
PRINCIPAL COMPONENT ANALYSIS (Q-PCA)**

BY

Emad Sami Jaha

A Thesis Presented to the
DEANSHIP OF GRADUATE STUDIES

KING FAHD UNIVERSITY OF PETROLEUM & MINERALS

DHAHRAN, SAUDI ARABIA

In Partial Fulfillment of the
Requirements for the Degree of

MASTER OF SCIENCE

In

COMPUTER SCIENCE

November, 2010

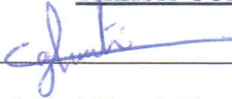
King Fahd University of Petroleum & Minerals

Dhahran 31261, Saudi Arabia

Deanship of graduate Studies

This thesis, written by **EMAD SAMI MOHAMMED JAHA** under the direction of his thesis advisor and approved by his thesis committee, has been presented to and accepted by the Dean of Graduate Studies, in partial fulfillment of his requirements for the degree of **MASTER OF SCIENCE IN COMPUTER SCIENCE**.

THEISIS COMMITTEE



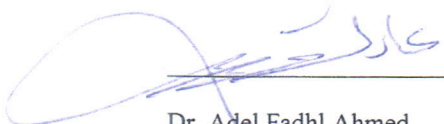
Dr. Lahouari Ghouti (Thesis Advisor)



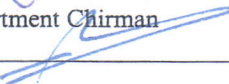
Dr. Naser Darwish (Member)



Dr. Adel Fadhl Ahmed (Member)



Dr. Adel Fadhl Ahmed
Department Chairman



Dr. Salam A. Zummo
Dean of Graduate Studies

Date 28/11/10



I would like to dedicate my thesis to

My Parents

My Wife

and my two children

ACKNOWLEDGMENT

All my thanks are due to Almighty Allah (Subhanahu Wa Taalaa) who gave me courage and patience to carry out this work.

I would like to thank Dr. Lahouari Ghouti for his precious time and continuous advice, support and encouragement throughout this research. Also, my thesis committee members, Dr. Nasir Al-Darwish and Dr. Adel Fadhil Ahmed, provided very helpful advice, comments and feedback to improve the content of this research.

Furthermore, I would like to thank all faculty members, colleagues and friends who shared with me the path of learning and knowledge throughout my graduate studies.

I wish to express my gratitude to my family and my wife's family members for their encouragement and being patient with me.

Special thanks are to King Abdul-Aziz University (KAU) for their generous support and scholarship to complete my Master degree and to King Fahd University of Petroleum and Minerals (KFUPM) for their support of this research.

TABLE OF CONTENT

	Page
DEDICATION	ii
ACKNOWLEDGMENT	iii
TABLE OF CONTENT	iv
LIST OF TABLES	vi
LIST OF FIGURES	vii
THESIS ABSTRACT	ix
ملخص الرسالة	x
CHAPTER 1	1
1. INTRODUCTION	1
1.1. Biometrics	3
1.2. Face Recognition	4
1.2.1. Face Recognition Processing	6
1.3. Problem Statement	8
1.4. Motivation	8
1.5. Thesis Contributions	9
1.6. Thesis Outline	10
CHAPTER 2	11
2. LITERATURE REVIEW	11
2.1. Grayscale-based Face Recognition	11
2.1.1. Grayscale PCA-based Approach	11
2.1.2. Grayscale Gabor Filters Approach	12
2.1.3. Grayscale Wavelet-based Approach	13
2.2. Color-based Face Recognition	13
2.2.1. Color PCA-based Approach	15
2.2.2. Color Quaternion-based Approach	15
CHAPTER 3	19
3. QUATERNION (HYPERCOMPLEX) REPRESENTATION	19
3.1. Quaternion Numbers	19
3.2. Properties of Quaternion Numbers	20
3.3. Quaternion Representation of Color Face Images	22

3.4.	Quaternion Fourier Transform (QFT)	23
3.5.	Quaternion Gabor Filters	25
CHAPTER 4.....		26
4.	PRINCIPAL COMPONENT ANALYSIS (PCA).....	26
4.1.	Eigenfaces.....	27
4.2.	Solving PCA Using SVD	28
4.3.	Quaternion Principal Component Analysis (Q-PCA).....	28
4.3.1.	Quaternion Singular Value Decomposition (Q-SVD).....	29
4.3.2.	QSVD-Based Color Image Compression	32
4.3.3.	Proposed Q-PCA Algorithm.....	34
CHAPTER 5.....		36
5.	METHODOLOGY AND EXPERIMENT	36
5.1.	Research Methodology	36
5.2.	Color Face Image Database	36
5.2.1.	Georgia Tech Face Database (GTDB).....	37
5.2.2.	Color FERET Database	37
5.3.	Performance Evaluation	39
5.3.1.	Standard Testing Subsets.....	40
5.3.2.	Test Design.....	42
5.3.3.	Standard Performance Measures	43
5.3.4.	Identification Performance against Probe Categories.....	49
5.3.5.	Performance Comparison Using CMC in Different Resolutions	57
5.3.6.	Variation in Identification Performance	72
5.3.7.	GD versus ID.....	79
5.3.8.	FAR versus FRR errors	84
5.3.9.	ROC Curves.....	89
CHAPTER 6.....		94
6.	CONCLUSION AND FUTURE WORK	94
6.1.	Summary and Findings.....	94
6.2.	Future Work.....	97
REFERENCES		99
Vita.....		104

LIST OF TABLES

	Page
Table 5.1: Summary of FERET color face database.....	39
Table 5.2: Summary of PCA-based algorithms used in this thesis.....	40
Table 5.3: Gallery and four probe sets.....	40
Table 5.4: Resolution of gallery and probe sets.....	40
Table 5.5: Subsets used to investigate the variation in performance.....	42
Table 5.6: Summary of used gallery and probe categories.....	49
Table 5.7: Match scores of the top-rank for each PCA-based algorithm.....	50
Table 5.8: Average score of the total match scores of rank 50 for each PCA-based algorithm.....	50
Table 5.9: Average score of the full rank for each PCA-based algorithm in two resolutions.....	57
Table 5.10: Variation in identification performance using five different galleries from the FB probes (top match).....	72
Table 5.11: Variation in identification performance using five different galleries from the FB probes (average of rank scores).....	73
Table 5.12: Variation in identification performance using five different galleries from the duplicate I probes (top match).....	76
Table 5.13: Variation in identification performance using five different galleries from the duplicate I probes (average of rank scores).....	76
Table 5.14: Decidability index (d) for each algorithm.....	79
Table 5.15: The EER of each algorithm.....	84

LIST OF FIGURES

	Page
Figure 1.1: Main processing steps in pattern recognition systems.	2
Figure 1.2: Biometric categories.	3
Figure 1.3: Categorization of Face Recognition (FR) methods.	6
Figure 1.4: Face recognition processing flow.	6
Figure 1.5: Face detection and alignment processes.	7
Figure 1.6: Four areas of related work and the current research location.	9
Figure 3.1: Quaternion representation of a color face image.	22
Figure 4.1: The PCA concept, (Li et al. [14]).	26
Figure 4.2: In the top gray-eigenfaces and in the bottom color-eigenfaces.	28
Figure 4.3: Q-SVD-based image compression. (a),(b),(c) and (d) are the reconstructed images with $k=8,16,25,144$ respectively. Where (d) is the perfect reconstruction of the original image.	34
Figure 5.1: One subject face images (gallery and probes).	41
Figure 5.2: Design scheme of the testing procedure.	45
Figure 5.3: GD versus ID and FAR versus FRR errors.	47
Figure 5.4: FAR versus FRR curves.	48
Figure 5.5: Identification performance using the FB with 192×128 pixels resolution.	53
Figure 5.6: Identification performance using the FB with 384×256 pixels resolution.	53
Figure 5.7: Identification performance using the duplicate I with 192×128 pixels resolution.	54
Figure 5.8: Identification performance using the duplicate I with 384×256 pixels resolution.	54
Figure 5.9: Identification performance using the fc with 192×128 pixels resolution.	55
Figure 5.10: Identification performance using the fc with 384×256 pixels resolution.	55
Figure 5.11: Identification performance using the duplicate II with 192×128 pixels resolution. ...	56
Figure 5.12: Identification performance using the duplicate II with 384×256 pixels resolution. ...	56
Figure 5.13: The CMC curves for PCA using the FB probes.	58
Figure 5.14: The CMC curve for PCA using the duplicate I probes.	58
Figure 5.15: The CMC curves for PCA using the fc probes.	59
Figure 5.16: The CMC curves for PCA using the duplicate II probes.	59
Figure 5.17: The CMC curves for QPCA using the FB probes.	60
Figure 5.18: The CMC curves for QPCA using the duplicate I probes.	60
Figure 5.19: The CMC curves for QPCA using the fc probes.	61
Figure 5.20: The CMC curves for QPCA using the duplicate II probes.	61
Figure 5.21: The CMC curves for Red-PCA using the FB probes.	62
Figure 5.22: The CMC curves for Red-PCA using the duplicate I probes.	62
Figure 5.23: The CMC curves for Red-PCA using the fc probes.	63
Figure 5.24: The CMC curves for Red-PCA using the duplicate II probes.	63
Figure 5.25: The CMC curves for Green-PCA using the FB probes.	64
Figure 5.26: The CMC curves for Green-PCA using the duplicate I probes.	64
Figure 5.27: The CMC curves for Green-PCA using the fc probes.	65
Figure 5.28: The CMC curves for Green-PCA using the duplicate II probes.	65

Figure 5.29: The CMC curves for Blue-PCA using the FB probes.....	66
Figure 5.30: The CMC curves for Blue-PCA using the duplicate I probes.....	66
Figure 5.31: The CMC curves for Blue-PCA using the fc probes.....	67
Figure 5.32: The CMC curves for Blue-PCA using the duplicate II probes.	67
Figure 5.33: The CMC curves for Avg RGB-PCA using the FB probes.	68
Figure 5.34: The CMC curves for Avg RGB-PCA using the duplicate I probes.	68
Figure 5.35: The CMC curves for Avg RGB-PCA using the fc probes.	69
Figure 5.36: The CMC curves for Avg RGB-PCA using the duplicate II probes.	69
Figure 5.37: The CMC curves for SCFT-CPCA using the FB probes.	70
Figure 5.38: The CMC curves for SCFT-CPCA using the duplicate I probes.....	70
Figure 5.39: The CMC curves for SCFT-CPCA using the fc probes.....	71
Figure 5.40: The CMC curves for SCFT-CPCA using the duplicate II probes.....	71
Figure 5.41: Identification performance using the FB probes of (Set 1) and rank of 50.....	73
Figure 5.42: Identification performance using the FB probes of (Set 2) and rank of 50.....	74
Figure 5.43: Identification performance using the FB probes of (Set 3) and rank of 50.....	74
Figure 5.44: Identification performance using the FB probes of (Set 4) and rank of 50.....	75
Figure 5.45: Identification performance using the FB probes of (Set 5) and rank of 50.....	75
Figure 5.46: Identification performance using the duplicate I probes of (Set 1) and rank of 50....	77
Figure 5.47: Identification performance using the duplicate I probes of (Set 2) and rank of 50....	77
Figure 5.48: Identification performance using the duplicate I probes of (Set 3) and rank of 50....	78
Figure 5.49: Identification performance using the duplicate I probes of (Set 4) and rank of 50....	78
Figure 5.50: Identification performance using the duplicate I probes of (Set 5) and rank of 50....	79
Figure 5.51: GD versus ID for PCA algorithm	81
Figure 5.52: GD versus ID for QPCA algorithm.....	81
Figure 5.53: GD versus ID for Red PCA algorithm	82
Figure 5.54: GD versus ID for Green PCA algorithm.....	82
Figure 5.55: GD versus ID for Blue PCA algorithm.....	83
Figure 5.56: GD versus ID for Avg RGB PCA algorithm	83
Figure 5.57: GD versus ID for SCFT CPCA algorithm	84
Figure 5.58: FAR versus FRR curve for PCA algorithm	86
Figure 5.59: FAR versus FRR curves for QPCA algorithm.....	86
Figure 5.60: FAR versus FRR curves for Red PCA algorithm	87
Figure 5.61: FAR versus FRR curves for Green PCA algorithm	87
Figure 5.62: FAR versus FRR curves for Blue PCA algorithm	88
Figure 5.63: FAR versus FRR curves for Avg RGB PCA algorithm.....	88
Figure 5.64: FAR versus FRR curves for SCFT CPCA algorithm.....	89
Figure 5.65: PCA and QPCA algorithms ROC curves.....	90
Figure 5.66: ROC curve for Red PCA algorithm	91
Figure 5.67: ROC curve for Green PCA algorithm.....	91
Figure 5.68: ROC curve for Blue PCA algorithm	92
Figure 5.69: ROC curve for Avg RGB PCA algorithm.....	92
Figure 5.70: ROC curve for SCFT CPCA algorithm	93

THESIS ABSTRACT

Name: Emad Sami Jaha
Title: Color Face Recognition Using Quaternion Principle Component Analysis (Q-PCA)
Major Field: Information and Computer Science
Date of Degree: November 2010

Recently, biometric systems have attracted the attention of both academic and industrial communities. Advances in hardware and software technologies have paved the way to such growing interest. Nowadays, efficient and cost-effective biometric solutions are continuously emerging. Fingerprint-based biometric systems have pioneered the commercial applications. Face and iris traits have been proven to be reliable candidates. Until recently, face recognition research literally followed the research undertaken in the field of fingerprint recognition which is inherently gray-scale. In this research, efforts are restricted to the investigation of subspace representations in the color domain. The concept of principal component analysis (PCA) implemented via singular value decomposition (SVD) is carried over into the hypercomplex (i.e., quaternionic) to define quaternionic PCA (Q-PCA) where color faces are compactly represented. Unlike the existing approaches for handling the color information, the proposed research implicitly accounts for the correlation that exists between the color components (i.e., red, green and blue components).

ملخص الرسالة

الاسم:	عماد بن سامي بن محمد جاها
عنوان الرسالة:	التعرف على صور الوجوه الملونة باستخدام تحليل المكونات الأساسية المركبة الرباعية الأبعاد
التخصص:	علوم الحاسب الآلي
تاريخ التخرج:	ذو القعدة 1431هـ

في الآونة الأخيرة انصرف اهتمام الأوساط الأكاديمية والصناعية لنظم التعرف الحيوية على هوية الأشخاص. إن التطور في تقنيات العتاد والبرمجيات قد مهّد الطريق لمثل هذا الاهتمام المتزايد. وبالتالي في هذه الأيام ظهرت و بشكل مستمر الكثير من نظم التعرف الحيوية كحلول اقتصادية وعالية الكفاءة. إن نظم التعرف الحيوية المعتمدة على بصمات الأصابع كان لها السبق في التطبيقات التجارية. وقد ثبت أن سمات الوجه والقزحية مرشح يمكن الاعتماد عليه في بناء مثل هذه النظم الحيوية. حتى وقت قريب كانت البحوث في مجال التعرف على صور الوجوه تتبع حرقياً مسار البحوث التي أجريت في مجال التعرف على بصمات الأصابع والتي تعتمد بطبيعتها على الصور الممثلة في نطاق تدرجات اللون الرمادي. أما في هذا البحث فتقتصر الجهود على مساحة جزئية لتمثيل الصور في نطاق الألوان. إن مفهوم تحليل المكونات الأساسية التي يتم حسابها بواسطة تحليل القيم المفردة ومن ثم تمثيل صور الوجوه بشكل مدمج باستخدام الصيغة المركبة الرباعية الأبعاد. بخلاف الأساليب الموجودة لمعالجة معلومات الألوان، فإن البحث المقترح يضع في الحسبان الارتباط القائم بين الألوان المكونة للصورة (أي الأحمر والأخضر والأزرق).

CHAPTER 1

1. INTRODUCTION

The revolution in the realm of modern technologies has influenced explicitly the people daily life. Technology has become widely used in many forms and everywhere. In fact, it has facilitated several needs such as communication, automated processes, and enforced security. Many of existing security-based systems such as banking systems are using different forms of technology. In such sensitive systems, a facility for user authentication and identification is considered an urgent need. Several of the commonly used solutions are username/password, electronic and smart cards. Although these solutions are effective and have many advantages, they suffer from serious uncontrollable disadvantages. Several violations could be easily performed such as using a stolen username/password or electronic/smart card by unauthorized persons. Another drawback consists in losing or forgetting the identity mean (i.e., username/password or smart card), which can also prevent the legal person from accessing the system. Also, other various forms of violations and problems can occur effortlessly.

Due to such disadvantages, biometric solutions have taken place and started playing a main role in developing efficient authentication and identification systems which are free from the above mentioned drawbacks. Biometric-based systems make use of various unique human traits. The majority of earlier research efforts have focused on fingerprint-based biometric systems. After that, face and iris traits have become the focus of very active research. Face recognition (FR) has many advantages over other biometric traits because it is natural, nonintrusive, and easy to use. Face recognition research has literally

followed fingerprint recognition research in methodologies and techniques used; therefore most of published research has used inherently gray-scale images. However, a number of promises were carried out from research which has used color images for FR purposes. The FR problem can be cast into the broader area of pattern recognition.

A simplified description of any automated pattern recognition system is using a computer with its integrated components (either hardware or software), instead of human observation, to recognize or identify the different samples by using a previous knowledge of similar models.

Any pattern recognition system comprises three main steps: preprocessing, feature extraction, and classification, as shown in Figure 1.1. Preprocessing is a set of prior operations applied, as preparation, on the input data such as resizing, normalizing, filtering, localization, and normalization. Features are the individual measurable heuristic properties of the phenomena being observed. These properties are used within comparisons between a new unknown sample and already known models to recognize to which class it belongs. Classifiers are mechanisms to assign each point that represents a pattern in the space with a class label or membership scores to the defined classes.



Figure 1.1: Main processing steps in pattern recognition systems.

1.1. Biometrics

A biometric is defined as “a measurable, physical characteristic or personal behavioral trait used to recognize the identity, or verify the claimed identity, of an enrollee” [1].

There exist several different biometrics comprise some methods for uniquely recognizing humans based on one or more essential (innate) physical or behavioral characteristic.

Biometric characteristics can be classified into two main categories listed below and depicted in Figure 1.2:

- Physiological biometrics are related to the shape of the body, e.g. fingerprint, face and iris recognition, hand and palm geometry, and DNA.
- Behavioral biometrics are related to the behavior of a person, e.g. typing rhythm or Keystroke, gait, signature, and voice.

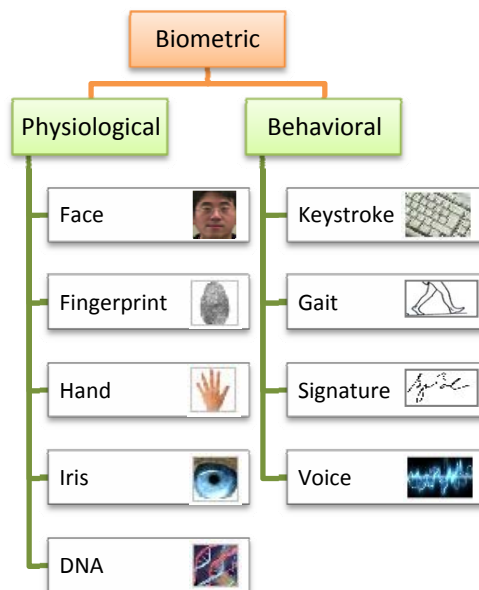


Figure 1.2: Biometric categories.

A biometric system can operate in the following two modes [4]:

- Verification (or authentication) which is a one-to-one matching or comparison of a captured biometric with a stored template to verify that the individual is the one he claimed by comparing a query face image against a template face image.
- Identification (or recognition) which is a one-to-many matching or comparison of the captured biometric against all the template images in a biometric database in attempt to identify an unknown individual, where a query face is matched to a list of suspects can be one-to-few matches.

1.2. Face Recognition

A face recognition (FR) system is simply an attempt to emulate the typical human face recognition task that a human performs routinely, effortlessly, and frequently along his life. Thus face recognition defined as the ability of a computer to receiving and interpreting of face image input. Such face recognition system is supposed to identify faces presented in images and videos automatically. It can operate in either a single or dual mode. Like other biometric systems, an FR system is capable of [1]:

- 1) Capturing a face sample from an end user.
- 2) Extracting biometric data from that sample.
- 3) Comparing the biometric data with that contained in one or more reference templates.
- 4) Deciding how well they match.

- 5) Indicating whether or not an identification or verification of identity has been achieved.

Face recognition has undergone approximately fifteen years of intensive development in both the academic and commercial arenas [1]. Despite of there exist several different approaches in the academic literature, they can be divided into four major classes of algorithms:

- 1) Eigenface Systems based on eigenfaces and eigenvectors.
- 2) Local Feature Analysis System based on the analysis of local features.
- 3) Neural Network methods based on machine learning techniques.
- 4) Gabor filter methods based on Gabor and wavelets analogies.

Definitely, each class has its own advantages and disadvantages [1]. The diagram in, shown in Figure 1.3, demonstrates classification of FR methods.

Although, FR is a very popular and promising research topic, the task is also tending to be a difficult one due to the existence of unconstrained tasks such as viewpoint, illumination, expression, occlusion, and accessories.

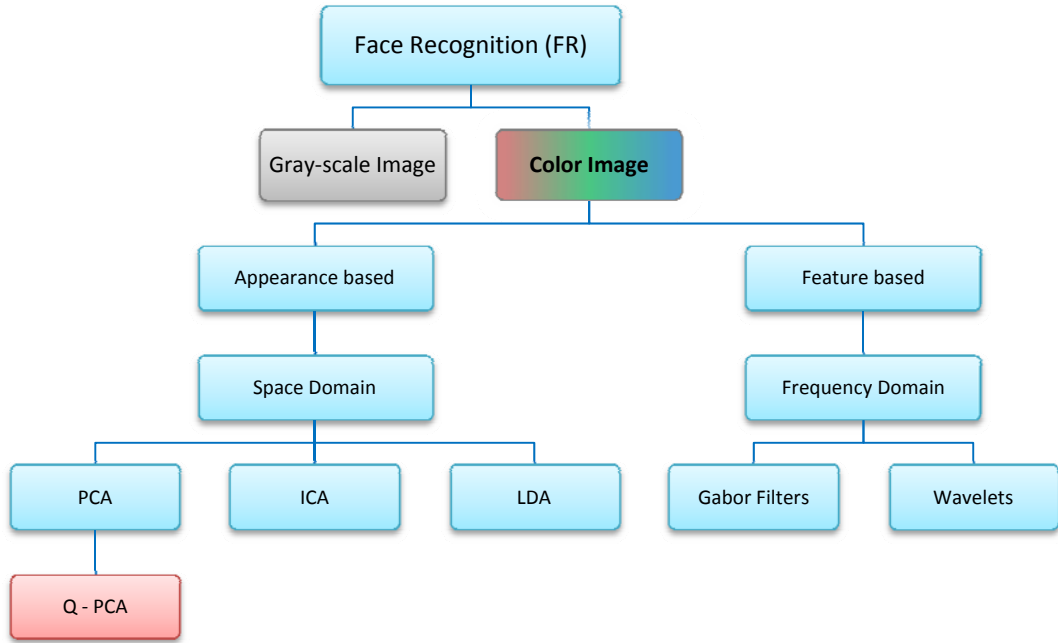


Figure 1.3: Categorization of Face Recognition (FR) methods.

1.2.1. Face Recognition Processing

The face recognition processing flow, depicted in Figure 1.4, consists of four modules: detection, alignment, feature extraction, and matching. Generally speaking, the whole system modules or steps can be divided into two main stages: preprocessing and recognition stages. The former stage includes face detection and alignment or localization and normalization. Facial feature extraction and matching constitute the latter stage.

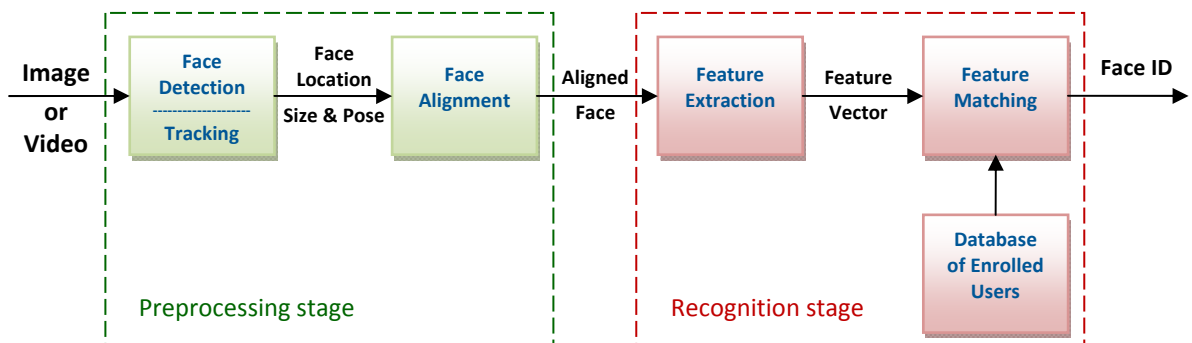


Figure 1.4: Face recognition processing flow.

Face detection segments the face areas from the background known as “nonface” segments. Face alignment is used to achieve more accurate localization, and at normalizing faces thereby it can treat the coarse estimates of the location and scale of each detected face which is detected and provided by face detection module. Figure 1.5 illustrates face detection and alignment processes. The two processes yield the outlines of located and normalized facial components outlines.

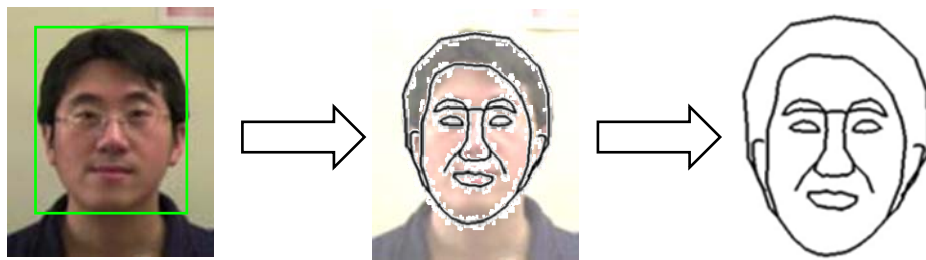


Figure 1.5: Face detection and alignment processes.

Feature extraction is performed to provide effective information that is useful for distinguishing between faces of different persons and stable with respect to the geometrical and photometrical variations. Face matching matches the extracted feature vector of the input face against those of enrolled faces in the database. It is worth noting that, the face recognition results depend highly on features that are extracted to represent the face pattern and classification methods used to distinguish between faces. Also, efficient distinct and effective features depend mainly on the face localization and normalization processes.

1.3. Problem Statement

Human face trait has been proven to be a reliable candidate for person identification. As a result, face recognition has become a very active research field. Consequently, several research efforts have been employed for this active field. However, the great majority of these efforts have used gray-scale representations of the face information. Although the usage of gray-scale representation is considered as one of the more powerful methods for face recognition, it has a major disadvantage of losing and discarding implicitly and explicitly the valued color information. As a remedy to this drawback, recent approaches have used the color information. However, each color component (i.e. red, green and blue) is used individually. In this case, color independence is assumed which violates basic principle of computer vision. Indeed, such approaches could perform better than their gray-scale counterparts if they make use of the color information constructively.

1.4. Motivation

In this thesis, a solution based on hypercomplex (i.e., quaternionic) image representation is proposed where the color information is used in a “holistic” manner. Hence, unlike most of the existing approaches to handle the color information separately, the proposed approach for face recognition implicitly accounts for the correlation that exists between the color components. Figure 1.6, illustrates the proposed approach as an intersection of four different areas.

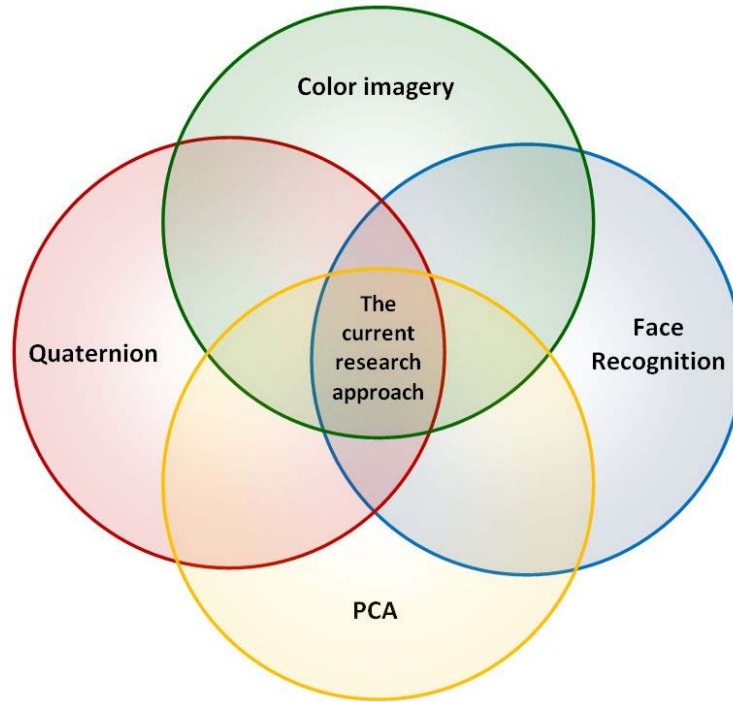


Figure 1.6: Four areas of related work and the current research location.

1.5. Thesis Contributions

The major contributions of this research work are:

- A novel scheme for efficient color face representation and processing for face-based biometric recognition system.
- The concept of principal component analysis (PCA) and singular value decomposition (SVD) are extended to the quaternionic and carried over into the hypercomplex to compactly represent color face images.
- Detailed analysis of the incorporation of color information in face recognition is provided.

- Performance improvement by using color information and the Q-PCA method.
- Extended performance evaluation is performed and comparisons from different perspectives are provided.

1.6. Thesis Outline

This thesis is organized as follows, Chapter 1 provides an introduction of biometric traits and systems. Face recognition concepts and techniques are laid out. In Chapter 2, a set of previous related works are presented and categorized into Grayscale-based and Color-based face recognition approaches.

An overview of Quaternion (Hypercomplex) concepts is provided in Chapter 3. Basic definitions, properties, and representations are discussed therein in details.. Chapter 4, defines Eigenface method for face recognition. Besides, a brief background of principal component analysis (PCA). Furthermore, a detailed description of the proposed quaternionic principal component analysis (Q-PCA) method is presented along with related mathematical expression of singular value decomposition (SVD) and its quaternionic counterpart (QSVD).

In Chapter 5, the methodology experimental results are reported and discussed along with a detailed performance analysis. A performance comparison with the current state-of-the-art methods is carried out. Finally, Chapter 6 gives a summary of the thesis work along with the contributions made in this thesis in light of the research and the testing results. The chapter concludes with an outline of some proposed research directions where the work described in this thesis can be further investigated.

CHAPTER 2

2. LITERATURE REVIEW

Biometrics is a very active area that has a lot of research efforts. Biometric systems provide novel solutions to different access, control and security application. Face recognition techniques evolved from being simple and limited to advanced, complicated, and less limited.

2.1. Grayscale-based Face Recognition

Zhao et al. [24] provide a good comprehensive and critical face recognition literature survey. Furthermore, relevant topics such as psychophysical studies, system evaluation, and issues of illumination and pose variation are discussed.

2.1.1. Grayscale PCA-based Approach

Eigenfaces were first considered for face recognition by Turk and Pentland [22]. 2D gray-face images are projected onto a feature space that captures the significant variation among known face images. These significant features include the eigenfaces because they are eigenvectors or principal components of the set of faces. The projection operation characterizes an individual face by a weighted sum of the eigenface features. Hence in order to recognize a particular face it is necessary only to compare these weights to those of known individuals.

A method for gray-face recognition using principal component analysis (PCA) and radial basis function (RBF) neural networks is presented by Thakur et al. [25]. PCA is employed to reduce the dimensionality of the image and to keep some of the variations in the image data. Adapted (RBF) neural networks are used under imposed conditions. Reported experimental results show that the proposed method enhances the recognition performance.

2.1.2. Grayscale Gabor Filters Approach

A novel algorithm for face recognition using Gabor features to train neural networks is introduced by Rahman and Bhuiyan [26]. The algorithm is applied to gray morphed face images within a constructed system using different scales and orientations. The Multi-Layer Perceptron (MLP) neural network with back-propagation algorithm is employed for face recognition and incorporates the convolution Gabor filter responses.

Wang et al. [27] propose an effective algorithm for face recognition using gray-face Gabor image and Support Vector Machine (SVM) for face recognition. The proposed approach derives the face Gabor image by down-sampling and concatenating the Gabor wavelets representations. These Gabor wavelets are convolution of the face image with a family of Gabor kernels, and then (2D-PCA) method is used to extract the feature space. Then, the extracted features are fed to the SVM classifier.

2.1.3. Grayscale Wavelet-based Approach

In [28], Liu and Dai propose a facial representation based on the dual-tree complex wavelet transform (DT-CWT). The proposed method effectively represents the structures in gray facial image with low redundancy.

By exploiting the DT-CWT and independent component analysis (ICA), a novel face recognition method is proposed by Chai et al. [29]. It provides a better representation for feature extraction. Using PCA, the dimension of the DT-CWT feature vectors is further reduced. Then, the ICA is exploited to reduce the feature redundancies and derive the independent feature vectors.

2.2. Color-based Face Recognition

Several approaches make use of color information [6-8, 16, 20].

Choi et al. [6, 7] propose a metric called “variation ratio gain” (VRG) to theoretically prove the significance of color effect on low-resolution faces. In addition, extensive performance comparison studies are conducted.

Yang and Liu [8] introduced a General Discriminant Model (GDM) for color face recognition. It deals with two sets of variables: a set of color component combination coefficients for color image representation and a set of projection basis vectors for image discrimination. In order to find the optimal solution of the model an iterative whitening-maximization (IWM) algorithm is designed and used.

An evolutionary two-fold framework is proposed by Shih and Liu [16]. First, two new color spaces are defined as linear transformations of the input RGB (i.e., red, green and blue) color space. The first color space is defined by one luminance (L) channel and two chrominance channels (C1, C2). The second color space incorporates one luminance channel (L) and three chrominance channels (C1, C2, C3). A genetic Algorithm (GA) searches for the optimal transformations from the RGB color space to the (LC1C2) and (LC1C2C3) color spaces, respectively.

Since color inputs have large dimensionality which increases the computational cost in FR systems, it is important to determine the scenarios in which usage of color information helps the FR system. Ganapathi [20] provides an empirical study for this purpose and indicates the following observations: the inclusion of chromatic information in FR systems is shown to be particularly advantageous in poor illumination conditions, a color input of optimal dimensionality would improve the FR performance.

The diagonal nonnegative matrix factorization (BDNMF) is proposed by Wang et al. [3] for color face representation and recognition. The approach employs block diagonal matrix to encode color information of different channels. An adapted Nearest Neighborhood classifier is used to identify color face samples. Whereas the obtained experimental results on (CVL) and (CMU PIE) color face databases verify the effectiveness of the proposed approach.

Thomas et al. [21] investigate the use of the characteristics of a 3D color to generate a color Linear Discriminant Analysis (LDA) subspace, which could be used to recognize a new testing image. In order to test the potential improvement in accuracy, a recognition

rate across two color face databases is computed. The observed results indicated that the LDA color subspace significantly improves recognition accuracy over the standard grayscale approach.

2.2.1. Color PCA-based Approach

The PCA technique is used repeatedly in various adaptations for color face recognition. Actually, the algorithm based on PCA, form the basis of numerous studies in the psychological and algorithmic face recognition literature as indicated in [12].

Wang et al. [2] propose a color face recognition approach based on 2D-PCA. The proposed approach comprises a matrix-representation model that encodes the color information directly to describe the color face image. In this way, color face images are represented efficiently in the matrix format. Consequently, color-eigenfaces are computed for feature extraction using 2D-PCA, and the Nearest Neighborhood classification is adapted to identify the color face samples.

Moon and Phillips [12] introduce a generic modular PCA-algorithm in order to investigate the influence of the computational and performance aspects of PCA-based for face recognition algorithms.

2.2.2. Color Quaternion-based Approach

The first attempt of using the quaternion concept for color images is attributed to Pei and Cheng [13]. They propose a quaternion model called the quaternion-moment block

truncation coding (QMBTC). It is proposed for compressing color-pixel blocks. It is mainly based on color (BTC) algorithm and is derived by using the quaternion arithmetic and moment preserving principle.

2.2.2.1. Color Quaternion PCA (Q-PCA) Approach

A technique for quaternion matrix algebra which can be used to process the *eigen* analysis of a color image is proposed by Le Bihan and Sangwine [10]. This technique introduces extensions of two classical techniques to their quaternionic case: Singular Value Decomposition (SVD) and Karhunen-Loeve Transform (KLT). It also introduces the problem of Eigen Value Decomposition (EVD) of quaternion matrix. The properties of these quaternion tools are given and their behavior on natural color images is presented. Furthermore, a method to compute the decomposition using complex matrix algebra is provided. In addition, another consequent work by Sangwine and Le Bihan [31], the Jacobi algorithm for computing the quaternion SVD (Q-SVD) is presented.

Based on Q-SVD, Shi [30] implements the Q-PCA, and applies it to several applications such as color image segmentation. Trilateral filtering is proposed by locally adapting color and changing the shape of the filter to achieve the effect of smoothing colors that preserve the edges.

Ding and Feng [11] propose another method of quaternion Karhunen-Loeve Transform (Q-KLT) and biomimetic pattern recognition (BPR) for color face recognition. The model of (Q-KLT) is used to extract the eigen-faces of training samples and algebraic features for each by BPR method.

A method proposed by some researchers called Extended Two-Dimensional PCA (E2D-PCA) which is an extension to the original 2D-PCA for gray face recognition. E2D-PCA is promoted by a new covariance matrix preserving more local geometric structure information than previous 2D-PCA methods. It avoids small sample size problem of the PCA method. Although the new E2D-PCA improves the previous 2D-PCA, the former one still has some limitation that, it is only considering the global information of face images. Besides, it is only applied for gray face recognition. Where some local and color information may be ignored. Thus, Chen et al. [15] provides a solution to such problems by proposing SpE2D-PCA a hybrid approach based on sub-pattern technique and E2D-PCA.

2.2.2.2. Color Quaternion Gabor Filters Approach

Numerous adapted biometric approaches by using quaternion concept with the well-known Gabor-based methods are defined in [4] for color iris recognition and [1, 9, 23] for color face recognition with distinct specifications of each.

A novel method for the automatic recognition and matching of color iris images is proposed by Al-Qunaieer [4]. Particularly, the well-known IrisCode algorithm, developed by Daugman for gray-scale iris images, is extended to the color domain by compact quaternionic Gabor wavelets representation.

The Gabor filter, which is typically defined as a complex function, is extended to the hypercomplex (quaternion) domain by Jones and Abbott [1, 9]. Several extensions to the hypercomplex domain are discussed and a preferred formulation is selected.

Wei et al. [23] proposes a novel color face recognition method based on Local Binary Patterns (LBP) of Quaternionic Gabor features (QGF). The approach is mainly based on quaternion Gabor analysis within color image representation. This approach is characterized by making full use of the interrelationship among different color channels to enhance the performance of the face recognition system. (QGF) are used to encode the positions and attributes of face elements. Then by using (LBP) which is a non-parametric method was imposed on these (QGF) to obtain the robustness against variations of phase, illumination, and facial expressions.

CHAPTER 3

3. QUATERNION (HYPERCOMPLEX) REPRESENTATION

3.1. Quaternion Numbers

Quaternions were first proposed in 1843 by W.R. Hamilton [36]. They are associative but non-commutative and they belong to a specific class of hypercomplex numbers. Such numbers are used in several applications such as mechanics in 3D space and 3D rotations [4]. Also, quaternions are being applied and used in image processing to represent and process color images in a holistic manner rather than each color separately. Complex numbers represented as a combination of a real and an imaginary parts such as:

$$c = a + b \cdot i \quad (3.1)$$

where i is the imaginary unit, a and bi represent the real and imaginary parts, respectively. Quaternions can be considered as a generalization of the complex numbers having one real part and three imaginary parts [30]. A quaternion number can be written as a linear combination defined as follows:

$$q = a + b \cdot i + c \cdot j + d \cdot k \quad (3.2)$$

where the quaternion q is made of one real part (a) and three imaginary parts (b , c , and d), with i , j and k being the imaginary units. \mathbb{Q} is the quaternionic set, \mathbb{C} is the complex set and \mathbb{R} is the real set satisfying:

$$\mathbb{R} \subseteq \mathbb{C} \subseteq \mathbb{Q} \quad (3.3)$$

The imaginary parts i, j , and k satisfy the following properties:

$$\blacksquare \quad ijk = i^2 = j^2 = k^2 = -1 \quad (3.4)$$

$$\blacksquare \quad (ij = -ji = k), (jk = -kj = i), \text{ and } (ki = -ik = j) \quad (3.5)$$

3.2. Properties of Quaternion Numbers

Quaternions satisfy the multiplication rules which are sometimes known as Hamilton's rules.

- A quaternion with a zero real part is called a pure quaternion (i.e., $a = 0$):

$$q = 0 + bi + cj + dk \quad (3.6)$$

- The conjugate of a quaternion, q , is defined by negating its imaginary parts:

$$\bar{q} = \overline{a + bi + cj + dk} = a - bi - cj - dk \quad (3.7)$$

- The modulus or magnitude of a quaternion, q , is defined by:

$$|q| = \sqrt{a^2 + b^2 + c^2 + d^2} \quad (3.8)$$

- The addition or the sum of two quaternions, q_1 and q_2 is given by:

$$q_1 + q_2 = (a_1 + a_2) + (b_1 + b_2)i + (c_1 + c_2)j + (d_1 + d_2)k \quad (3.9)$$

- The multiplication or the product of two quaternions, q_1 and q_2 is given by:

$$\begin{aligned}
q_1 \times q_2 = & (a_1a_2 - b_1b_2 - c_1c_2 - d_1d_2) \\
& + (a_1b_2 - b_1a_2 - c_1d_2 - d_1c_2)i \\
& + (a_1c_2 - b_1d_2 - c_1a_2 - d_1b_2)j \\
& + (a_1d_2 - b_1c_2 - c_1d_2 - d_1a_2)k
\end{aligned} \tag{3.10}$$

- The quaternion norm is defined by:

$$norm(q) = \sqrt{q \times \bar{q}} = \sqrt{\bar{q} \times q} = \sqrt{a^2 + b^2 + c^2 + d^2} \tag{3.11}$$

The norm is multiplicative such that:

$$norm(q_1 \times q_2) = norm(q_1) \cdot norm(q_2) \tag{3.12}$$

- The division is uniquely defined except division by zero, therefore quaternions form a division algebra. The inverse of a quaternion is defined by:

$$q^{-1} = \frac{\bar{q}}{q \times \bar{q}} \tag{3.13}$$

Given that the norm of q is non-zero.

- To convert a quaternion to a regular complex number, where the quaternions can be represented using its uniquely defined equivalent complex 2×2 matrices such that:

$$q = \begin{bmatrix} z & w \\ -\bar{w} & \bar{z} \end{bmatrix} = \begin{bmatrix} a + bi & c + di \\ -c + di & a - bi \end{bmatrix} \tag{3.14}$$

where z and w are complex numbers, a , b , c and d are real numbers, and \bar{z} and \bar{w} are the complex conjugate of z and w , respectively.

3.3. Quaternion Representation of Color Face Images

Each pixel in a color image has the property of having the values of the three color channels or components. These three colors simultaneously represent a pixel and are defined as the three imaginary parts of the quaternion. Thus, any pixel or point, (x, y) , of a color face image can be represented by a pure quaternion as follows:

$$q_{xy} = 0 + R_{xy}i + G_{xy}j + B_{xy}k \quad (3.15)$$

where x and y are the pixel coordinates, respectively. Figure 3.1 illustrates the approach adopted to represent RGB color face images using a quaternionic form.

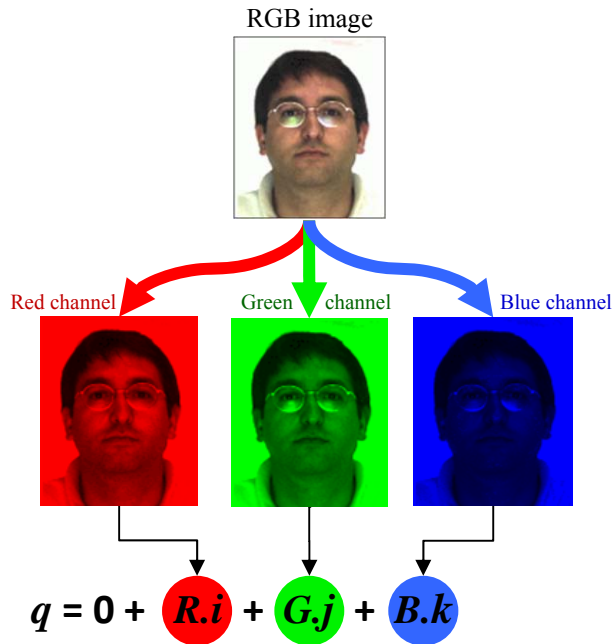


Figure 3.1: Quaternion representation of a color face image.

In this method, quaternions are used to represent the RGB color space. Therefore, the three colors channels are processed equally in arithmetic and geometric operations such as multiplication.

3.4. Quaternion Fourier Transform (QFT)

The 2D Fourier Transform known as Fast Fourier Transform (FFT) is a useful image processing method used to decompose a grayscale image into its sine and cosine components. This method transforms a given image from spatial domain to Fourier or frequency domain, where each pixel represents a specific frequency. It is employed in several applications such as image analysis, filtering and compression. The 2D FFT can be given by [4]:

$$I(u, v) = \int_{-\infty}^{\infty} \int_{-\infty}^{\infty} I(x, y) e^{-iux} e^{-ivx} dx dy \quad (3.16)$$

where $I(u, v)$ is the frequency-domain representation of the image, and u and v are the frequency coordinates, $I(x, y)$ is the spatial-domain representation of the image, x and y are the spatial coordinates.

While the FFT is applied on real and complex numbers, it can be extended to the QFT for handling quaternionic numbers defined as [30]:

$$H_q(u, v) = \int_{-\infty}^{\infty} \int_{-\infty}^{\infty} e^{-iux} \cdot h(x, y) \cdot e^{-jvy} \cdot dx dy \quad (3.17)$$

Equation (3.17) can be generalized to obtain three different types of the QFT: the left-side QFT, the right-side QFT and the two-side QFT. Moreover, The Inverse Quaternion Fourier Transform (IQFT) can be performed for all types. The two-side QFT is defined as [38]:

$$H_{L-R}(u, v) = \int_{-\infty}^{\infty} \int_{-\infty}^{\infty} e^{-\mu_1 ux} \cdot h(x, y) \cdot e^{-\mu_2 vy} \cdot dx dy \quad (3.18)$$

where $h(x, y)$ is the input Quaternion image, μ_1 and μ_2 are two pure quaternionic units, orthogonal to each other, w and v are the spatial frequencies in x and y directions, respectively.

The two-side IQFT is defined as:

$$h(x, y) = \frac{1}{4\pi} \int_{-\infty}^{\infty} \int_{-\infty}^{\infty} e^{-\mu_1 ux} \cdot H_{L-R}(u, v) \cdot e^{-\mu_2 vy} \cdot dudv \quad (3.19)$$

The left-side QFT is defined as:

$$H_L(u, v) = \int_{-\infty}^{\infty} \int_{-\infty}^{\infty} e^{-\mu_1(ux+vy)} \cdot h(x, y) \cdot dx dy \quad (3.20)$$

The left-side IQFT is defined as:

$$h(x, y) = \frac{1}{4\pi} \int_{-\infty}^{\infty} \int_{-\infty}^{\infty} e^{-\mu_1(ux+vy)} \cdot H_L(u, v) \cdot dudv \quad (3.21)$$

The right-side QFT is defined as:

$$H_R(u, v) = \int_{-\infty}^{\infty} \int_{-\infty}^{\infty} h(x, y) \cdot e^{-\mu_1(ux+vy)} \cdot dx dy \quad (3.22)$$

The right-side IQFT is defined as:

$$h(x, y) = \frac{1}{4\pi} \int_{-\infty}^{\infty} \int_{-\infty}^{\infty} H_R(u, v) \cdot e^{-\mu_1(ux+vy)} \cdot dudv \quad (3.23)$$

3.5. Quaternion Gabor Filters

The Gabor filters are well known technique used for image characterization, texture analysis and feature extraction [9]. The complex Gabor filters are widely used in the literature, whereas very few research works make use of the extended Gabor filters in the Quaternion domain. A 2D Gabor filter can be defined by [1]:

$$g(x, y) = \frac{1}{2\pi\sigma_x\sigma_y} \exp\left\{-\frac{1}{2}\left[\frac{x^2}{\sigma_x^2} + \frac{y^2}{\sigma_y^2}\right]\right\} \exp\{j2\pi(ux + uy)\} \quad (3.24)$$

where σ_x and σ_y are the space constants of the Gaussian envelope along the x and y axes. They also characterize the bandwidth of the filter. Each different frequency is given by:

$$F = \sqrt{u^2 + v^2} \quad (3.25)$$

The Quaternion Gabor filters can be implemented by the QFT. Therefore, a 2D Quaternion Gabor filter can be defined by an extension of Equation (3.25) as [1]:

$$g(x, y) = \frac{1}{2\pi\sigma_x\sigma_y} \exp\left\{-\frac{1}{2}\left[\frac{x^2}{\sigma_x^2} + \frac{y^2}{\sigma_y^2}\right]\right\} \exp\{i2\pi(ux + uy)\} \exp\{j2\pi(ux + uy)\} \quad (3.26)$$

Another extension of Equation (3.25) can define a pure Quaternion Gabor filter is achieved by multiplying the quaternion unit μ by the real part of the filter such as [1]:

$$g(x, y) = \mu \frac{1}{2\pi\sigma_x\sigma_y} \exp\left\{-\frac{1}{2}\left[\frac{x^2}{\sigma_x^2} + \frac{y^2}{\sigma_y^2}\right]\right\} \cos\{2\pi(ux + uy)\} \quad (3.27)$$

CHAPTER 4

4. PRINCIPAL COMPONENT ANALYSIS (PCA)

The PCA or KLT is a dimensionality reduction technique based on extracting the desired number of principal components of the multidimensional data [14]. Another definition of PCA is a general method of finding orthogonal axes that contain the most information about a set of sample vectors in a multidimensional space [1].

PCA is the simplest of the true eigenvector-based multivariate analysis. It is considered as a standard tool in modern data analysis in several fields including computer graphics. The concept of PCA can be diagrammatically represented as shown in Figure 4.1. PCA is usually related to the mathematical technique of SVD. A typical PCA mechanism can be summarized in the following steps [17]:

- 1) Organize data as an $m \times n$ matrix, where m is the number of measurement types and n is the number of samples.
- 2) Subtract off the mean from each row or column of the $m \times n$ matrix.
- 3) Apply SVD to calculate the eigenvectors of the covariance.

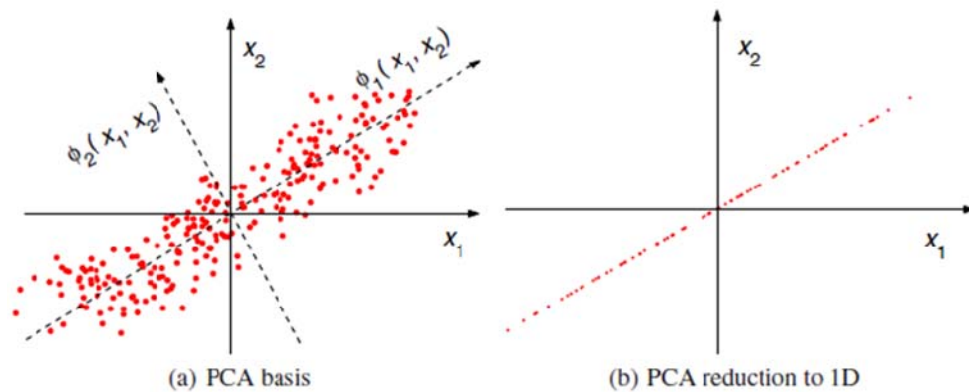


Figure 4.1: The PCA concept, (Li et al. [14]).

Suppose $T = \{t_1, t_2, \dots, t_n\}$, is a training set of (facial) images consisting of n samples. Each t_k is an $(i \times j)$ image matrix representing the k^{th} sample in the training set T . In PCA, each t_k is first reshaped into a high-dimensional vector, $h \in (i * j) \times 1$, by concatenating its columns or its rows. Therefore, an $(m \times n)$ matrix, H , of all reshaped training samples is obtained. m is the number of measurement types and n is the number of samples. Then, the mean of whole training set, μ , is computed as follows [9]:

$$\mu = \frac{1}{n} \sum_{k=1}^n t_k \quad (4.1)$$

The covariance matrix, C , is computed as follows [17]:

$$C = \frac{1}{n} \sum_{k=1}^n (h_k - \mu) (h_k - \mu)^T \quad (4.2)$$

4.1. Eigenfaces

Eigenfaces are a set of eigenvectors used in PCA-based human face recognition. The use of eigenfaces for recognition was first proposed by Sirovich and Kirby in 1987 [22]. Informally, eigenfaces can be considered as a set of standardized face ingredients or substances, derived from statistical analysis of many face images. The generated eigenfaces can be represented visually as shown in Figure 4.2. In this case, a face image can be considered as a combination of standard faces (eigenfaces).

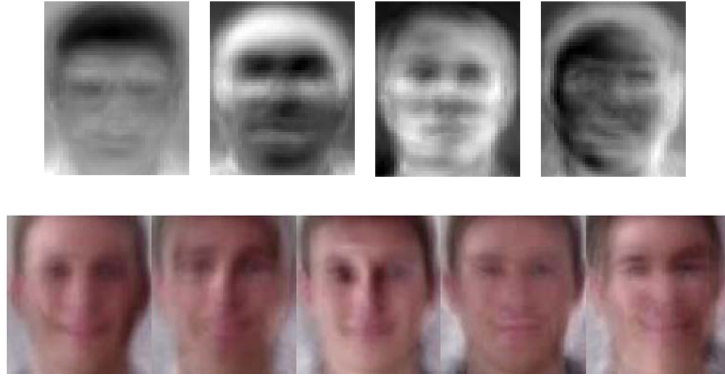


Figure 4.2: In the top gray-eigenfaces and in the bottom color-eigenfaces.

4.2. Solving PCA Using SVD

The PCA calculation can be implemented via the SVD technique. The SVD of an $(m \times n)$ matrix A ($m \geq n$) is given by:

$$A = U \cdot \Sigma \cdot V^T \quad (4.3)$$

where the $m \times n$ matrix U and the $n \times n$ matrix V have orthonormal columns. The $n \times n$ matrix Σ has the singular values of A with $\sigma_1 \leq \sigma_2 \leq \dots \leq \sigma_n \leq 0$ along its main diagonal and zero elsewhere. It should be noted that a singular value of a matrix, A , is the square root of an eigenvalue of matrix AA^T . Note that, the SVD allows for efficient and robust computation of the PCA without the need to estimate the data covariance matrix.

4.3. Quaternion Principal Component Analysis (Q-PCA)

In the real domain, the eigenvalues and eigenvectors of real matrix can be easily computed. However, computing those of a quaternion matrix is a difficult task [15]. In order to calculate the PCA projection matrix based on a quaternion representation, it is

necessary to obtain the orthogonal eigenvector set of the covariance. The orthogonal eigenvectors of the PCA covariance matrix can be obtained using three PCA-based methods: Quaternion Singular Value Decomposition (Q-SVD), Quaternion Eigen-Value Decomposition (Q-EVD), and Quaternion Karhunen-Loeve Transform (Q-KLT).

The Q-SVD can be considered as a generalization of the real or complex SVD. It inherits similar properties [30]. The decomposition of a quaternion matrix by means of classical complex algorithms is based on the SVD computation of the *complex adjoint matrix* (CAM). Therefore, in the Q-SVD solution, a quaternion matrix can be decomposed into its singular value form by converting it into complex matrix representation. Each quaternion matrix \mathbb{Q} of size $M \times N$ has an equivalent complex matrix \mathbb{C} of size $2M \times 2N$ [30, 31]. Hence, the existing complex SVD algorithm can be applied to this equivalent complex matrix \mathbb{C} to obtain the eigenvectors and eigenvalues (i.e. singular values) of the corresponding quaternion matrix \mathbb{Q} .

4.3.1. Quaternion Singular Value Decomposition (Q-SVD)

The Q-PCA calculation can be implemented via the Q-SVD technique. Based on a theorem given in [34] to show the existence of the SVD of a quaternion matrix. Let $Q_q \in \mathbb{Q}_{n \times n}$ be a $n \times n$ quaternion valued matrix with rank k , and there exist two unitary quaternion matrices $U_q \in \mathbb{Q}_{n \times n}$ and $V_q \in \mathbb{Q}_{n \times n}$ such that:

$$U_q^H \cdot Q_q \cdot V_q = \begin{pmatrix} \Sigma_r & 0 \\ 0 & 0 \end{pmatrix}_{n \times n} \quad (4.4)$$

where (H) represents the Hermitian transpose (or conjugate-transposition) operator. Note that, ($_q$, $_c$ and $_r$) denote data types (quaternion, complex and real), respectively. The unitary quaternion matrices U_q and V_q have the property such that:

$$U_q \cdot U_q^H = V_q \cdot V_q^H = \mathbf{I}_r \quad (4.5)$$

Hence, the multiplication of quaternion matrices actually yields the real identity matrix \mathbf{I}_r . The notation Σ_r is a real diagonal matrix ($\Sigma_r \in \mathbb{R}_{k \times k}$) (i.e., the number of non-null singular values), k is the rank of Q_q . The values on the diagonal of $\Sigma_r = \text{diag}\{\lambda_1, \dots, \lambda_k\}$ with ($1 \leq k \leq n$), λ 's are the real positive *singular values* of the quaternion matrix Q_q , arranged in decreasing magnitude order along the diagonal. Thus, Equation (4.5) can be rewritten as:

$$Q_q = U_q \cdot \begin{pmatrix} \Sigma_r & 0 \\ 0 & 0 \end{pmatrix}_{n \times n} \cdot V_q^H \quad (4.6)$$

According to a definition of the equivalent complex matrix of a quaternion matrix [34].

Each quaternion defined by:

$$q = w + x \cdot i + y \cdot j + z \cdot k \quad (4.7)$$

This quaternion q can be decomposed using:

$$q = (w + x \cdot i) + (y + z \cdot i) \cdot j = a + b \cdot j \quad (4.8)$$

where a and b are two complex numbers.

For instance, an $n \times n$ quaternion valued matrix Q_q defined as:

$$Q_q = A_c + B_c \cdot j \quad (4.9)$$

where A and B are $n \times n$ complex matrices, then from equation (3.14) in Chapter 3 and equation (4.9) the equivalent $2n \times 2n$ complex matrix C_c of Q_q is

$$C_c = \begin{bmatrix} A_c & B_c \\ -\bar{B}_c & \bar{A}_c \end{bmatrix}_{2n \times 2n} = \begin{bmatrix} w + xi & y + zi \\ -y + zi & w - xi \end{bmatrix} \quad (4.10)$$

Thus, the classical complex SVD algorithm can be applied to C_c to generate the eigenbasis (i.e., eigenvectors) and the corresponding singular values ranked in descending order.

Let the SVD of a quaternion matrix Q_q be:

$$Q_q = U_q \cdot \Sigma \cdot V_q^H \quad (4.11)$$

Let the equivalent complex matrix C_c for Q_q be:

$$C_c = U_c \cdot \Sigma' \cdot V_c^H \quad (4.12)$$

then,

$$\Sigma = \text{row}_{\text{odd}}(\text{col}_{\text{odd}}(\Sigma')) \quad (4.13)$$

If

$$U_c = \begin{bmatrix} [U_c^1]_{n \times 2n} \\ [U_c^2]_{n \times 2n} \end{bmatrix}_{2n \times 2n} = \begin{bmatrix} A_c \\ B_c \end{bmatrix} \quad (4.14)$$

Then,

$$\begin{aligned} U_q &= \text{col}_{\text{odd}}(U_c^1) + \text{col}_{\text{odd}}(-\bar{U}_c^2) \cdot j \\ &= \text{col}_{\text{odd}}(A_c) + \text{col}_{\text{odd}}(-\bar{B}_c) \cdot j \end{aligned} \quad (4.15)$$

where, $row_{odd}(M)$ means the odd rows and $col_{odd}(M)$ means the odd columns of matrix M . In addition, some of the most significant properties of the Q-SVD, when applied to color images, are listed below by Le Bihan et al. [10]:

- 1) Invariance to spatial rotation (also true in the case of greyscale images with SVD).
- 2) Invariance to spatial shift (vectors in U and V are shifted by the same amount).
- 3) Invariance to color space rotation.

4.3.2. QSVD-Based Color Image Compression

Several useful methods applied to the SVD can be extended to color images using Q-SVD. Such extensions are achieved without separating the color image into three channels and processing each color channel independently. One very useful SVD-based method is image compression which definitely can be extended to color images. The robustness of this compression method is in storing large images as smaller more manageable ones. QSVD-based compression accomplished by reproducing the original image with each succeeding non-zero singular value ($\lambda_i \in \Sigma$). Furthermore, by using fewer singular values (λ 's) it can achieve more compression to produce approximate image [30]. Using equation (4.12), the image can be decomposed as:

$$Q = U \cdot \Sigma \cdot V^H \quad (4.16)$$

Then, to construct the eigen-image of original one, the SVD of a color image, Q , can be decomposed into:

$$Q = U \cdot \Sigma \cdot V^H = \sum_{i=1}^R \lambda_i \cdot (u_i \times v_i^H) \quad (4.17)$$

where u_i and v_i are the column vectors of matrix U and V , respectively. The λ_i 's are the diagonal elements of the real matrix Σ and R is the rank of Q . Here, each i product $(u_i \times v_i^H)$ generates an eigen-image. Therefore, the constructed color image, \mathbf{x} , can be considered as the linear combination of R color eigen-images. Note that, in quaternion and complex matrices, the preceding eigen-images represent the low-frequency components of the original image, and the later ones represent the high-frequency components [30]. Therefore, an approximate Q_{approx} of a color image can be obtained by summing the first k eigen-images such that:

$$Q_{approx} = \sum_{i=1}^k \lambda_i \cdot (u_i \times v_i^H) \quad (4.18)$$

where the real part of Q_{approx} is small, and decreases to zero when k increases to R . However, a good approximation of the original color image can be provided by a small k . Due to this compression, the storage requirements for the color image is reduced from $(3 \times N \times N)$ to $k(2 \times 4N + 1)$.

Figure 4.3 illustrates four estimated images based on Q-PCA and its approximation reconstruction applied to a facial image of size 213×144 . Note that when the image has more high-frequency components, a larger k is necessary to have a good approximation. Otherwise, for images containing mostly low-frequency signals, small k is good for the reconstruction. As shown in the two approximations in (c) and (d), it is clear that a satisfactory approximate representation can be found with far fewer singular values. This

simple example illustrates the power and efficiency of the Q-SVD method. The reconstructed image is produced by the first 16 singular values requiring only $16 \times 213 \times 4 = 13,632$ entries. Another major advantage is performance optimization of a recognition system.



Figure 4.3: Q-SVD-based image compression. (a),(b),(c) and (d) are the reconstructed images with $k=8,16,25,144$ respectively. Where (d) is the perfect reconstruction of the original image

4.3.3. Proposed Q-PCA Algorithm

The most significant concepts (i.e., Quaternion, PCA, SVD) associated with the novel proposed scheme have been defined previously. The proposed QPCA algorithm, called Quaternion Principle Component Analysis, can be described and summarized under a list of steps needed to carry out Q-PCA procedure as follows:

- 1) For each facial color image t_q in the training data, convert t_q into pure quaternionic representation.

$$t_q = 0 + R \cdot i + G \cdot j + B \cdot k \quad (4.19)$$

- 2) Organize the data as an $(m \times n)$ design matrix, A_q , where m is the number of measurement types (also rows) and n is the number of samples (also columns). Each matrix cell $m_x n_y$ is a quaternion number. Hence, each column n_y represents a single vector or orthogonal representation of quaternion image pixels.
- 3) Subtract off the mean, μ_q , and divide by the variance, σ_q , each measurement type, m_x , to obtain n orthonormal vectors of the design matrix A_q .
- 4) Calculate the Q-SVD or the quaternion eigenvectors, U_q , of the covariance matrix, defined as:

$$A_q = U_q \cdot \Sigma \cdot V_q^H \quad (4.20)$$

- 5) To recognize or match a query color face image, f_q , the quaternion form of f_q is normalized and projected onto the eigen-face space by:

$$P_q = U_q^H \cdot \left(\frac{f_q - \mu_q}{\sigma_q} \right) \quad (4.21)$$

where P_q is the projection of the image f_q , and $(^H)$ represents the Hermitian transpose (or conjugate-transposition) of the eigenvectors, U_q . μ_q and σ_q are the mean and variance vectors of the design matrix, A_q , respectively.

CHAPTER 5

5. METHODOLOGY AND EXPERIMENT

5.1. Research Methodology

This research proposes a novel scheme for color face recognition. Particularly, the proposed scheme is based on the well-known PCA method. In this research, the PCA is naturally extended to the hypercomplex (quaternionic) domain to define the Q-PCA. Besides the benefit of combining the existing color information, Q-PCA supports and emphasizes the usage of other beneficial information (such as color correlation and interaction) that would not be obtained using a mere parallel (and independent) processing of the color components. The added-value brought in by the proposed scheme is made possible by the holistic representation of the color information in the hypercomplex domain. Moreover, a comparative analysis is carried out to highlight the improvement attributed to the holistic processing of the color components. The experimental work is conducted using standard color face databases.

5.2. Color Face Image Database

Within the experimental work of this thesis, two standard databases are used. The first one is used as a minor database and the other one is used as major. The minor database is the “Georgia Tech Face Database (GTDB)” which is used at earlier stages of the development of the PCA technique for gray-level and color face images. The major database is “The Color FERET Database” which is used in all experiments reported therein.

5.2.1. Georgia Tech Face Database (GTDB)

The GTDB was collected and prepared at the Center for Signal and Image Processing at Georgia Institute of Technology. It contains images of 50 people taken in two or three sessions between 06/01/1999 and 11/15/1999 to take into account the variations in illumination conditions, facial expression and appearance. Furthermore, the faces were captured at different scales and orientations. Each subject (a person) in the database is represented by 15 color JPEG images with cluttered background taken at a resolution of 640×480 pixels. Hence, the database contains 750 face images. The average image is 150×150 pixels. The GTDB also provides a preprocessed set (GTDB_crop) of cropped and relabeled images where each in the database was cropped and background removed. An addition at preprocessing step is performed in this thesis. Due to the various sizes of the cropped images, each image is resized to 213×144 pixels.

5.2.2. Color FERET Database

The FERET database is a well known standard facial database in both color and grayscale representations provided by the US National Institute of Standards and Technology (NIST). It has been designed to advance the state of the art in face recognition. The database collection was a collaborative effort between Dr. Wechsler and Dr. Phillips. The database was collected at various angles in 15 sessions between August 1993 and July 1996. It contains 1564 sets of images for a total of 14,126 images that includes 1199 individuals and 365 duplicate sets of images. A duplicate set is a second set of images of a person already in the database and was usually taken on a different day. For some

individuals, two years have elapsed between their first and last sittings, with some subjects being photographed multiple times. This period of time was important to enable researchers to study the effects of changes in a subject's appearance that occur over years. Thus, the FERET database introduces variability by the inclusion of images taken at different dates and locations. This results in changes in lighting, scale and background.

The whole database is divided into a development set, provided to researchers, and a set of sequestered images for testing. The images in the development set are used as a representative of the sequestered images. However, the available database for researchers is a subset of the database consisting of 11,338 images from the total of 14,126. These images represent 994 individuals from the total of 1199 individuals. The remaining individuals and images were not provided for the researchers. The database, provided in color PPM-format, represents images in three different resolutions:

- 1) Full size images 768×512 pixels.
- 2) Half size images 384×256 pixels.
- 3) Quarter size images 192×128 pixels.

There are 13 different poses in the collected database representing the person's face at various angles. Table 5.1 gives a summary of the database content and the imagery pose types.

<i>Two letter code</i>	<i>Pose Angle (degrees)</i>	<i>Description</i>	<i>Number of images in Database</i>	<i>Number of Subjects (persons)</i>
fa	0 =	Regular facial expression	1364	994
fb	0	Alternative facial expression	1358	993
ql	-22.5	quarter left - head turned about 22.5 degrees left	761	501
qr	+22.5	quarter right - head turned about 22.5 degrees	761	501
hl	-67.5	half left - head turned about 67.5 degrees left	1267	917
hr	+67.5	half right - head turned about 67.5 degrees right	1320	953
pl	-90	Profile left - head turned about 90 degrees left	1312	960
pr	+90	Profile right - head turned about 90 degrees	1363	994
ra	-45	random image - head turned about 45 degree	321	261
rb	-15	random image - head turned about 15 degree	321	261
rc	+15	random image - head turned about 15 degree	610	423
rd	+45	random image - head turned about 45 degree	290	236
re	+75	random image - head turned about 75 degree	290	236

Table 5.1: Summary of FERET color face database.

5.3. Performance Evaluation

A biometric evaluation protocol determines how to test a system, select the data, and measure the performance. In order to apply validation and verification to the proposed approach, the (FERET) evaluation protocol is used, which is a standard method for evaluating face-recognition algorithms [32]. This biometric evaluation protocol investigates the performance of Q-PCA-based versus the typical PCA-based algorithms. The PCA-based algorithms considered in this thesis are: gray-PCA, Red-component-PCA, Green-component-PCA, Blue-component-PCA, Avg-RGB-PCA of the three components, and SCFT-CPCA (complex PCA of Spatio-chromatic Fourier transform) [37].

A number of stress test experiments are performed for these different implementations to evaluate and compare their performance. All these algorithms are examined by applying a number of proper performance evaluation methods and using the same data sets. Table 5.2 shows the PCA-based algorithms used in this work.

<i>Algorithm</i>	<i>Description</i>
PCA	Calculates PCA for grayscale face images
QPCA	Calculates Quaternion PCA for color face images
Red PCA	Calculates PCA for the Red component of color face images
Green PCA	Calculates PCA for the Green component of color face images
Blue PCA	Calculates PCA for the Blue component of color face images
Avg RGB PCA	Calculates PCA for the Average of the three color channels (i.e. red, green and blue) of color face images
SCFT CPCA	Calculates Complex PCA for the spatio-chromatic Fourier transform of color face images

Table 5.2: Summary of PCA-based algorithms used in this thesis.

5.3.1. Standard Testing Subsets

In this experimental work, FERET standard testing subsets are used to carry out the performance and statistical evaluation. Particularly, the gallery and probe sets used in FERET tests (September 1996) are selected for this purpose. Therefore, the identification scores are carried out for four categories of probes and all the tests for these probes are using a single gallery containing 993 images as indicated in Table 5.3.

<i>Evaluation Task</i>	<i>Recognized Names</i>	<i>Gallery (993)</i>	<i>Probe Set</i>
Facial Expression	FB	gallery.names	probe fafb *.names (993)
Low aging of subjects	duplicate I	gallery.names	probe dup 1 *.names
Illumination	fc	gallery.names	probe fafc *.names (98)
High aging of subjects	duplicate II	gallery.names	probe dup 2 *.names

Table 5.3: Gallery and four probe sets.

Table 5.4 gives the identification scores derived two times for the same gallery and probes in two different versions (or resolutions). This redundancy aims at assessing the effect of image resolution on the system performance.

<i>Dataset</i>	<i>No. of images / Resolution version</i>	
Gallery	(993) / 192×128 pix	(993) / 384×256 pix
FB (probe)	(993) / 192×128 pix	(993) / 384×256 pix
duplicate I (probe)	(736) / 192×128 pix	(736) / 384×256 pix
fc (probe)	(98) / 192×128 pix	(98) / 384×256 pix
duplicate II (probe)	(228) / 192×128 pix	(228) / 384×256 pix

Table 5.4: Resolution of gallery and probe sets.

The first probe category is the FB probes. In each set of images, there are two frontal images denoted by fa and fb pose types. One of the images is randomly placed in the gallery, and the other image is placed in the FB probe set. This category is aimed to evaluate the algorithm performance against the variation in facial expressions. The second probe category is the duplicate I probe, which contains all duplicate frontal images in the FERET database for the gallery images. This category is aimed to evaluate the algorithm performance against the variation in low degree of subject aging. The third probe category is the fc probe, where images are taken the same day with a different camera and lighting. This category is aimed to evaluate the algorithm performance against the variation in illumination. The fourth probe category is the duplicate II probe, which consists of duplicates where there is at least one year between the acquisition of the probe image and the corresponding image in the gallery. This category is aimed to evaluate the algorithm performance against the variation in high degree of subject aging. Figure 5.1 gives the face images of one subject samples from the gallery and all the four probes.

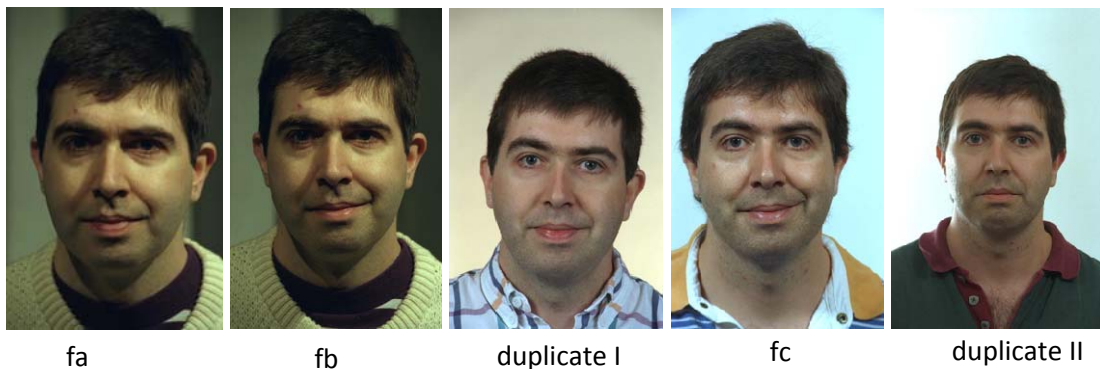


Figure 5.1: One subject face images (gallery and probes).

Another subpart of color FERET database consists of five subsets. Each subset has its own gallery and probes (one gallery and two probes). The gallery of each subset contains approximately 200 individuals. For each subset, one of the two probes represents the FB

category and the other represents the duplicate I category. Table 5.5 lists the five subsets with their details.

<i>Probe Name</i>	<i>Gallery size</i>	<i>FB Probe set size</i>	<i>duplicate I Probe set size</i>
Set 1	200	200	145
Set 2	200	200	70
Set 3	200	200	204
Set 4	200	200	283
Set 5	193	193	34

Table 5.5: Subsets used to investigate the variation in performance.

5.3.2. Test Design

The adopted biometric evaluation protocol investigates the performance aspects to several FR algorithms. In this testing protocol, each evaluated algorithm can use a different similarity measure and it does not compare similarity measures from different algorithms. However in the current experimental work the similarity measure is the same for all compared algorithms, since they are all PCA-based algorithms. A significant advantage of this protocol is that for any two images, q_i and t_k , the similarity measure, $si(k)$, is known which allows for a greater flexibility and more comprehensive evaluation methodology. This flexibility is achieved and satisfied by computing scores for virtual galleries and probe sets. The algorithm performance is characterized by different categories of images:

- 1) Rotated images.
- 2) Duplicates taken within a week of the gallery image.
- 3) Duplicates where the time between the images is at least one year.
- 4) Galleries containing one image per person.
- 5) Galleries containing duplicate images of the same person.

A gallery \mathcal{G} is a virtual gallery if \mathcal{G} is a subset of the target set \mathcal{T} . Similarly, \mathcal{P} is a virtual probe set if \mathcal{P} is a subset of query set \mathcal{Q} . For a given gallery \mathcal{G} and probe set \mathcal{P} , the performance scores are computed by examination of similarity measures $si(k)$ such that $q_i \in \mathcal{P}$ and $t_k \in \mathcal{G}$.

In all the conducted experiments, for all Algorithms the number of eigenvectors is adopted to be 200 eigenvectors. This decision is obtained after performing a number of trials using 25, 50 and 100 eigenvectors. Selecting this certain number of eigenvectors to be used for projecting a tested facial image onto the eigenface space improves the accuracy in general about 3-9%.

5.3.3. Standard Performance Measures

For the sake of comparison with existing algorithms, a set of standard biometric evaluation methods are provided and described in this section. Such evaluation methods or measures are commonly used to allow a fair comparison and a precise statistical evaluation.

Cumulative Match Characteristic (CMC): It is usually computed and visually represented as a curve of ranked cumulative match scores form rank of 1 to rank of $k \leq$ the number of enrolled persons.

In order to define the decision theory of CMC measure for evaluating the performance of an algorithm, there exist two basic models are: the closed and open universes. In the closed universe, every probe is in the gallery whereas in an open universe, some probes

are not in the gallery. Since the concern of this research is concerned with identification, the appropriate model is the closed-universe model which reports different performance statistics and reflects important aspects of FR algorithms. Such aspects allow evaluators to ask how good an algorithm is at identifying a probe image. Note that, the question is not always “is the top match correct?” but it could be “is the correct answer in the top n matches?”. The answer of such question allows evaluators to know how many images (what are the k -images) have to be examined to get a desired level of performance. The reported performance statistics are based on the CMC curve wherein the rank is plotted along the horizontal axis and the percentage of correct matches is plotted in the vertical axis. The cumulative match score can be calculated for any algorithm against any subset of the probe set. The computation of an identification score as follows:

Let $|\mathcal{P}|$ be the size of probe \mathcal{P} . The probe set \mathcal{P} is scored against gallery \mathcal{G} , where $\mathcal{G} = \{g_1, \dots, g_m\}$ and $\mathcal{P} = \{p_1, \dots, p_n\}$ by comparing the similarity scores $si(*)$ such that p_i in \mathcal{P} and g_k in \mathcal{G} , where $*$ indicates the similarities of all g_k images in a gallery set, \mathcal{G} , to be computed against each p_i in \mathcal{P} . For each probe image, p_i in \mathcal{P} , $si(*)$ is scored for all gallery images g_k in \mathcal{G} . A smaller similarity score implies a closer match. If g_k and p_i are the same image, then $si(k) = 0$. The function $id(i)$ gives the index of the gallery image of the person in probe p_i , i.e., p_i is an image of the person in $g_{id(i)}$. A probe p_i is correctly identified if $si(id(i))$ is the smallest scores for $g_k \in \mathcal{G}$. A probe p_i is in the top k if $si(id(i))$ is one of the k -th smallest score $si(*)$ for gallery \mathcal{G} . Let R_k denotes the number of probes in the top k . Thus, the fraction of probes in the top k is reported, such that $R_k / |\mathcal{P}|$. For example, let $k = 5$, $R_5 = 80$ and $|\mathcal{P}| = 100$. Based on this formula, the performance score

for R_5 is $80/100 = 0.8$. The design scheme of the testing procedure, used in this research is illustrated in Figure 5.2.

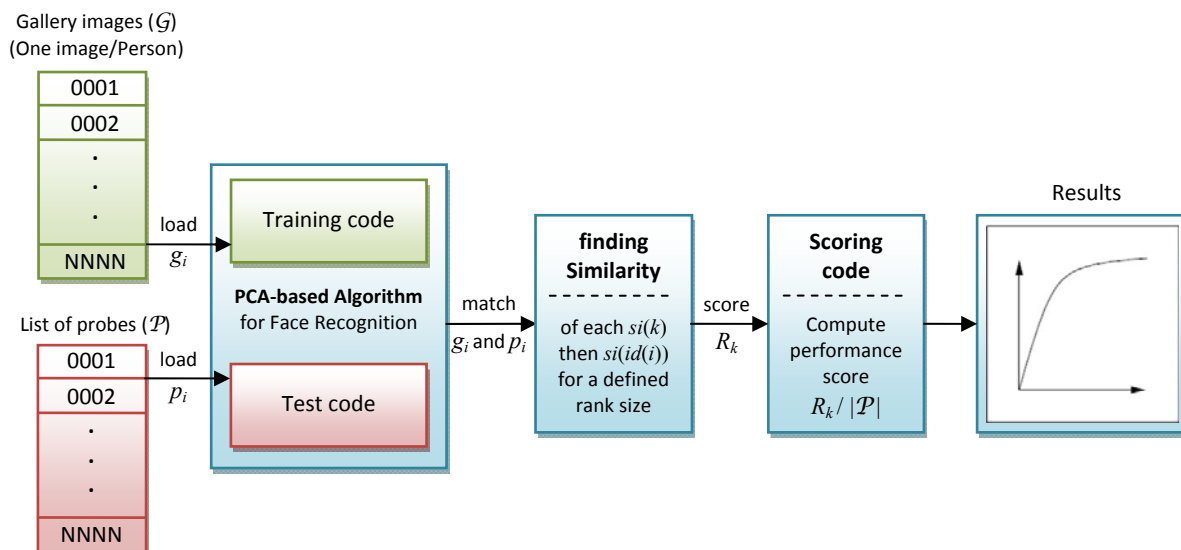


Figure 5.2: Design scheme of the testing procedure.

In all reported performance results, the size of the gallery is the number of different faces (people) contained in the images that are in the gallery. Hence, there is one image per person in the gallery. Therefore, the size of the gallery is also the number of images in this gallery. The number of probes scored is also the size of the probe set (i.e., $|\mathcal{P}|$). However, the probe set may contain more than one image of a person and the probe set may not contain an image of everyone in the gallery. Every image in the probe set has a corresponding image in the gallery (closed-universe model).

Genuine distribution (GD): A distribution which is estimated by comparing different face image samples that belong to the same person against each other.

It should be noted that there is no need to inverse the comparisons between any two samples i and j since the comparison is symmetric.

Imposter distribution (ID): A distribution which is estimated by comparing different face images that belong to different persons.

Such that, the i^{th} sample of each person is compared to the i^{th} sample of all the remaining persons in the dataset. In this case, the comparison is also symmetric.

For illustration, a sample of GD and ID distributions is given in Figure 5.3. The more separated are the GD and ID curves, the better is the matching process. Furthermore, the intersection areas represent errors in the matching process.

Within this error area, two subareas exist:

False Accept Rate (FAR): A subarea which is the region of ID that is considered to belong to the GD.

False Reject Rate (FRR): A subarea which is the portion of GD that is considered as part of the ID.

Both error areas are illustrated in Figure 5.3. Consequently, the selection of a specific threshold represents a trade-off between the FAR and FRR errors. The selection of a proper threshold depends significantly on the application of the biometric system at hand. For instance, the FAR error is selected to be large in forensic applications for criminal identification to reduce the possibility of missing a wanted criminal. On other hand, the FRR error is selected to be large in highly secure access control systems to guarantee that authorized genuine users can gain access.

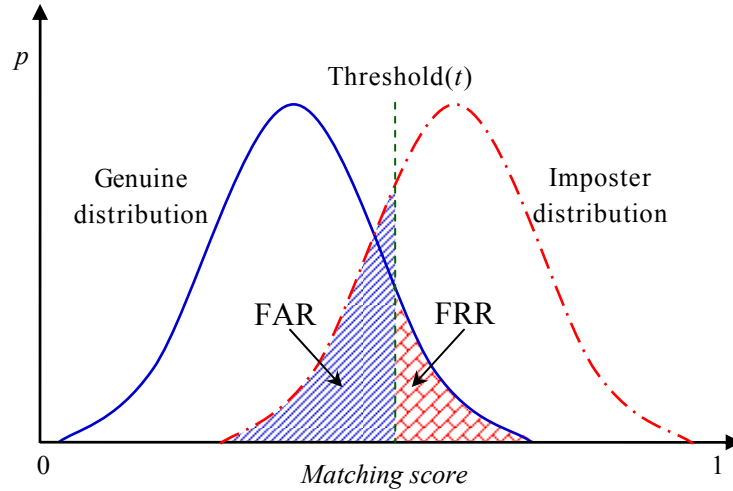


Figure 5.3: GD versus ID and FAR versus FRR errors.

Generally speaking, better results are achieved if the two distributions are well separated.

Decidability index (d): The separation or the distance between the two means the GD and ID considered as a hint about the system performance.

The decidability index, d , can be calculated as follows [4]:

$$d = |\mu_g - \mu_i| \quad (5.1)$$

where μ_g and μ_i are the means of the GD and ID, respectively. Large values for the decidability index do not necessarily mean that the performance is better. In some cases, although the decidability index is large, the errors can be large and should be taken into account with the decidability index.

The FAR and FRR error curves can be calculated from the GD and ID by using a threshold t that ranges from 0 to 1. Thus, the $FAR(t)$ and $FRR(t)$ are functions of t , where $FAR(t)$ is the percentage of imposters greater than or equal to the threshold, and $FRR(t)$ is the percentage of genuine less than the threshold [35]. Besides, the following information can be estimated from the FAR and FRR curves as illustrated in Figure 5.4:

Equal-Error Rate (EER): The error rate where accept and reject errors are equal ($FAR(t) = FRR(t)$), so that lower EER values indicate less errors.

ZeroFRR: The lowest FAR where no FRR occurs.

ZeroFAR: The lowest FRR where no FAR occurs.

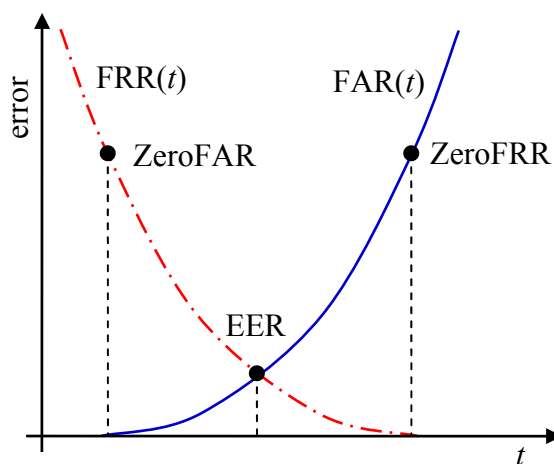


Figure 5.4: FAR versus FRR curves.

Receiver Operating Characteristic (ROC): A curve is used to measure and summarize the performance of a biometric identification or verification systems.

An ROC curve is based on the representation of the decision thresholds, therefore it shows the system performance at all thresholds. Note that it is threshold independent, allowing performance comparison of different systems under similar conditions. It plots the percentage of impostor attempts accepted which is the FAR on the x-axis, against the percentage of genuine attempts accepted which known as correct acceptance rate ($CAR=1 - FRR$) on the y-axis [35]. In ROC curves the relationship between FAR and FRR can be observed. Such that, as the FAR error is increased, the FRR is decreased and accordingly

the CAR or (1- FRR) is increased, and vice versa. The best curve is a straight horizontal line with zero FRR that means accordingly the genuine attempts acceptance is (1-0=100), which means that EER is equal to zero. Consequently, the lower curve means more errors.

5.3.4. Identification Performance against Probe Categories

The identification performance is investigated and reported for each of the compared algorithms against four different probe categories from the first standard dataset. This identification performance evaluation is based on a fraction of CMC scores ranked from 1 to 50 for the sake of comparison. Moreover, the identification performance for an algorithm is investigated and reported for the same dataset in different resolutions. Table 5.6 gives a summary of the properties of the test gallery and probes.

<i>Figure No.</i>	<i>Probe Category</i>	<i>Gallery size</i>	<i>Probe set size</i>	<i>Resolution</i>	
5.5 and 5.6	FB	993	993	192×128 pix	384×256 pix
5.7 and 5.8	duplicate I	993	736		
5.9 and 5.10	fc	993	98		
5.11 and 5.12	duplicate II	993	228		

Table 5.6: Summary of used gallery and probe categories.

Table 5.7 gives the fraction of probes whose gallery match is top ranked (i.e., the rank equals to 1). Hence, each number in this table represents the correct total match score considering the match with only one nearest-neighbor to each tested sample. This is effectively the performance on forced identification (i.e., best guess). As shown in the table, each probe category has two score numbers representing scores of two different resolutions.

Algorithm	Gallery Size / Scored Probes							
	993/993		993/736		993/98		993/228	
	FB		duplicate I		fc		duplicate II	
	192×128	384×256	192×128	384×256	192×128	384×256	192×128	384×256
PCA	0.624	0.626	0.135	0.132	0.010	0.010	0.004	0.004
QPCA	0.646	0.648	0.145	0.147	0.010	0.010	0.004	0.004
Red PCA	0.635	0.638	0.141	0.143	0.010	0.010	0.004	0.004
Green PCA	0.621	0.622	0.130	0.132	0.010	0.010	0.004	0.004
Blue PCA	0.599	0.600	0.128	0.129	0.010	0.010	0.004	0.004
Avg RGB PCA	0.619	0.620	0.133	0.135	0.010	0.010	0.004	0.004
SCFT CPCA	0.004	0.002	0.001	0.004	0.000	0.000	0.000	0.000

Table 5.7: Match scores of the top-rank for each PCA-based algorithm.

Table 5.8 gives the estimated average score of the total match score against each probes (i.e., the average of scores located along a rank from 1 to 50) which consider the average of the first 50 identification estimations. Hence, each number in this table represents the average of correct total match scores of the ranks from 1 to 50 (i.e., from 1 to 50 nearest-neighbors) for each test sample. This is effectively the total performance on forced identification (i.e., best 1,2, ..., 50 guesses). As shown in the table, each probe category has two score numbers representing scores of two different resolutions.

Algorithm	Gallery Size / Scored Probes							
	993/993		993/736		993/98		993/228	
	FB		duplicate I		fc		duplicate II	
	192×128	384×256	192×128	384×256	192×128	384×256	192×128	384×256
PCA	0.867	0.868	0.277	0.277	0.037	0.037	0.047	0.047
QPCA	0.880	0.881	0.284	0.285	0.042	0.041	0.052	0.052
Red PCA	0.887	0.887	0.290	0.290	0.030	0.029	0.035	0.035
Green PCA	0.862	0.862	0.273	0.274	0.045	0.045	0.054	0.054
Blue PCA	0.846	0.846	0.269	0.269	0.056	0.057	0.060	0.061
Avg RGB PCA	0.865	0.865	0.277	0.278	0.044	0.044	0.050	0.050
SCFT CPCA	0.059	0.047	0.025	0.035	0.017	0.035	0.020	0.030

Table 5.8: Average score of the total match scores of rank 50 for each PCA-based algorithm.

In order to evaluate and compare the performance of different FR algorithms, two aspects are taken in account. The first is the evaluation of an algorithm based on the achieved top-rank match score as reported in Table 5.7. The second is the total-average of total match scores that depends on averaging the total of scores achieved as listed in Table 5.8. So,

according to the scoring results summarized in Tables Table 5.7-Table 5.8, to a number of observations can be estimated.

By testing the PCA-based algorithms against FB probe data, as illustrated in Figures Figure 5.5-Figure 5.6, the Q-PCA algorithm yielded the highest top-rank match score, and achieved the best performance in the identification task. While the Red PCA achieved the second best top-rank score, it achieved a total-average score better than the Q-PCA algorithm. It should be noted that, the total-average score of each algorithm was not affected by the probe resolutions except in the case of the 384×256 pixels resolution, where the top-rank score of the SCFT CPCA algorithm is slightly decreased.

The performance of all algorithms against duplicate I probe data with 192×128 pixels resolution is illustrated in Figure 5.7. The best algorithm has the highest top-rank score and the worst algorithm has the lowest top-rank score. It can be seen that the Q-PCA algorithm achieved the best top-rank and the SCFT CPCA algorithm achieved the lowest top-rank. On the other hand, the performance was quite differed with respect to the total-average. The best total-average was achieved by the Red PCA algorithm. The Q-PCA algorithm was the second. However, against the duplicate I probe data using 384×256 pixels resolution, as illustrated in Figure 5.8 the performance trend has slightly changed. According to the reported top-rank scores the Q-PCA algorithm has still the best performance. From the total-average perspective, the performance has improved for the Q-PCA, Green PCA and Avg RGB PCA algorithms. The best total-average was achieved by the Red PCA algorithm followed by the Q-PCA algorithm.

Figures Figure 5.9 -Figure 5.10 illustrate the performance of all algorithms against the fc probe data at resolutions of 192×128 pixels and 384×256 pixels, respectively. The top-rank score value was the same for all algorithms in both resolutions as listed in Table 5.7 except for the SCFT CPCA algorithm. However, the total-average varies and can be used for comparing and ranking the competitor algorithms. Unlike in the FB and duplicate I datasets the best total-average is achieved by the Blue PCA algorithm. Then, the Green PCA and Avg RGB PCA algorithms achieved the next highest performance followed by the Q-PCA algorithm.

As illustrated in Figures Figure 5.11 -Figure 5.12, the performance of all algorithms against the duplicate II probe data at two resolutions of 192×128 pixels and 384×256 pixels, respectively. The top-rank score was the same for all algorithms in both resolutions as listed in Table 5.7 except for SCFT CPCA. However, the total-average varies for each algorithm. With the two resolutions, the best total-average was achieved by the Blue PCA algorithm followed by the Green PCA algorithm.

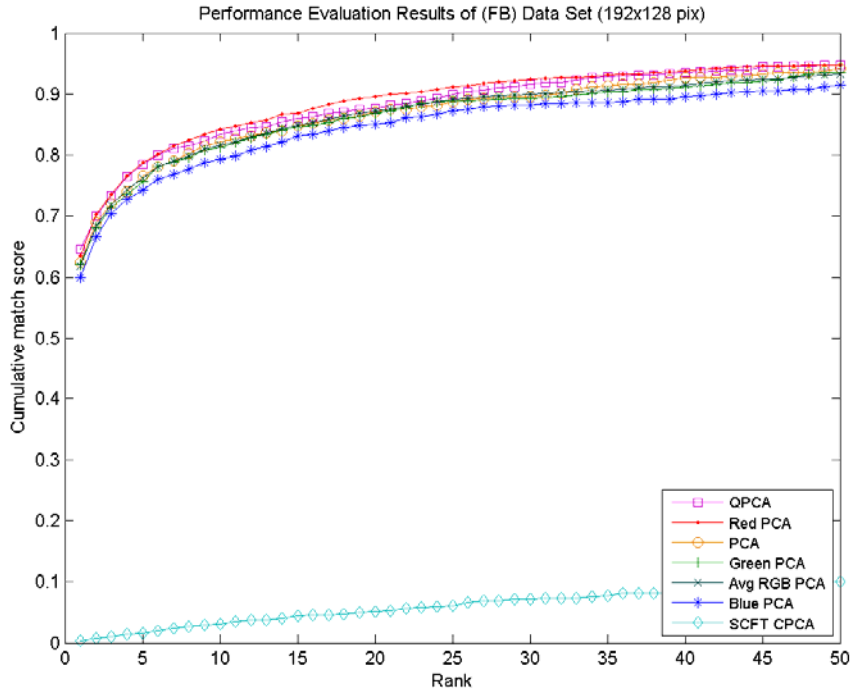


Figure 5.5: Identification performance using the FB with 192×128 pixels resolution.

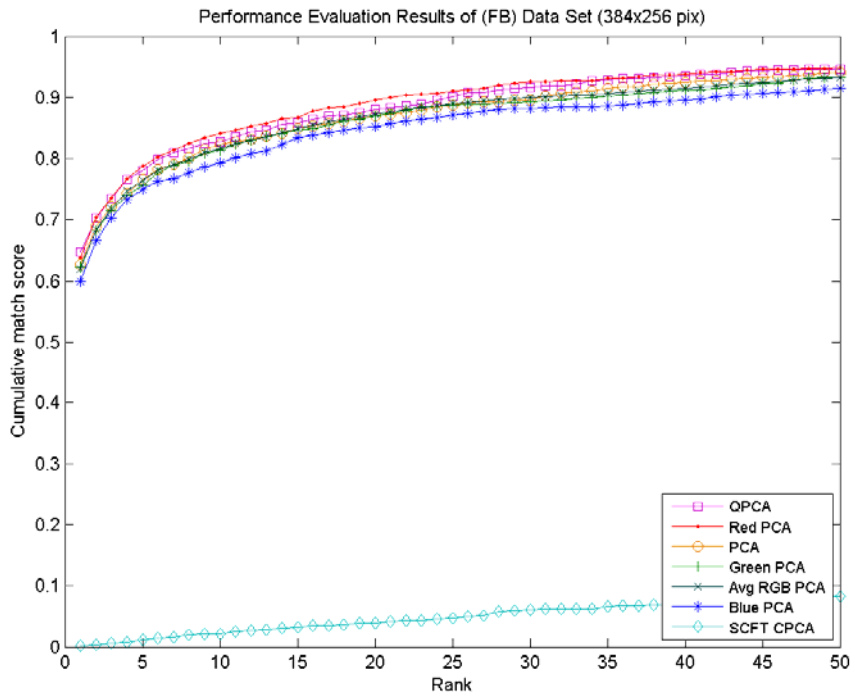


Figure 5.6: Identification performance using the FB with 384×256 pixels resolution.

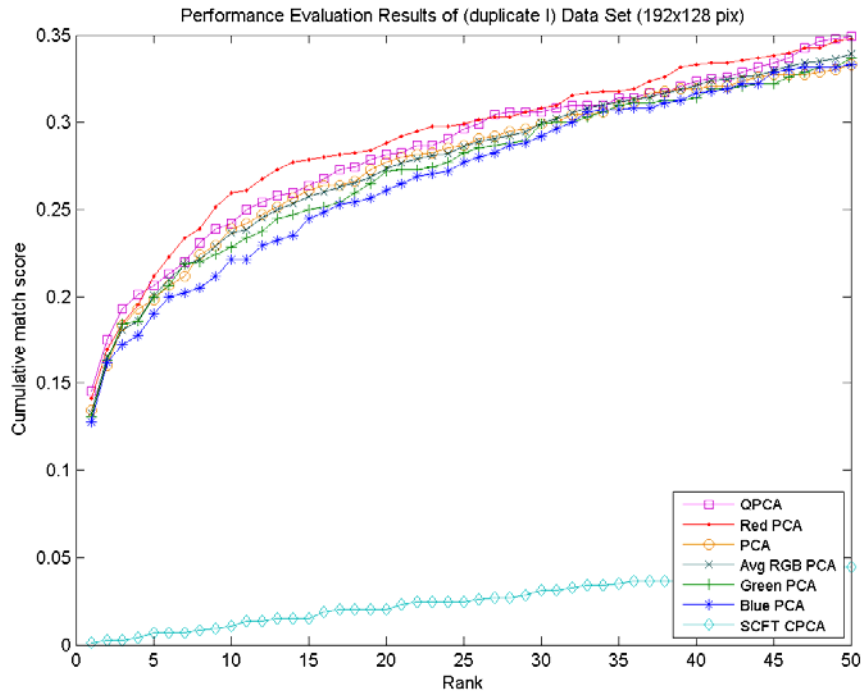


Figure 5.7: Identification performance using the duplicate I with 192×128 pixels resolution.

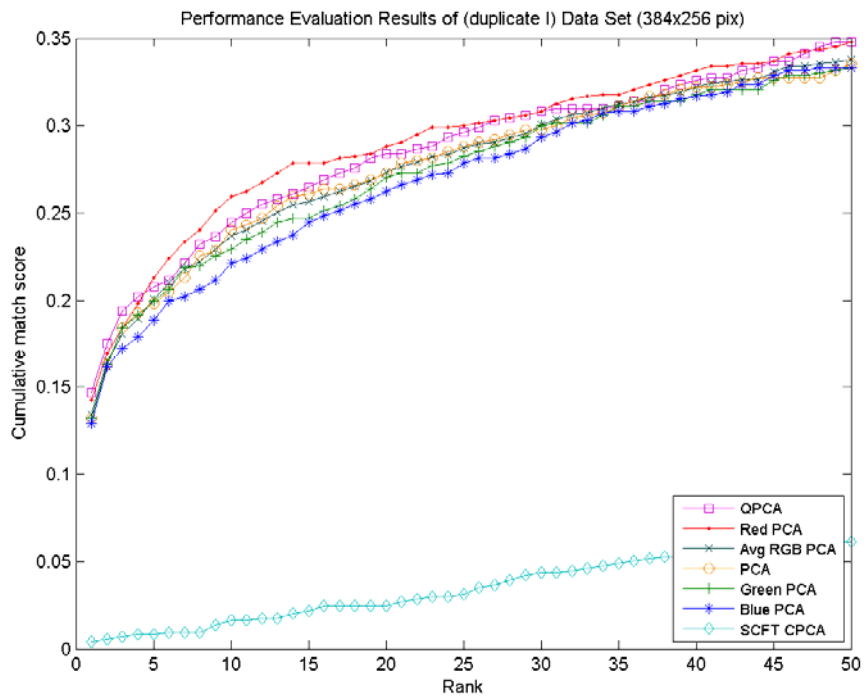


Figure 5.8: Identification performance using the duplicate I with 384×256 pixels resolution.

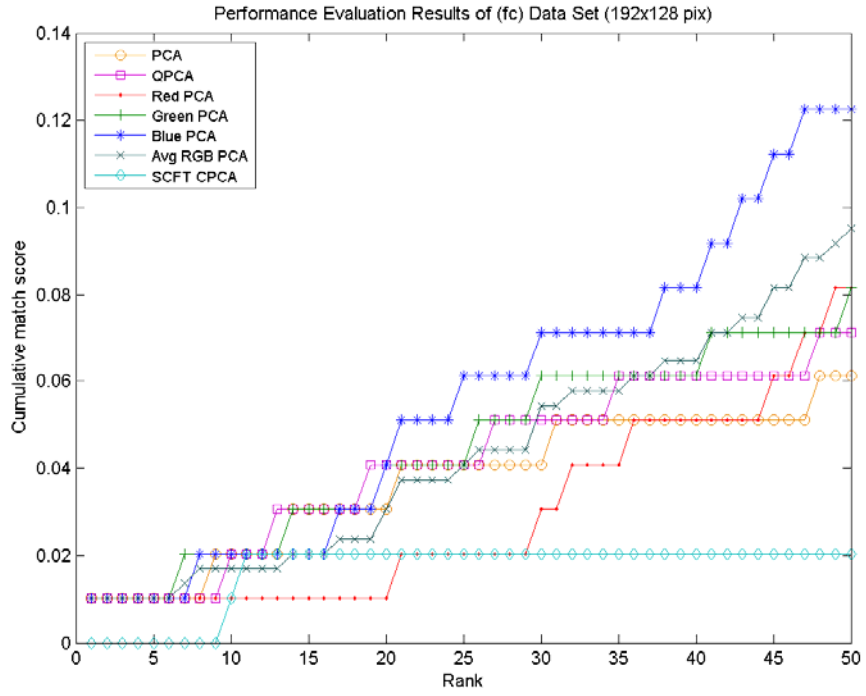


Figure 5.9: Identification performance using the fc with 192×128 pixels resolution.

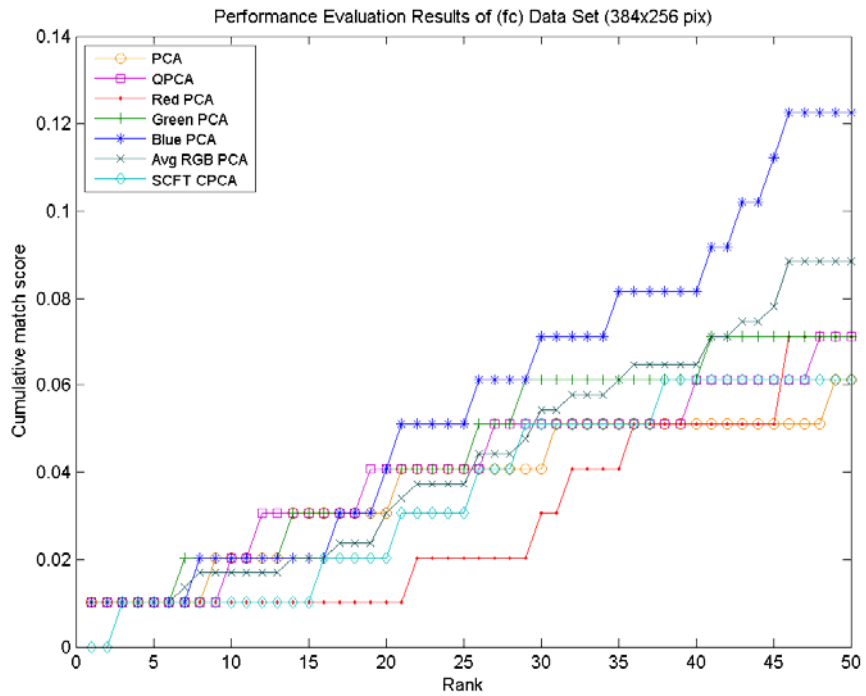


Figure 5.10: Identification performance using the fc with 384×256 pixels resolution.

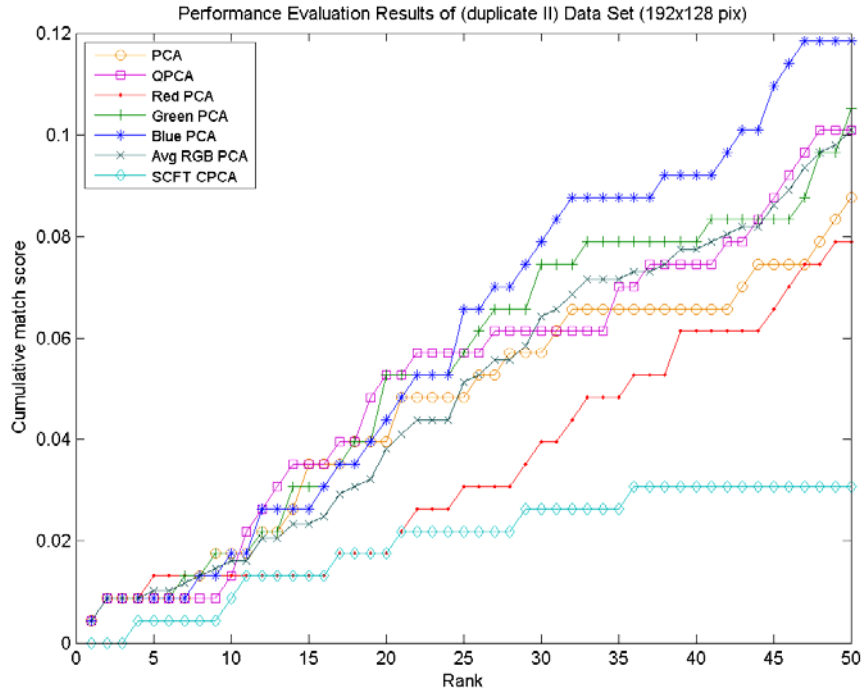


Figure 5.11: Identification performance using the duplicate II with 192×128 pixels resolution.

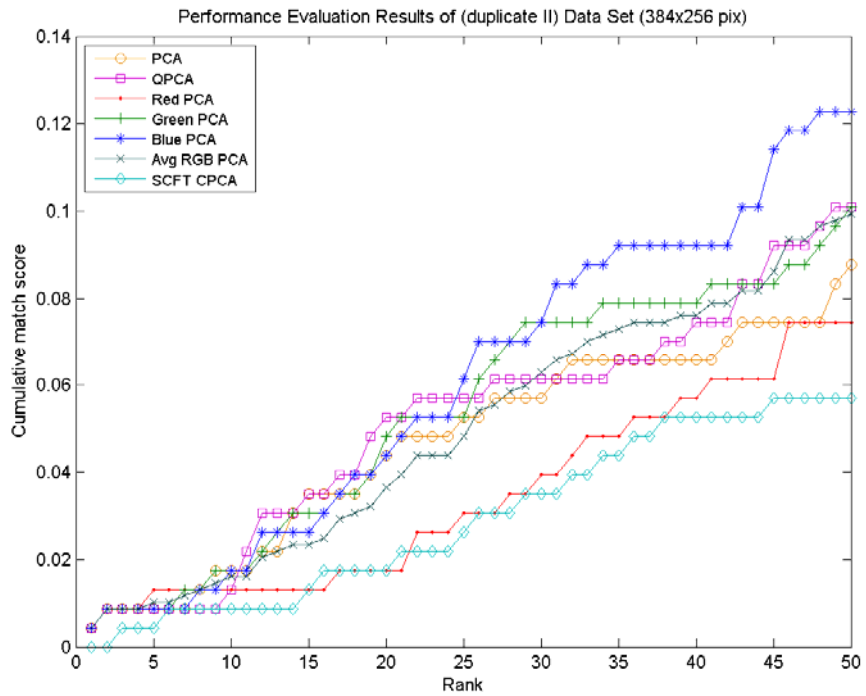


Figure 5.12: Identification performance using the duplicate II with 384×256 pixels resolution.

5.3.5. Performance Comparison Using CMC in Different Resolutions

The effect of image resolution on performance is investigated and reported in this experiment by comparing the CMC curves of each algorithm using the same probe categories in different resolution. Table 5.9 shows, for each PCA-based algorithm, the average score of the total match scores of the full rank applied to the four probe categories using two resolutions. It should be noted that the bolded numbers in the table represent the affected performance, either positively or negatively, by increasing the resolution.

Algorithm	Gallery Size / Scored Probes							
	993/993		993/736		993/98		993/228	
	FB		duplicate I		fc		duplicate II	
	192×128	384×256	192×128	384×256	192×128	384×256	192×128	384×256
PCA	0.987	0.987	0.612	0.613	0.086	0.085	0.193	0.194
QPCA	0.988	0.988	0.609	0.610	0.089	0.089	0.191	0.191
Red PCA	0.989	0.989	0.624	0.624	0.074	0.074	0.187	0.187
Green PCA	0.986	0.986	0.606	0.606	0.090	0.090	0.189	0.189
Blue PCA	0.981	0.981	0.588	0.589	0.112	0.112	0.186	0.187
Avg RGB PCA	0.985	0.985	0.606	0.606	0.092	0.092	0.187	0.188
SCFT CPCA	0.550	0.522	0.350	0.377	0.034	0.052	0.093	0.121

Table 5.9: Average score of the full rank for each PCA-based algorithm in two resolutions.

The comparison graphs for each algorithm are illustrated to represent the identification performance curves using each probe category in two resolutions. The illustrated graphs represent the full CMC with rank from 1 to the full rank size which is equals to full size of the probe set.

5.3.5.1. CMC for the Gray-PCA algorithm

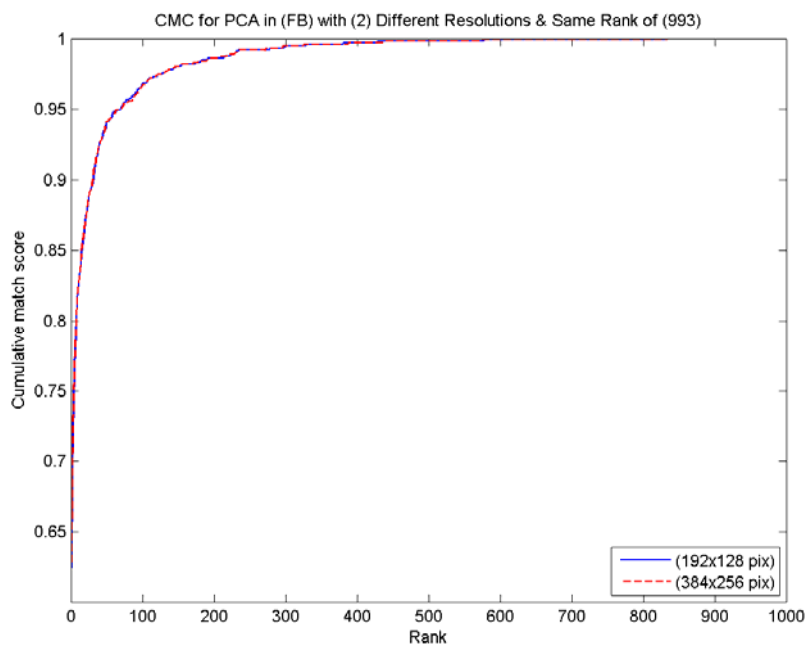


Figure 5.13: The CMC curves for PCA using the FB probes.

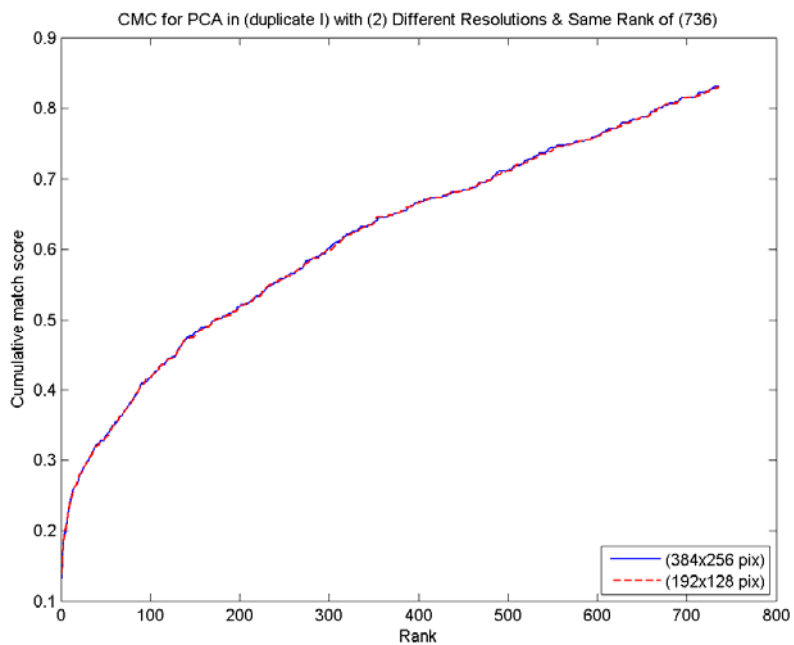


Figure 5.14: The CMC curve for PCA using the duplicate I probes.

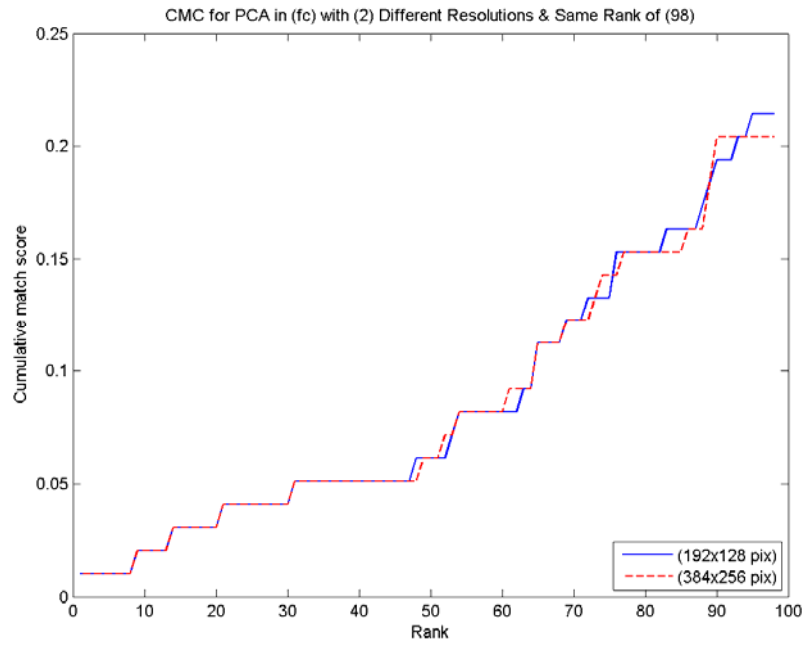


Figure 5.15: The CMC curves for PCA using the fc probes.

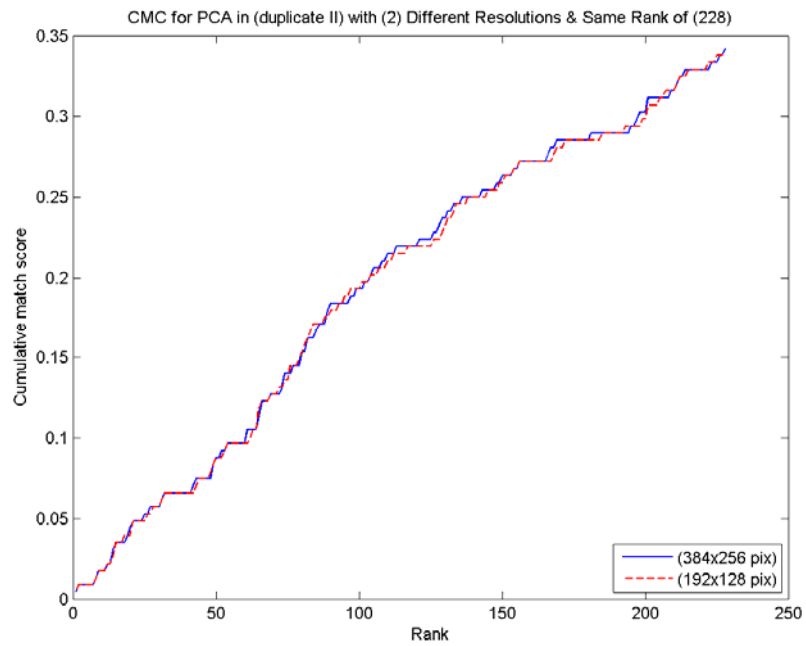


Figure 5.16: The CMC curves for PCA using the duplicate II probes.

5.3.5.2. CMC for the QPCA algorithm

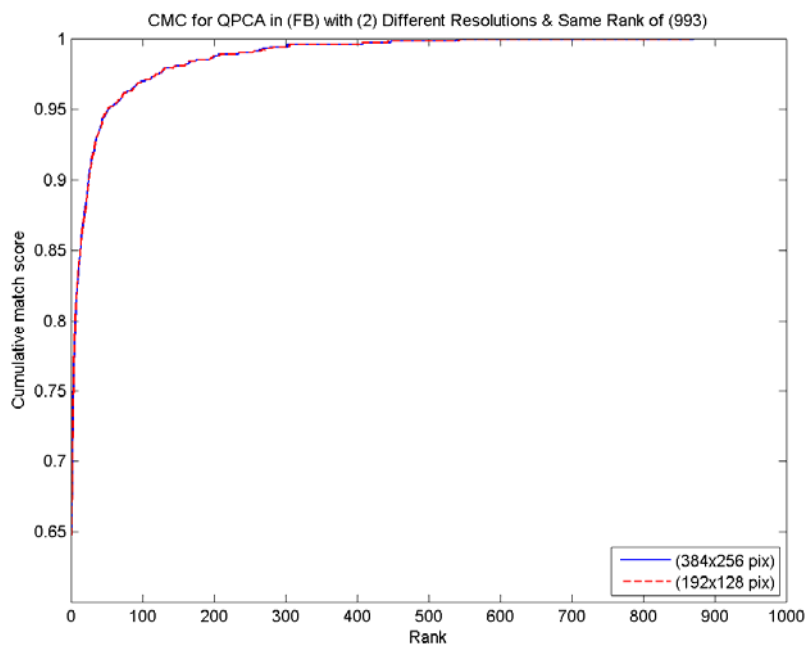


Figure 5.17: The CMC curves for QPCA using the FB probes.

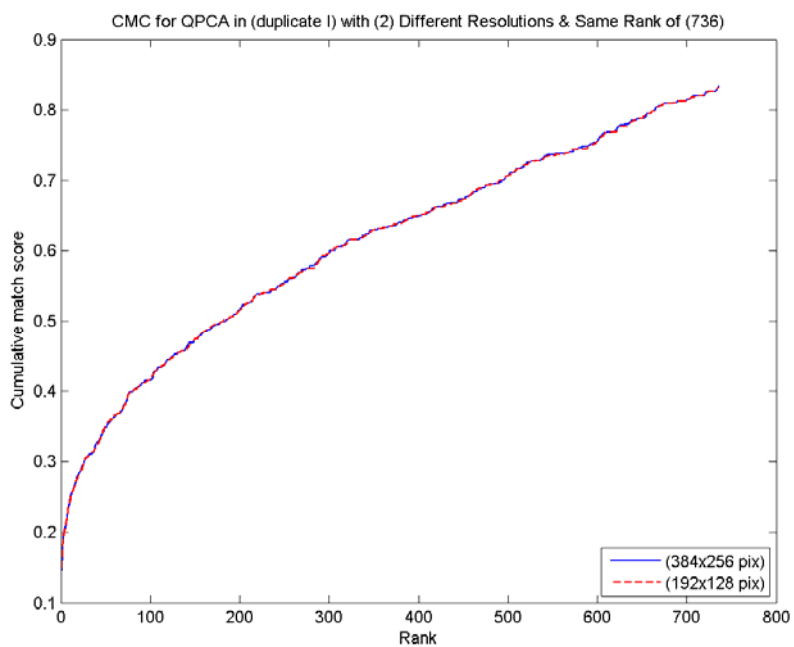


Figure 5.18: The CMC curves for QPCA using the duplicate I probes.

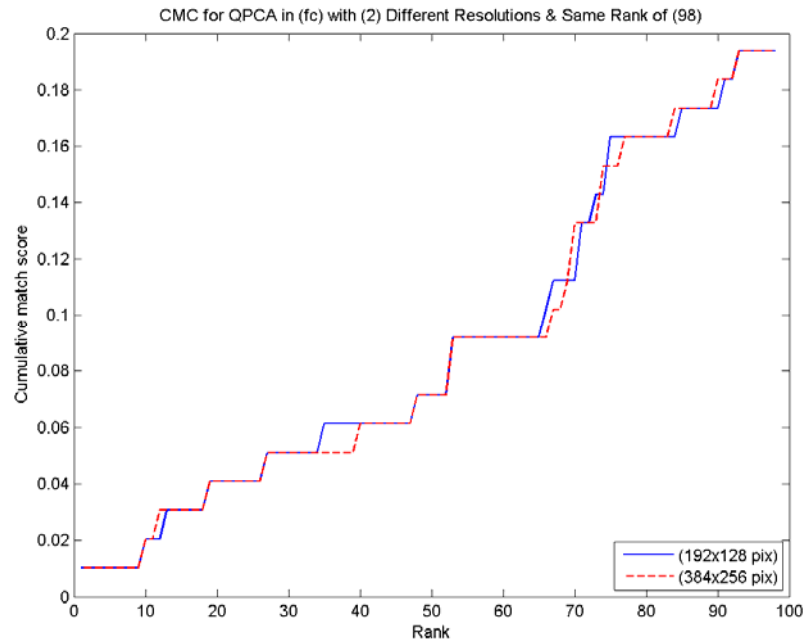


Figure 5.19: The CMC curves for QPCA using the fc probes.

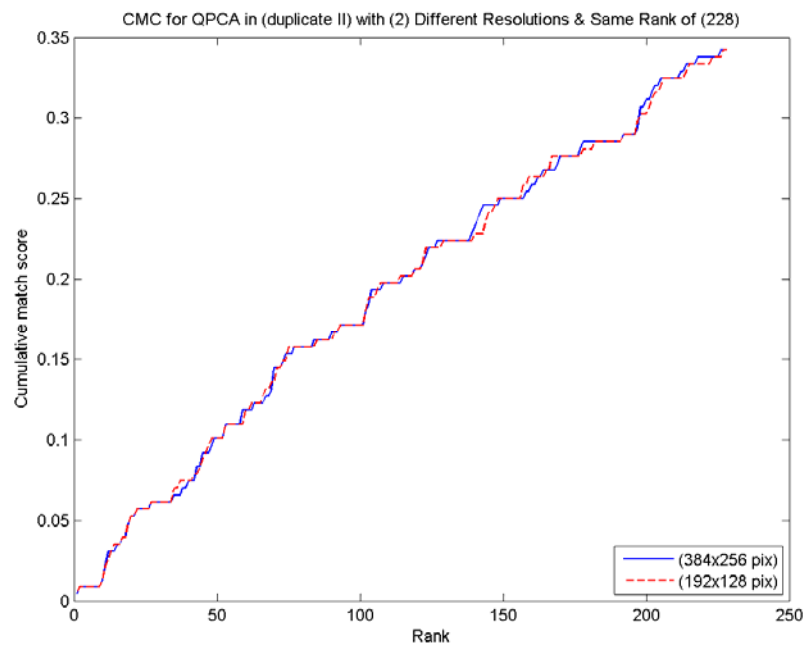


Figure 5.20: The CMC curves for QPCA using the duplicate II probes.

5.3.5.3. CMC for the Red-PCA algorithm

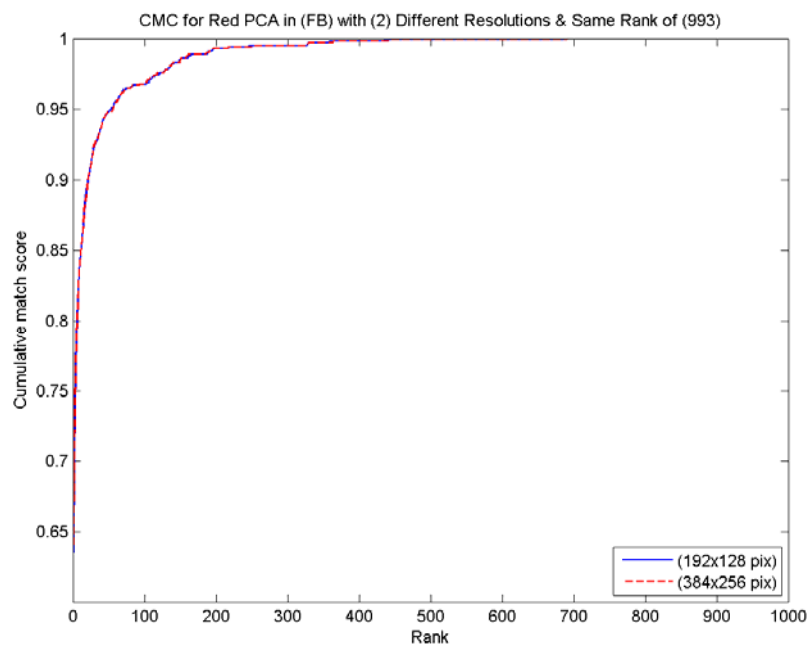


Figure 5.21: The CMC curves for Red-PCA using the FB probes.

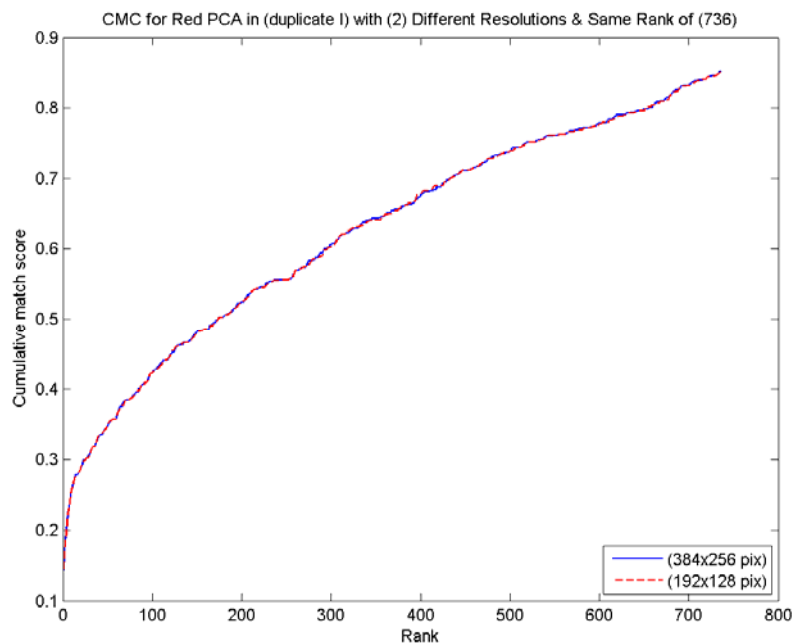


Figure 5.22: The CMC curves for Red-PCA using the duplicate I probes.

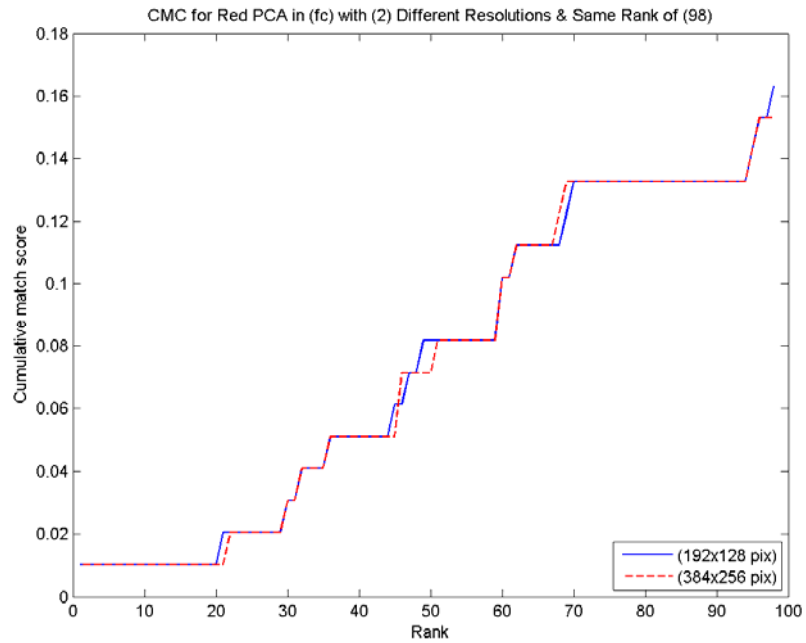


Figure 5.23: The CMC curves for Red-PCA using the fc probes.

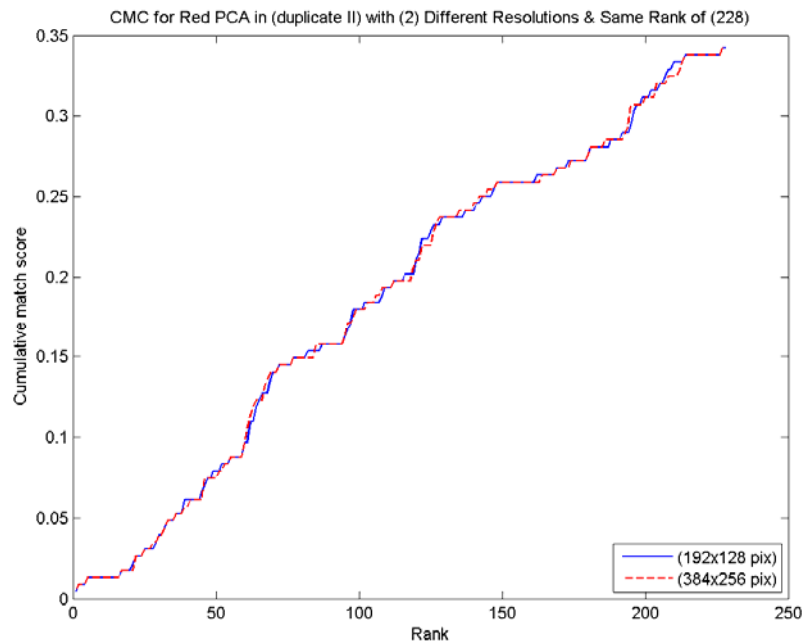


Figure 5.24: The CMC curves for Red-PCA using the duplicate II probes.

5.3.5.4. CMC for the Green-PCA algorithm

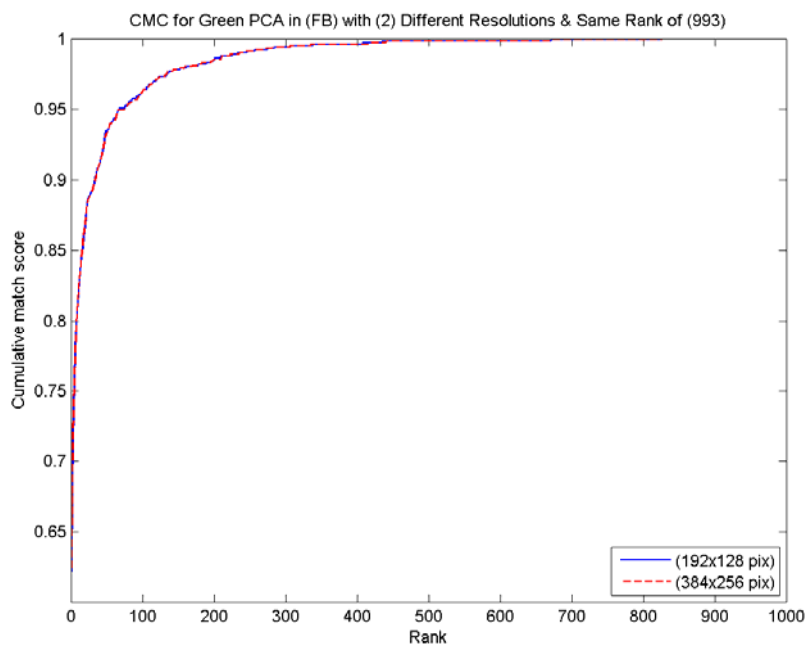


Figure 5.25: The CMC curves for Green-PCA using the FB probes.

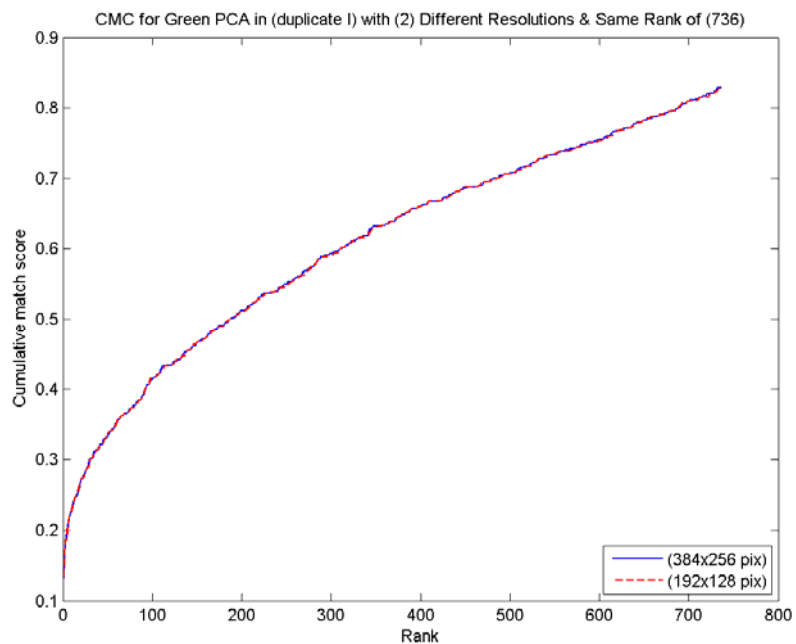


Figure 5.26: The CMC curves for Green-PCA using the duplicate I probes.

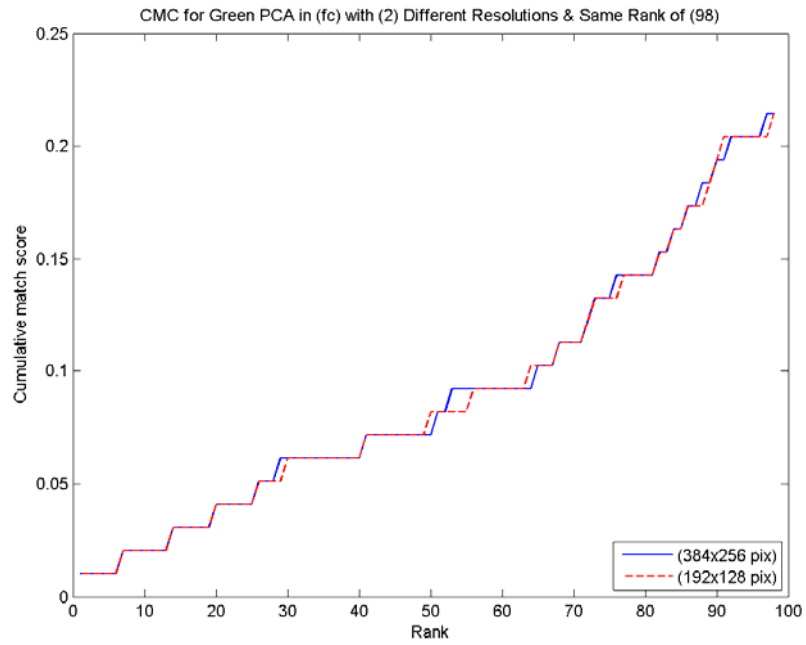


Figure 5.27: The CMC curves for Green-PCA using the fc probes.

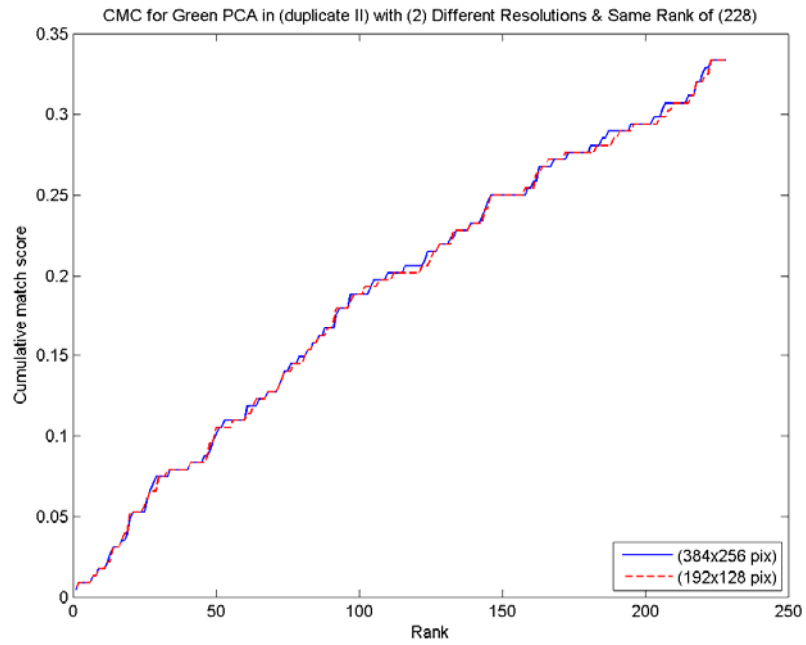


Figure 5.28: The CMC curves for Green-PCA using the duplicate II probes.

5.3.5.5. CMC for the Blue-PCA algorithm

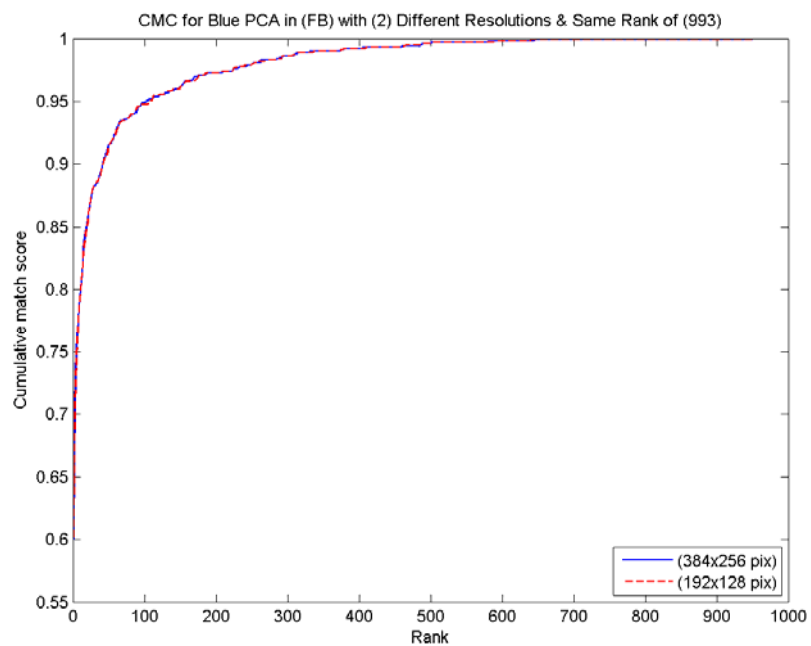


Figure 5.29: The CMC curves for Blue-PCA using the FB probes.

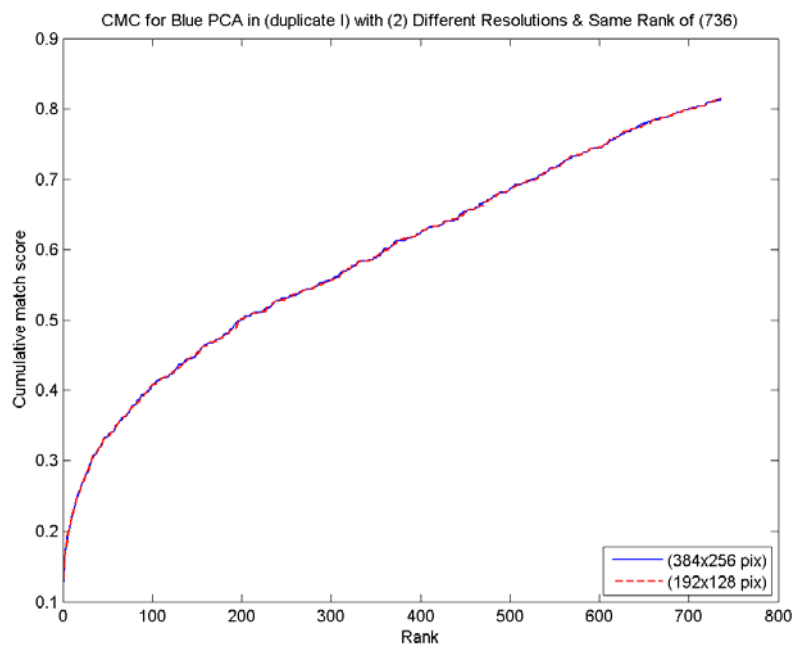


Figure 5.30: The CMC curves for Blue-PCA using the duplicate I probes.

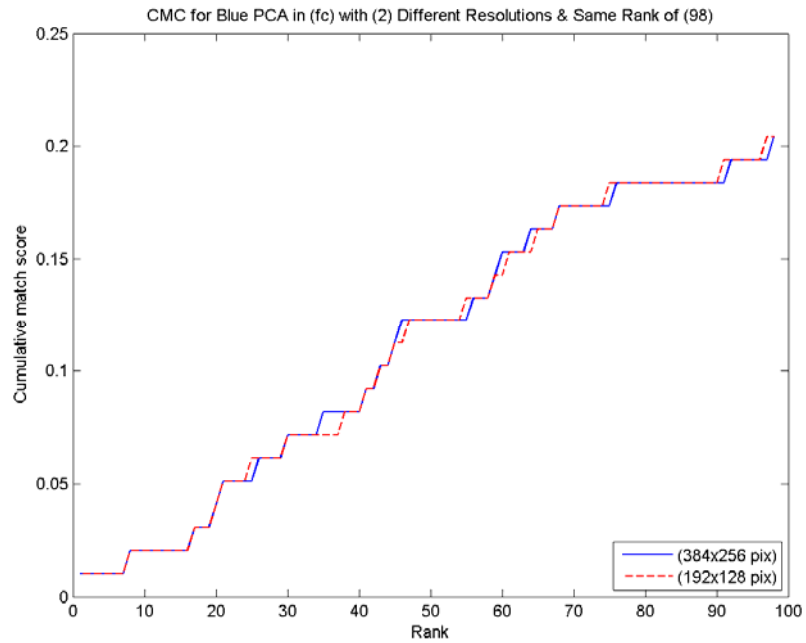


Figure 5.31: The CMC curves for Blue-PCA using the fc probes.

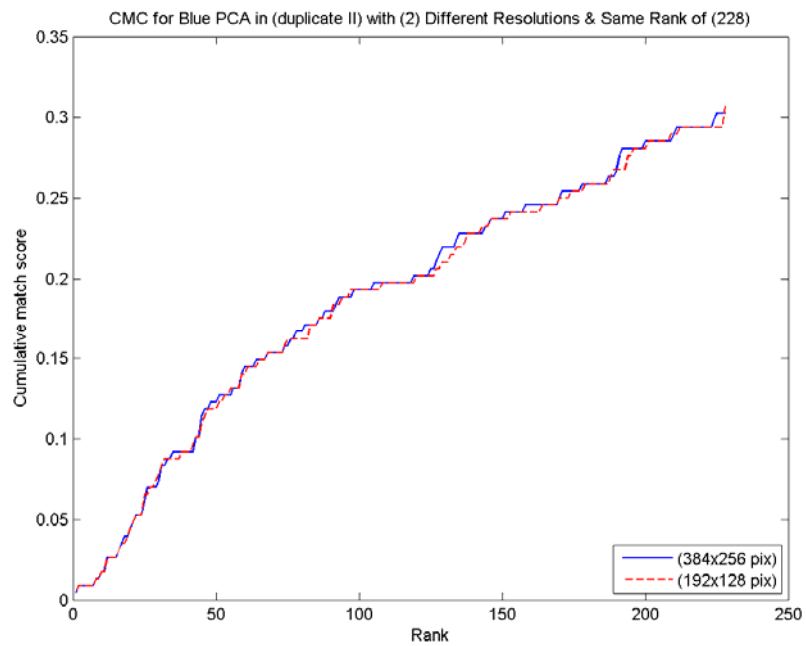


Figure 5.32: The CMC curves for Blue-PCA using the duplicate II probes.

5.3.5.6. CMC for the Avg RGB-PCA algorithm

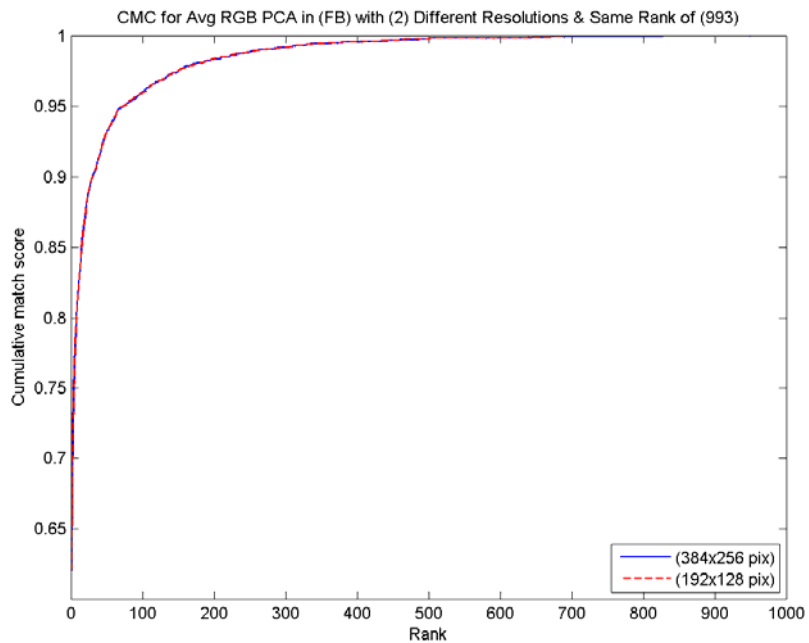


Figure 5.33: The CMC curves for Avg RGB-PCA using the FB probes.

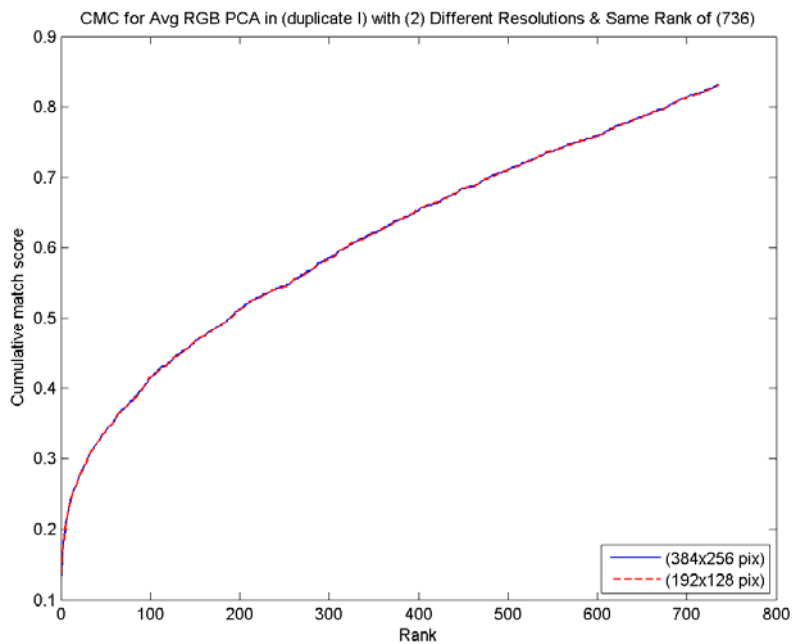


Figure 5.34: The CMC curves for Avg RGB-PCA using the duplicate I probes.

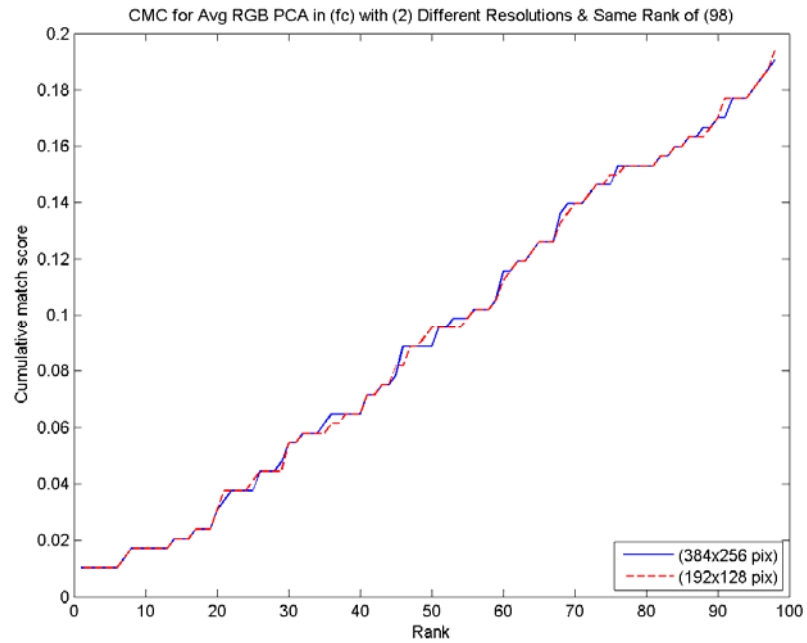


Figure 5.35: The CMC curves for Avg RGB-PCA using the fc probes.

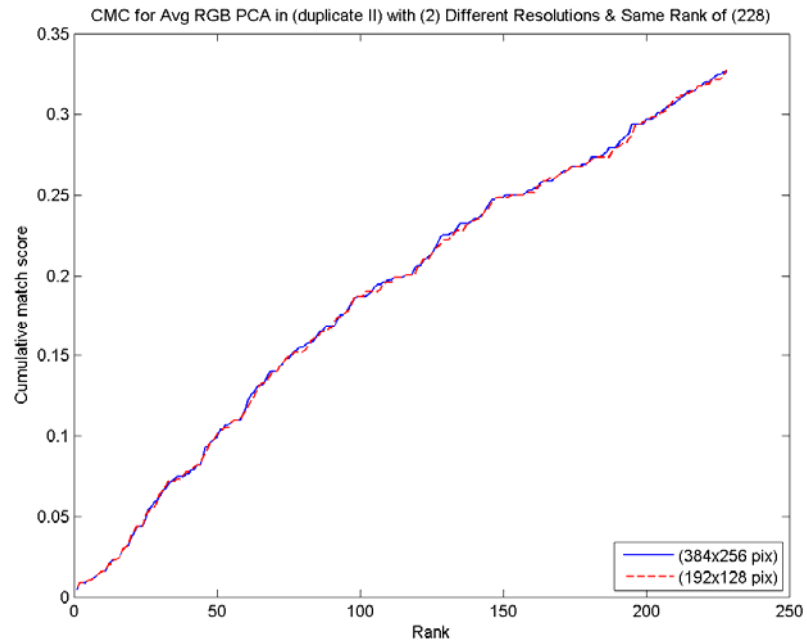


Figure 5.36: The CMC curves for Avg RGB-PCA using the duplicate II probes.

5.3.5.7. CMC for the SCFT-CPCA algorithm

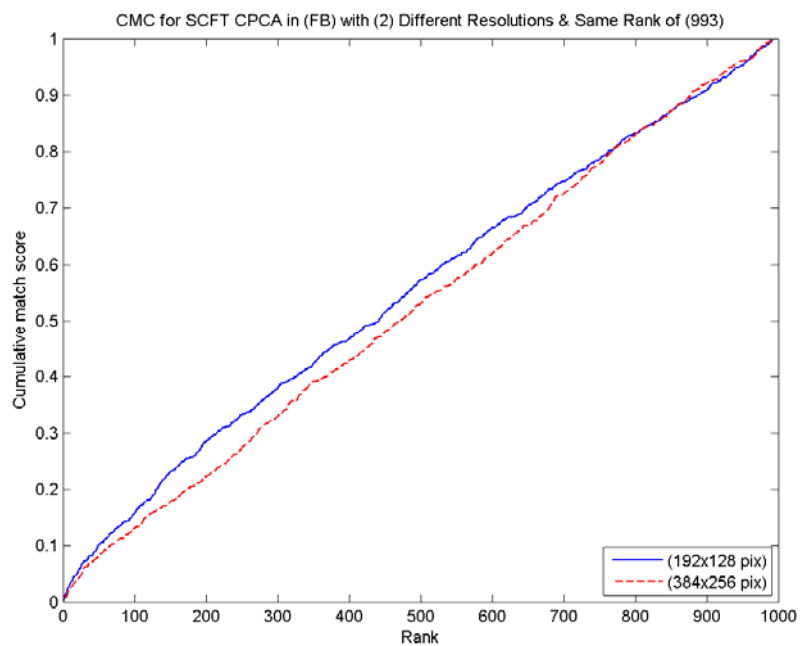


Figure 5.37: The CMC curves for SCFT-CPCA using the FB probes.

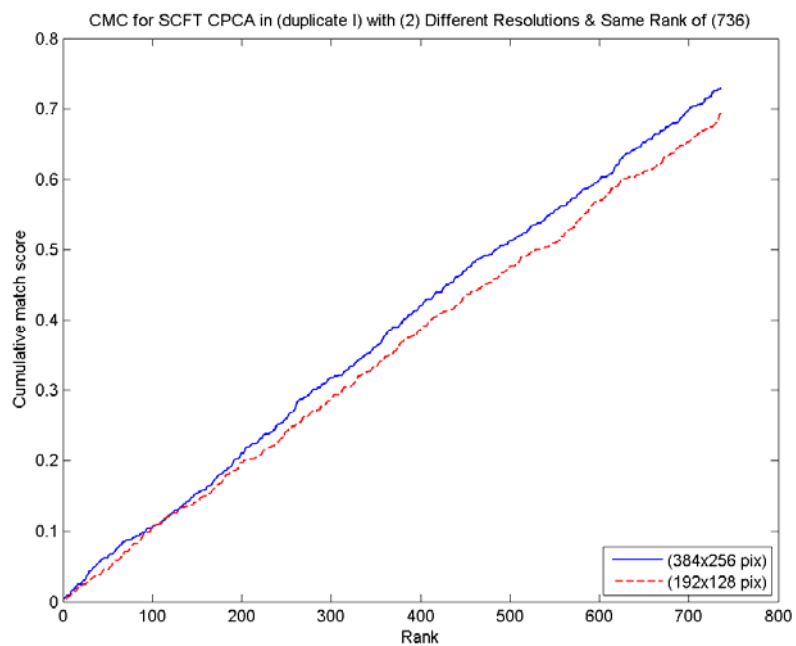


Figure 5.38: The CMC curves for SCFT-CPCA using the duplicate I probes.

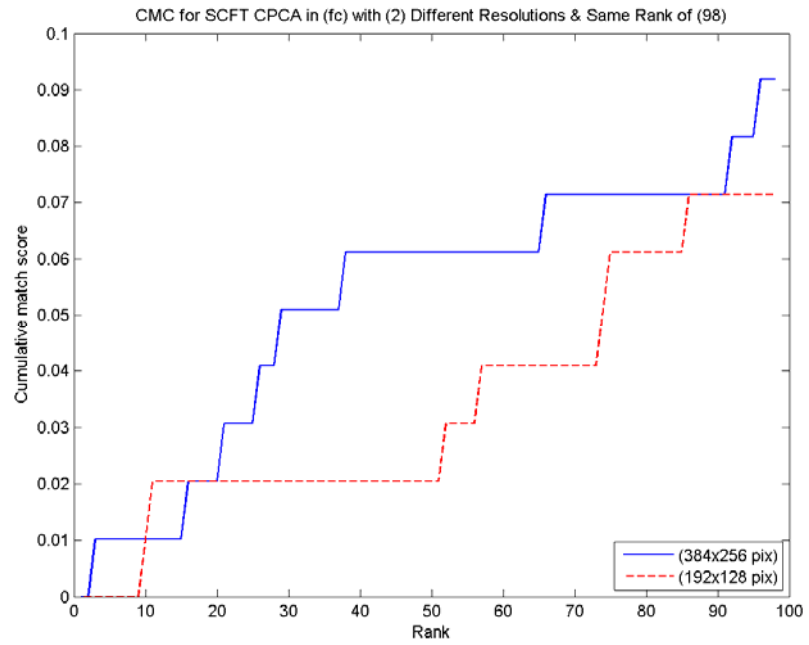


Figure 5.39: The CMC curves for SCFT-CPCA using the fc probes.

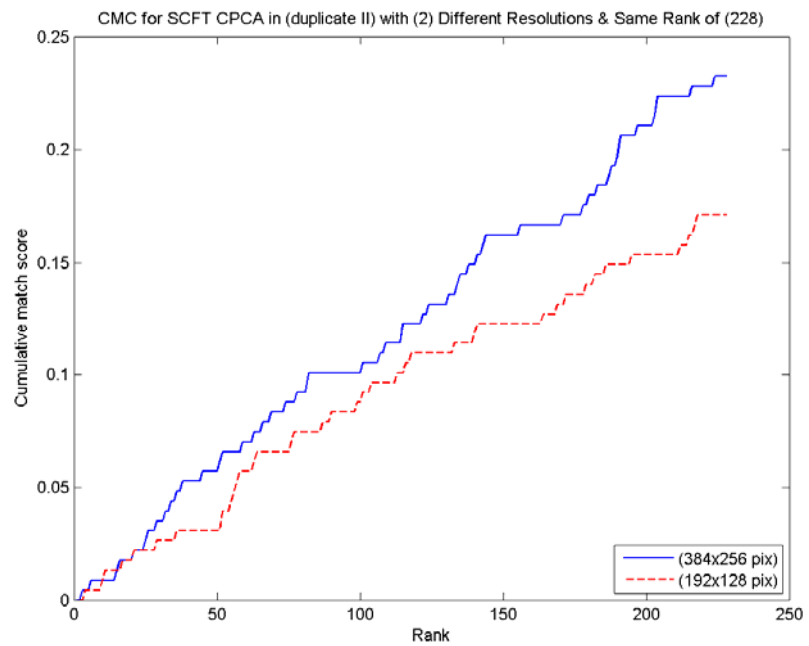


Figure 5.40: The CMC curves for SCFT-CPCA using the duplicate II probes.

5.3.6. Variation in Identification Performance

Another performance evaluation approach aims to investigate the identification performance using different galleries that contain different face images from the other galleries. While a face-recognition algorithm estimates the identity of a face, a possible question “how does the algorithm performance change using a different gallery and probe set?” Tables Table 5.10 - Table 5.12 show the change in algorithm performance if the galleries content is changed. In this experiment, a second standard dataset is constructed and used. This dataset consists of five galleries of approximately 200 individuals, where an individual is only in one gallery. Tables Table 5.10 - 5.13, summarize the results where the algorithms are ordered by top rank score and average of rank scores, respectively. For example, as indicated in Table 5.10, the QPCA algorithm scored highest on gallery of (Set 2). While Table 5.10 -Table 5.11 report results for the FB probes whereas Table 5.12 - Table 5.13 report results for the duplicate I probes. The last column in these tables represents the overall rank or order of each algorithm which indicates the general performance indicator.

Algorithm	Algorithm Ranking by Top Match					Overall rank
	Gallery Size / Scored Probes					
	200/200	200/200	200/200	200/200	193/193	
Set 1	Set 2	Set 3	Set 4	Set 5		
PCA	1	4	3	3	3	2
QPCA	1	1	2	1	1	1
Red PCA	6	3	1	2	2	2
Green PCA	5	2	5	5	2	3
Blue PCA	3	4	6	6	5	4
Avg RGB PCA	4	3	4	4	4	3
SCFT CPCA	2	5	7	7	6	5
Avg Score	0.3707	0.5843	0.4988	0.5745	0.4996	

Table 5.10: Variation in identification performance using five different galleries from the FB probes (top match).

Algorithm Ranking by Average of rank of 50 scores						
Gallery Size / Scored Probes						
Algorithm	200/200 Set 1	200/200 Set 2	200/200 Set 3	200/200 Set 4	193/193 Set 5	Overall rank
PCA	2	4	4	3	3	3
QPCA	1	3	3	2	2	1
Red PCA	7	2	1	1	1	2
Green PCA	5	6	6	5	5	6
Blue PCA	4	7	7	6	6	7
Avg RGB PCA	6	5	5	4	4	5
SCFT CPCA	3	1	2	7	7	4
Avg Score	0.6553	0.8434	0.8739	0.8751	0.8841	

Table 5.11: Variation in identification performance using five different galleries from the FB probes (average of rank scores).

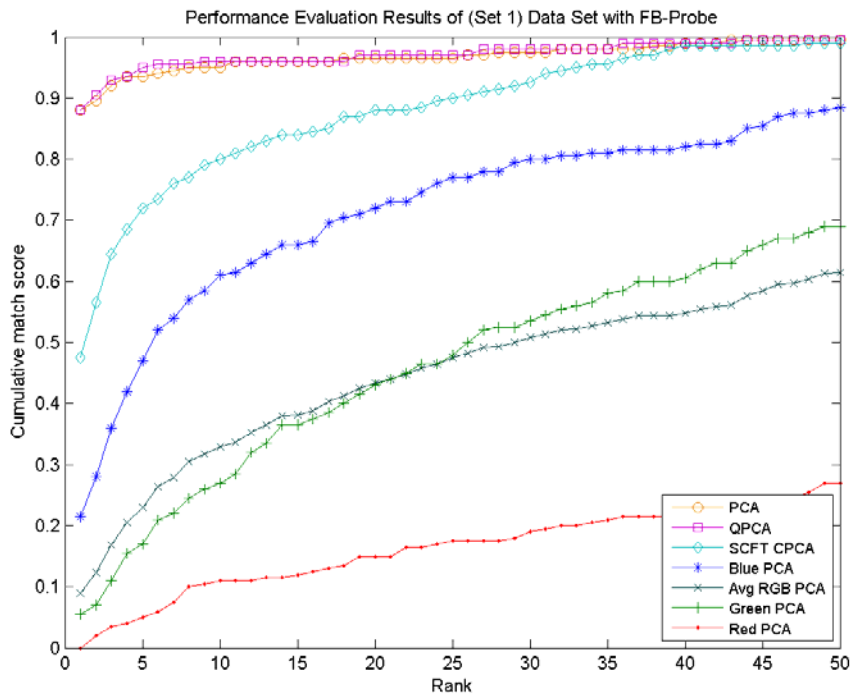


Figure 5.41: Identification performance using the FB probes of (Set 1) and rank of 50

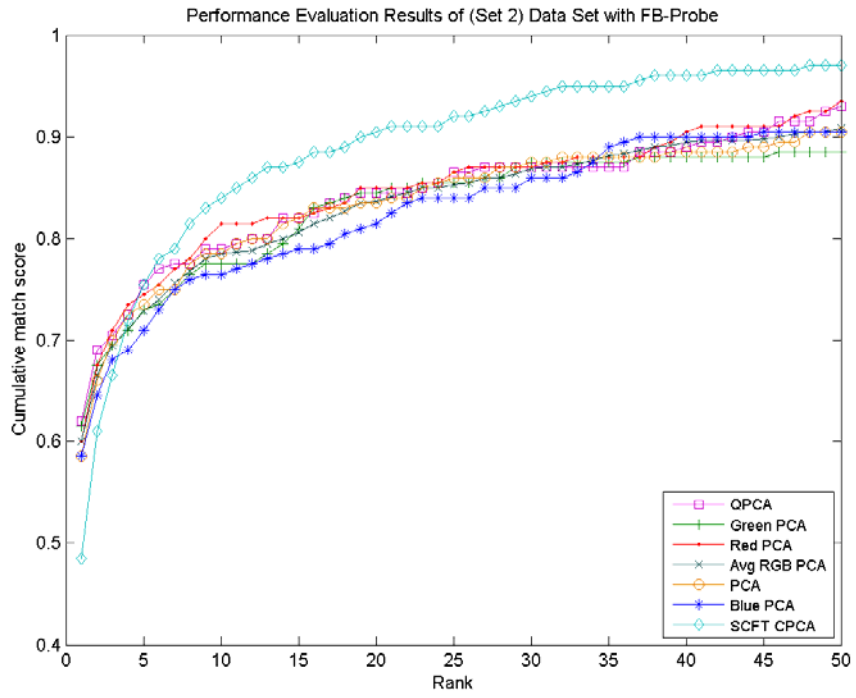


Figure 5.42: Identification performance using the FB probes of (Set 2) and rank of 50

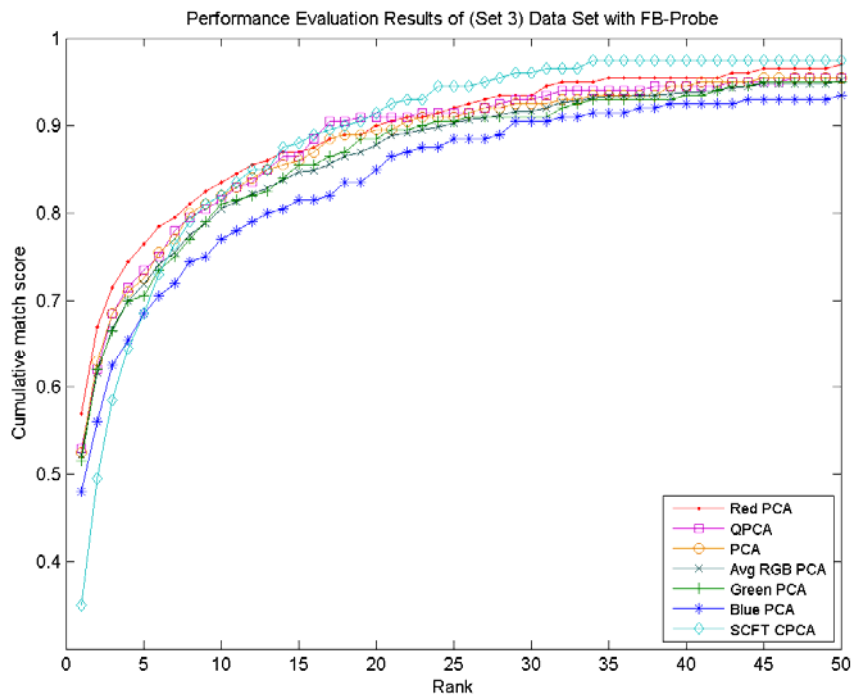


Figure 5.43: Identification performance using the FB probes of (Set 3) and rank of 50

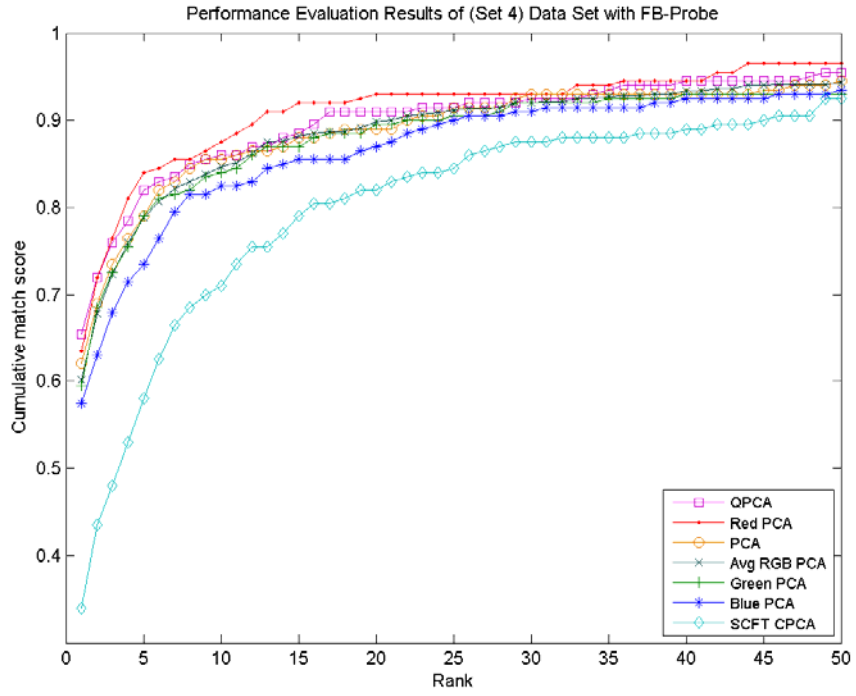


Figure 5.44: Identification performance using the FB probes of (Set 4) and rank of 50

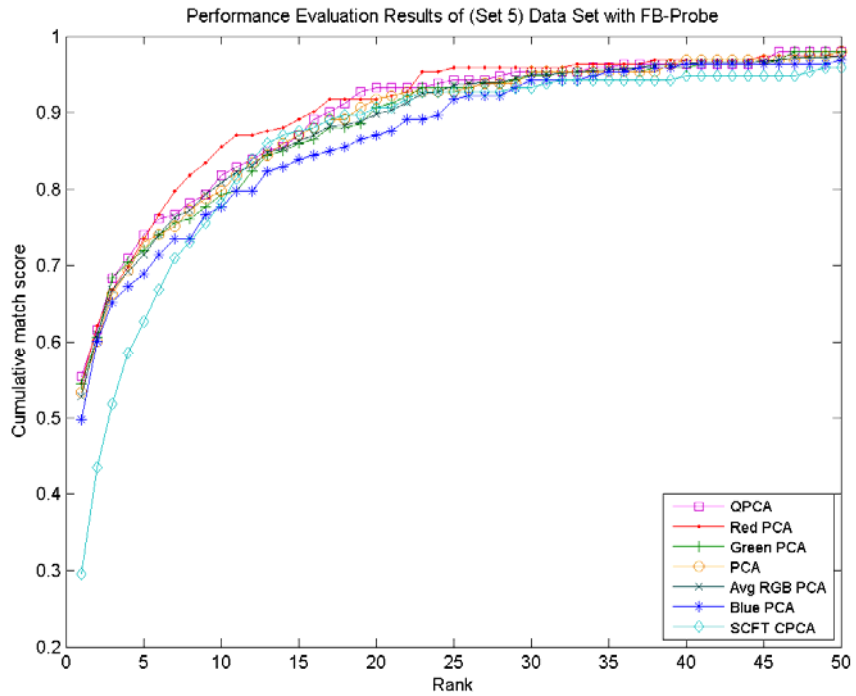


Figure 5.45: Identification performance using the FB probes of (Set 5) and rank of 50

Algorithm Ranking by Top Match						
Gallery Size / Scored Probes						
	200/200	200/200	200/200	200/200	193/193	Overall rank
Algorithm	Set 1	Set 2	Set 3	Set 4	Set 5	
PCA	2	3	2	3	3	2
QPCA	4	3	2	1	3	2
Red PCA	5	1	1	4	1	1
Green PCA	1	4	4	1	3	2
Blue PCA	6	4	4	3	3	3
Avg RGB PCA	3	2	3	2	2	1
SCFT CPCA	7	5	5	5	4	4
Avg Score	0.0269	0.2320	0.2829	0.0535	0.2283	

Table 5.12: Variation in identification performance using five different galleries from the duplicate I probes (top match).

Algorithm Ranking by Average of rank of 50 scores						
Gallery Size / Scored Probes						
	200/200	200/200	200/200	200/200	193/193	Overall rank
Algorithm	Set 1	Set 2	Set 3	Set 4	Set 5	
PCA	1	5	2	2	2	2
QPCA	4	6	1	1	3	3
Red PCA	2	1	3	1	1	1
Green PCA	3	7	5	3	4	5
Blue PCA	6	4	6	5	6	6
Avg RGB PCA	5	3	4	4	5	4
SCFT CPCA	7	2	7	6	7	7
Avg Score	0.1782	0.5068	0.5907	0.2620	0.7791	

Table 5.13: Variation in identification performance using five different galleries from the duplicate I probes (average of rank scores).

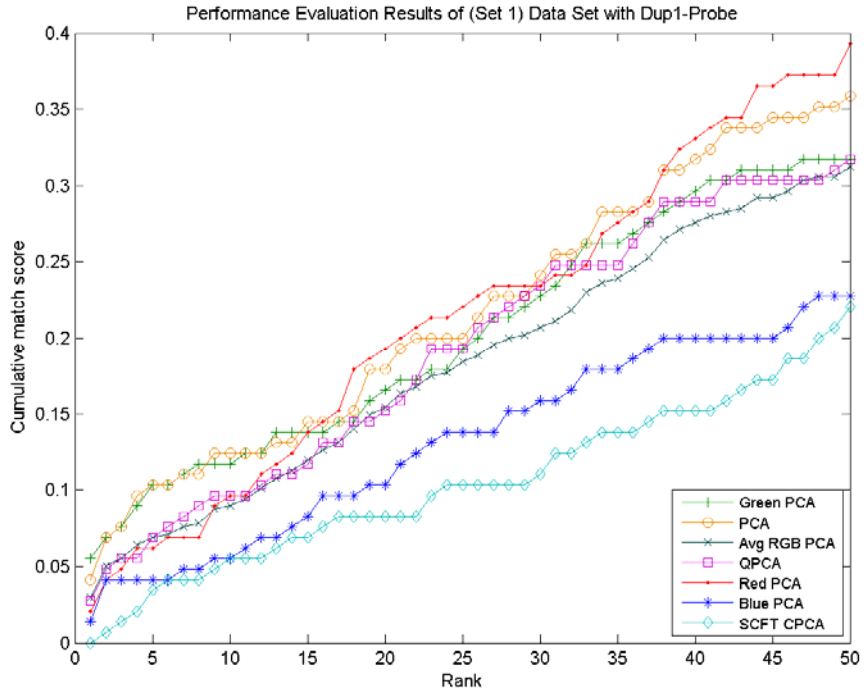


Figure 5.46: Identification performance using the duplicate I probes of (Set 1) and rank of 50

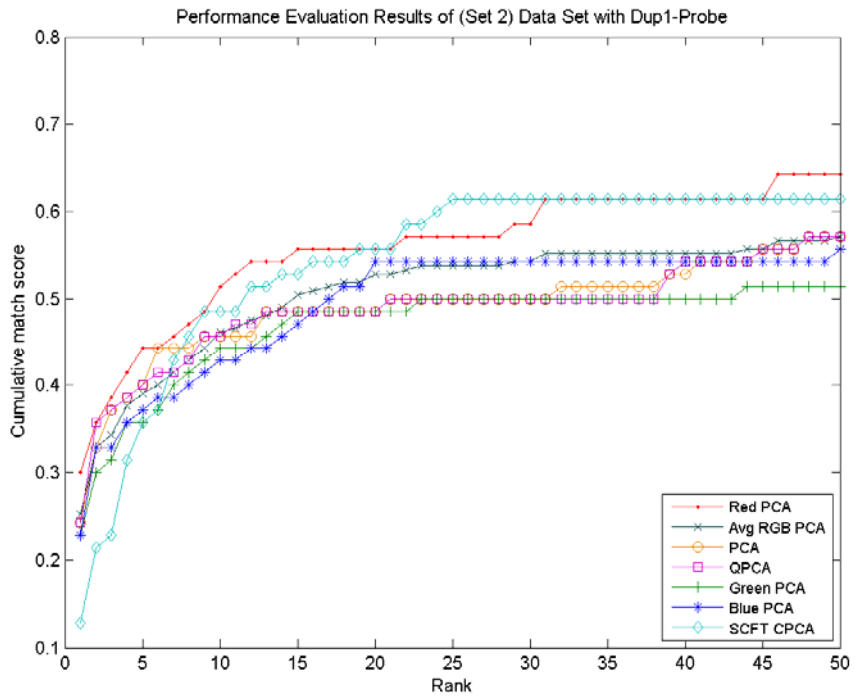


Figure 5.47: Identification performance using the duplicate I probes of (Set 2) and rank of 50

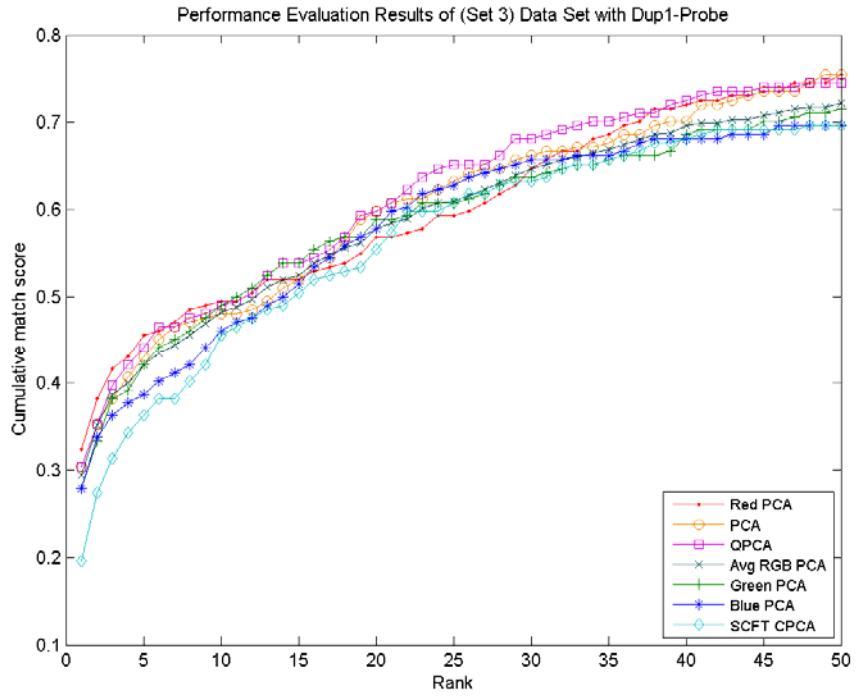


Figure 5.48: Identification performance using the duplicate I probes of (Set 3) and rank of 50

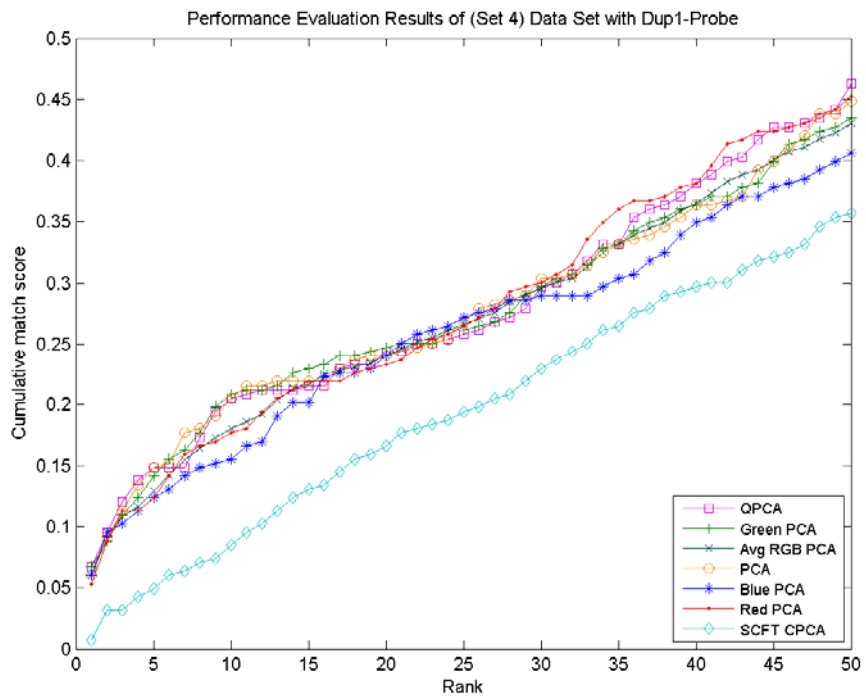


Figure 5.49: Identification performance using the duplicate I probes of (Set 4) and rank of 50

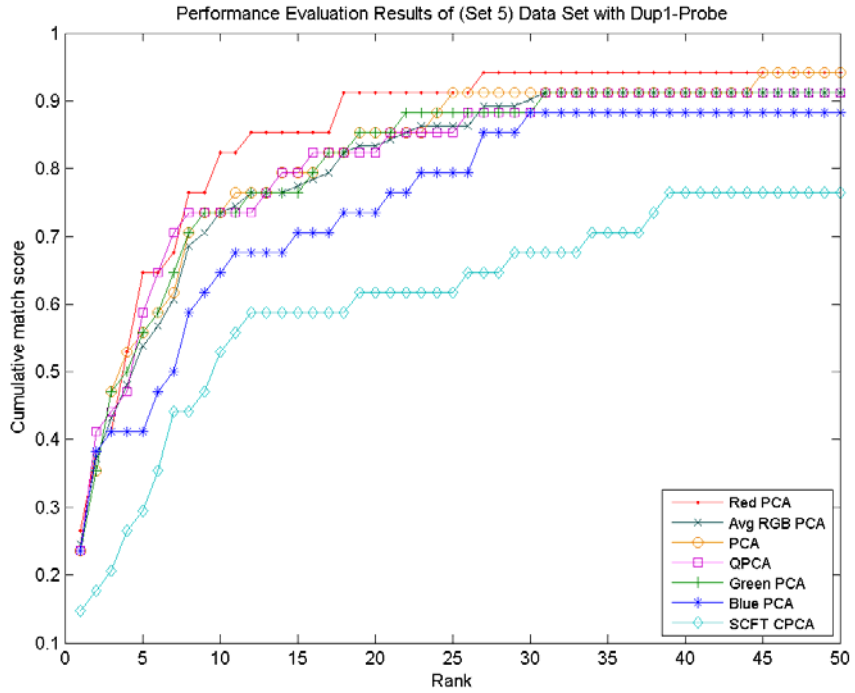


Figure 5.50: Identification performance using the duplicate I probes of (Set 5) and rank of 50

5.3.7. GD versus ID

The decidability indices for the used PCA-based algorithms are calculated and listed in Table 5.14.

<i>Algorithm</i>	<i>Decidability Index (d)</i>
PCA	0.1422
QPCA	0.1470
Red PCA	0.1694
Green PCA	0.1390
Blue PCA	0.1486
Avg RGB PCA	0.1475
SCFT CPCA	0.0251

Table 5.14: Decidability index (d) for each algorithm.

Figure 5.51 shows the genuine and imposter distributions using PCA. Blue and red dashed curves represent genuine and imposter distributions; respectively, vertical lines illustrate

the means of the two distributions, and the region underlie the two curves are overlapping indicates the errors resulting from their intersection. The developed QPCA algorithm yields genuine versus imposter distribution illustrated in Figure 5.52. It can be noted that QPCA achieved better separation between genuine and imposter distributions with less errors. In Figure 5.53, the distributions of using Red PCA are shown. The separation of genuine and imposter is better than that achieved by using QPCA, and in general it has the largest separation (i.e. decidability index). As shown in Figure 5.54, the use of Green PCA yields less separation than PCA, with more errors. The distributions using Blue PCA and Avg PCA are shown in Figure 5.55 and Figure 5.56, respectively. They are almost similar, although that the separation of Blue PCA is slightly better than what is achieved by Avg RGB PCA. In the case of SCFT CPCA, the separation is the worst separation overall algorithms as presented by its distributions in Figure 5.57. Moreover, it can be inferred that the separation is even far less than the closest (second lowest) algorithm of the remaining algorithms. Definitely, this indicates the highest error rate which increased rapidly due to the drastic overlapping between genuine an imposter distributions.

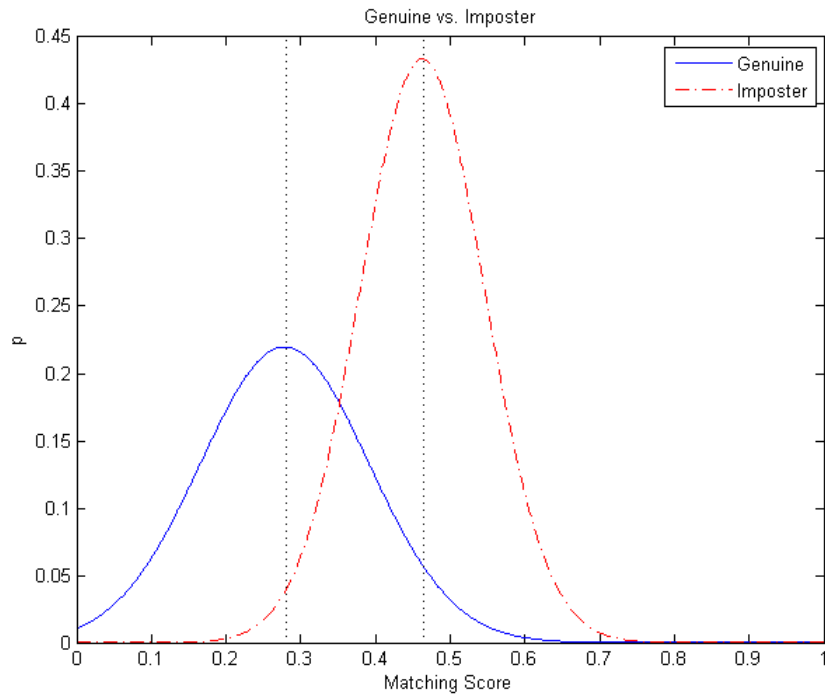


Figure 5.51: GD versus ID for PCA algorithm

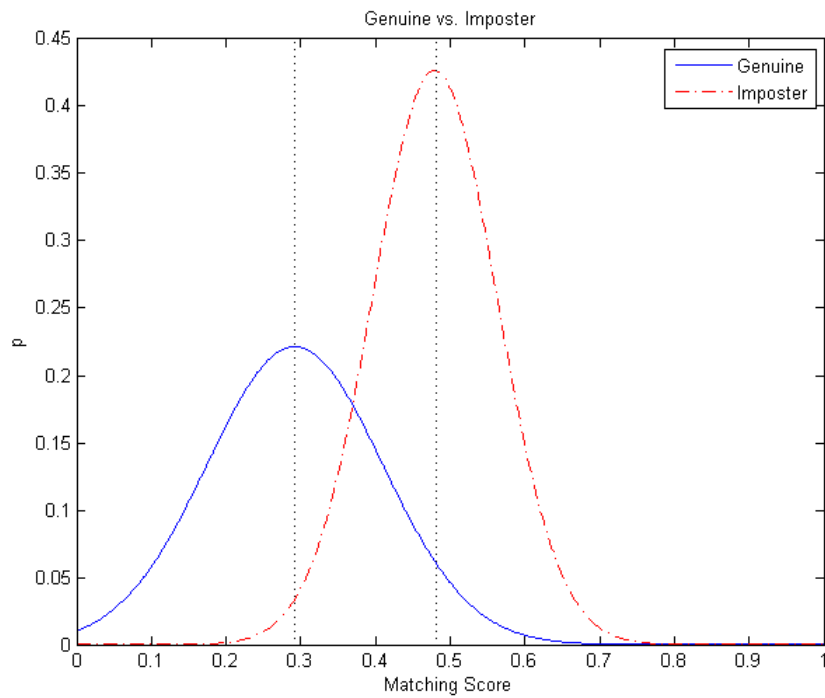


Figure 5.52: GD versus ID for QPCA algorithm

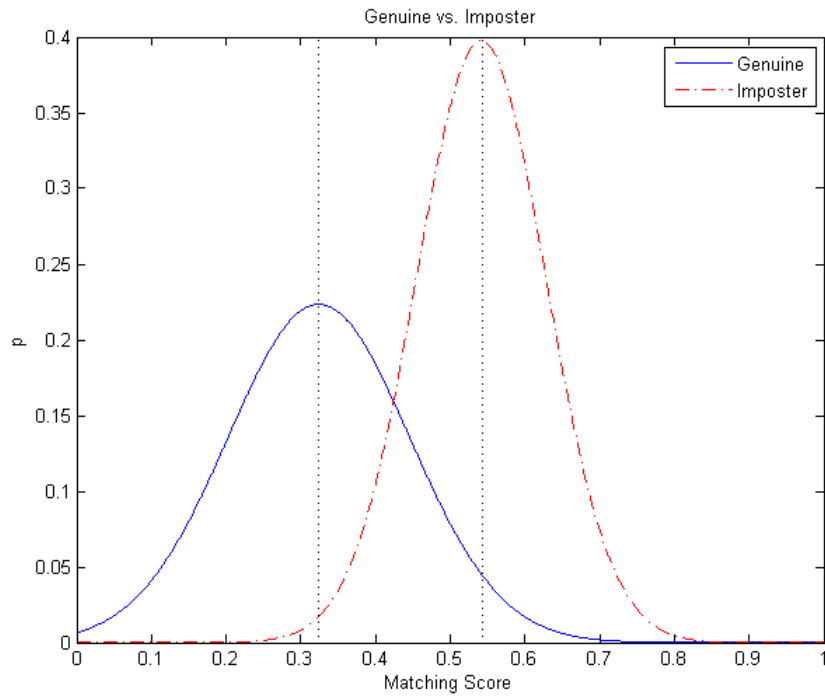


Figure 5.53: GD versus ID for Red PCA algorithm

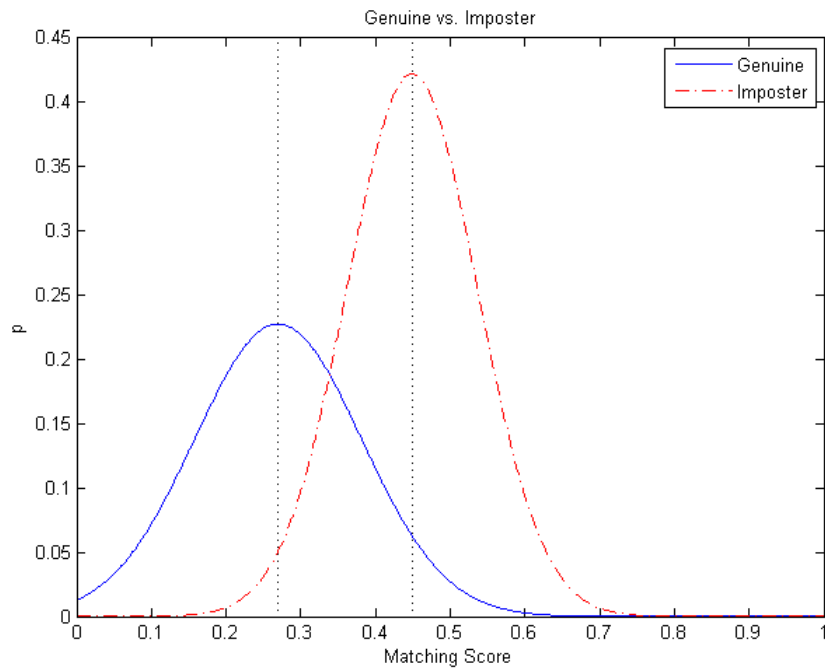


Figure 5.54: GD versus ID for Green PCA algorithm

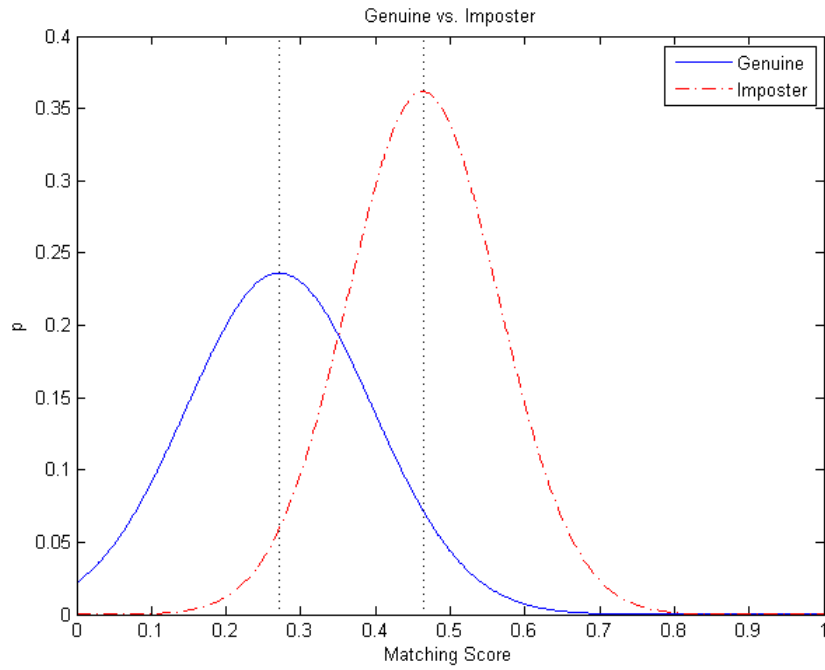


Figure 5.55: GD versus ID for Blue PCA algorithm

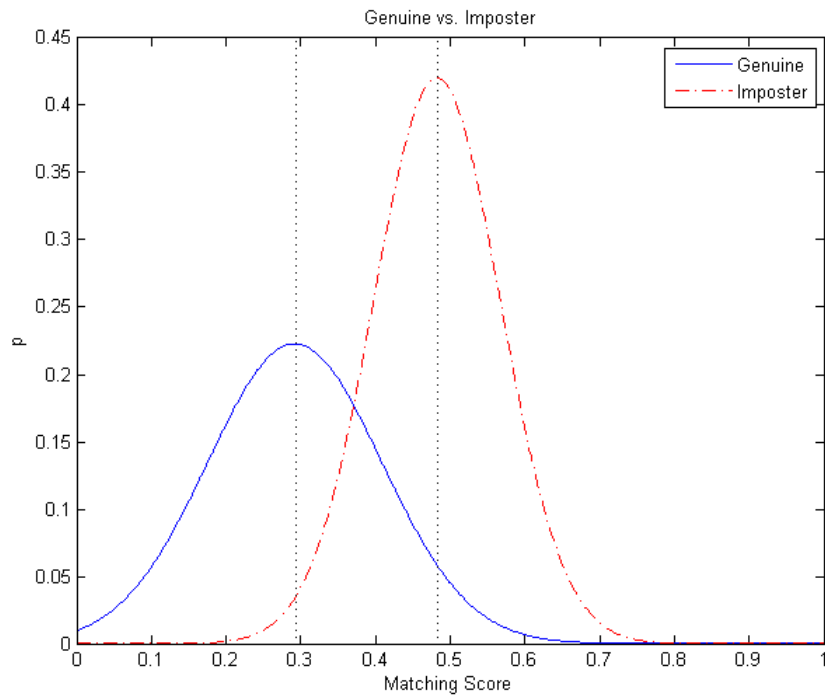


Figure 5.56: GD versus ID for Avg RGB PCA algorithm

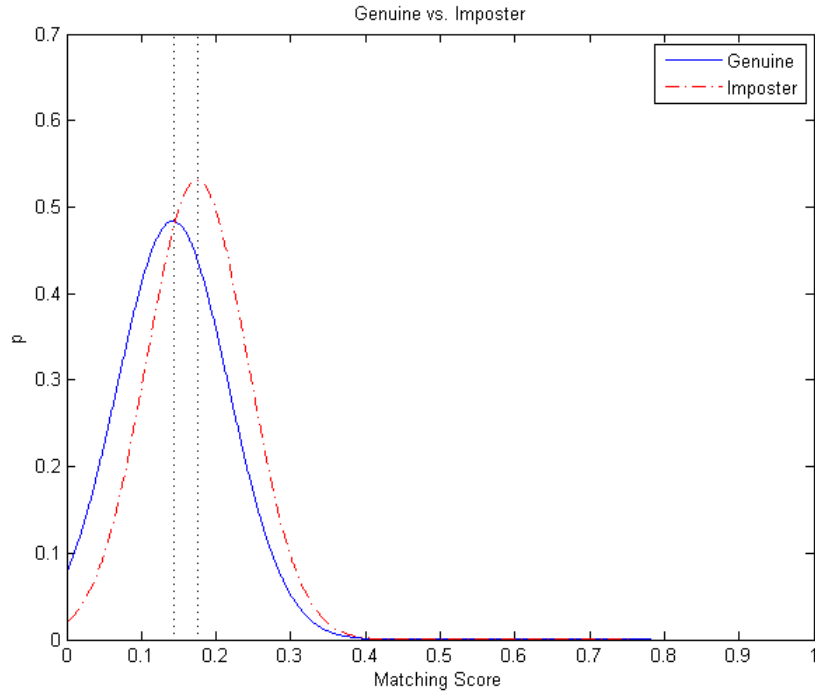


Figure 5.57: GD versus ID for SCFT CPCA algorithm

5.3.8. FAR versus FRR errors

Table 5.15 gives the EER value for each PCA-based algorithm.

<i>Algorithm</i>	<i>EER</i>
PCA	0.151
QPCA	0.152
Red PCA	0.130
Green PCA	0.168
Blue PCA	0.177
Avg RGB PCA	0.145
SCFT CPCA	0.457

Table 5.15: The EER of each algorithm.

Figure 5.58 shows the FAR and FRR curves when using PCA algorithm. It can be noted that EER is small, and consequently errors are low. Where the blue curve represents the FAR, whereas the other red dashed curve represents the FRR, and the cross point between

the two curves denotes the equal error rate (EER) of FAR and FRR. For the developed QPCA algorithm, Figure 5.59 illustrates the curves. The EER value is very similar to the one achieved with PCA, and thus QPCA, most likely, generates a close number of errors. This observation confirms the results obtained previously from the genuine and imposter distributions. Figure 5.60 shows the curves using Red PCA algorithm. Essentially, the EER value is the smallest among the others algorithms. The curves when using Green PCA and Blue PCA are illustrated in Figure 5.61 and Figure 5.62, respectively. It is clear that, EER of both are large compared to the previous mentioned algorithms (PCA, QPCA and Red PCA). Consequently, they both have more errors. While Green PCA has slightly less error than Blue PCA. The curves using Avg RGB PCA are shown in Figure 5.63. The value of EER is located between Red PCA and Green PCA, where it is greater than the first one and smaller than the other. Finally, the curves of SCFT CPCA are shown in Figure 5.64. The far greatest EER value is obtained, which indicates that the highest error rate is achieved by this algorithm.

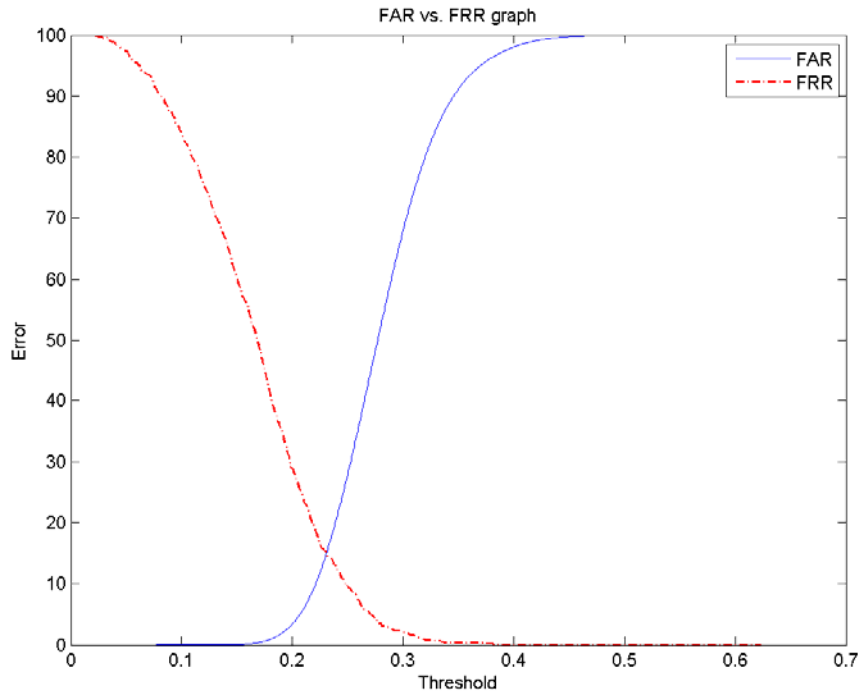


Figure 5.58: FAR versus FRR curve for PCA algorithm

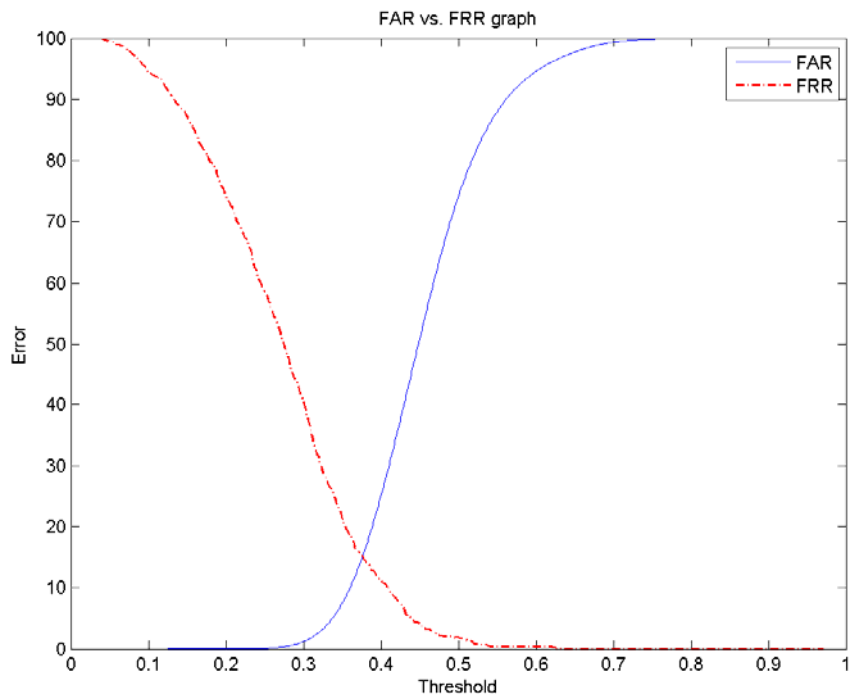


Figure 5.59: FAR versus FRR curves for QPCA algorithm

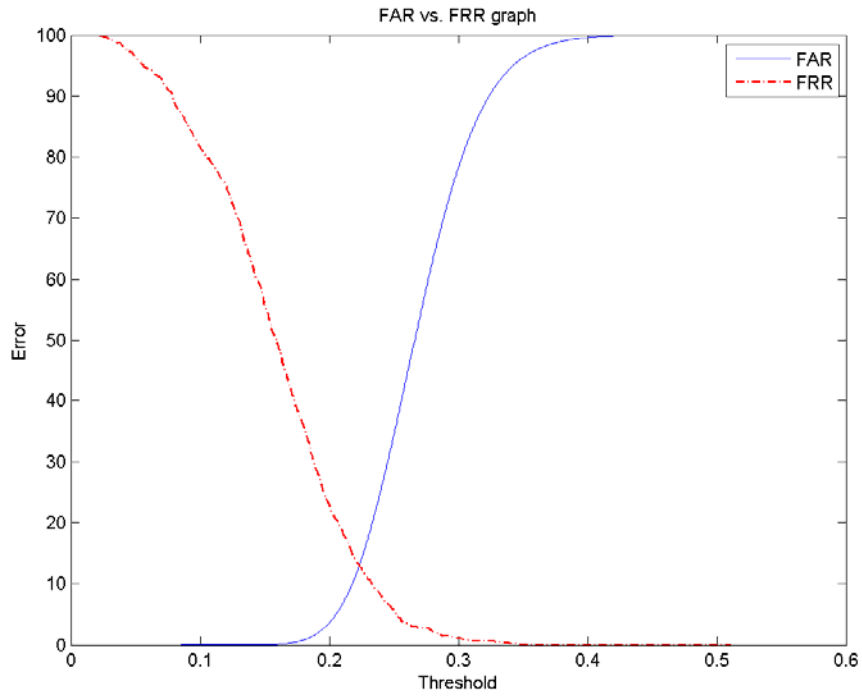


Figure 5.60: FAR versus FRR curves for Red PCA algorithm

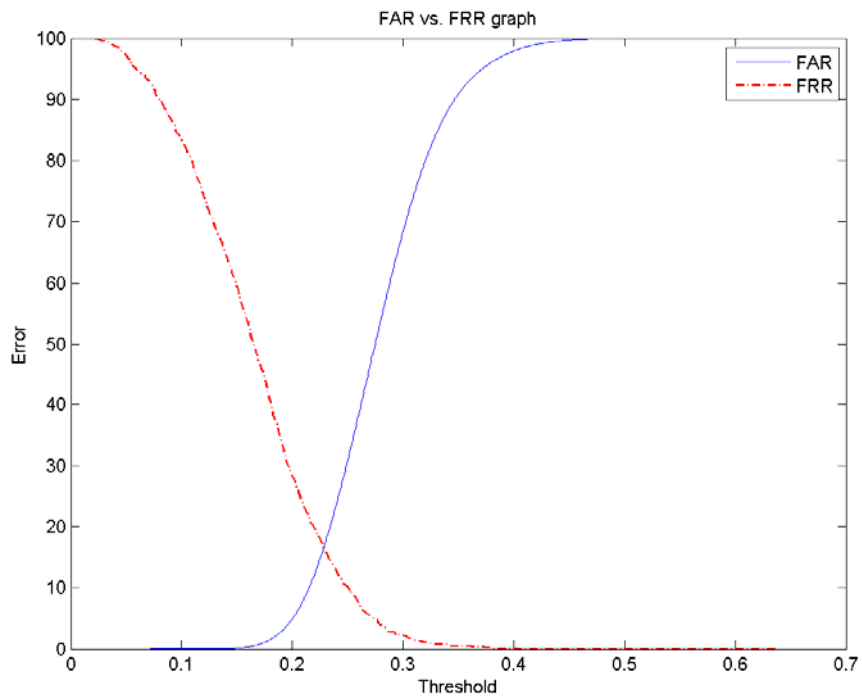


Figure 5.61: FAR versus FRR curves for Green PCA algorithm

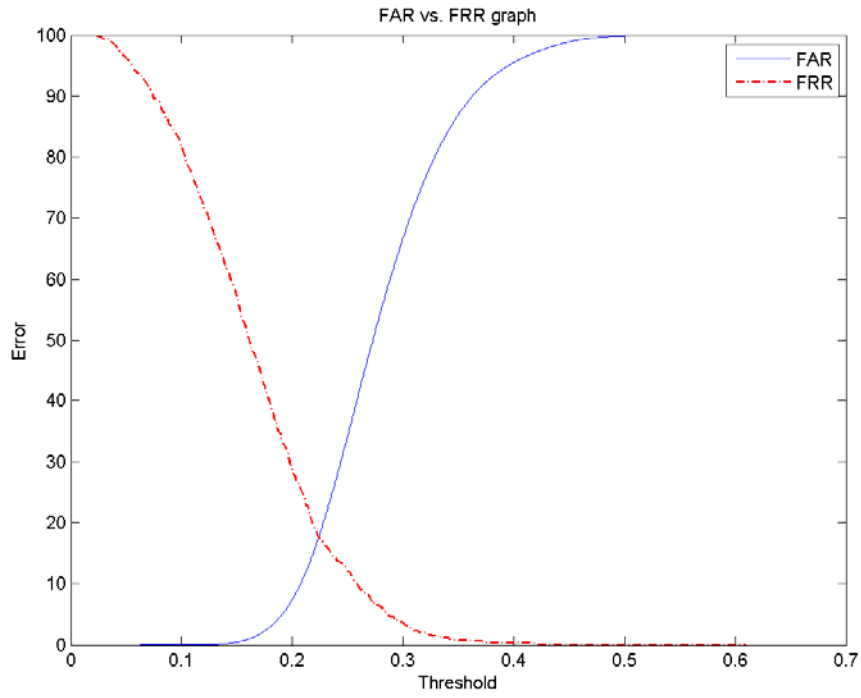


Figure 5.62: FAR versus FRR curves for Blue PCA algorithm

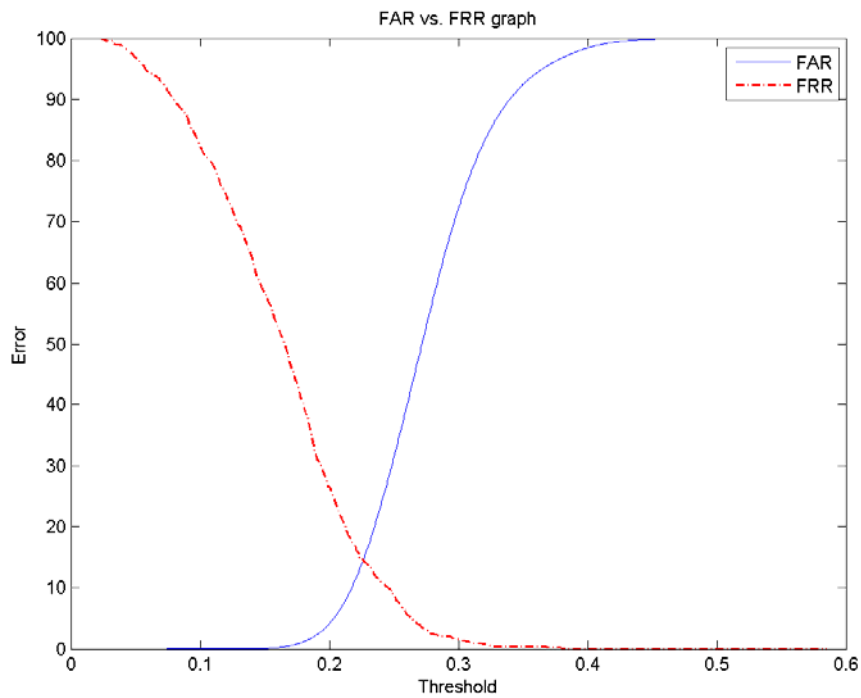


Figure 5.63: FAR versus FRR curves for Avg RGB PCA algorithm

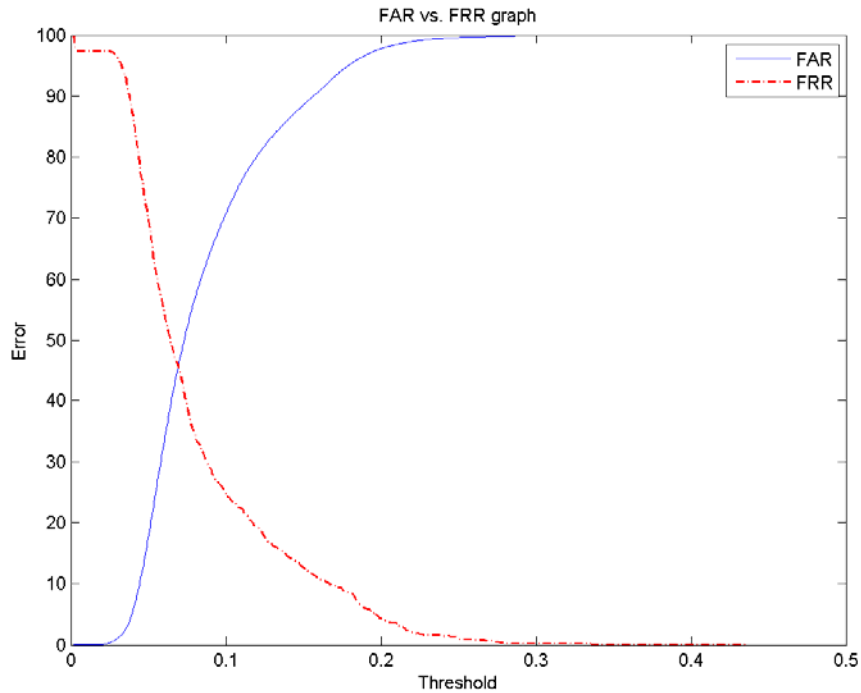


Figure 5.64: FAR versus FRR curves for SCFT CPCA algorithm

5.3.9. ROC Curves

Figure 5.65 shows the ROC curves when using PCA and QPCA algorithm. Where the relationship between FAR and FRR can be observed clearly As FAR is increased, FRR is decreased and accordingly $(1 - FRR)$ is increased, and vice versa. Where the small black circle denotes the estimated EER point where the FAR and FRR are equivalent. The obtained QPCA curve, Compared to the PCA curve, indicate that QPCA achieves higher accuracy than PCA with accepting the same number of errors. In Figure 5.66, the curve using Red PCA algorithm. It can be observed that the curve is the highest curve overall others, and thus it yields the least errors. This confirms the finding from genuine and imposter distributions and FAR and FRR curves. Figure 5.67 and Figure 5.68 show the

result when using Green PCA algorithm and Blue PCA Algorithm, respectively. It is clear that, they are both lower than PCA and QPCA curves, which means more errors are achieved. While Green PCA is better than Blue PCA with less error. The curve using Avg RGB PCA is shown in Figure 5.69. It can be inferred from this curve that it achieves results with fewer errors compared with Green and Blue PCA, but still lower than Red PCA. Finally, the lowest curve overall which yields the highest number of errors is SCFT CPCA as illustrated in the curve of Figure 5.70.

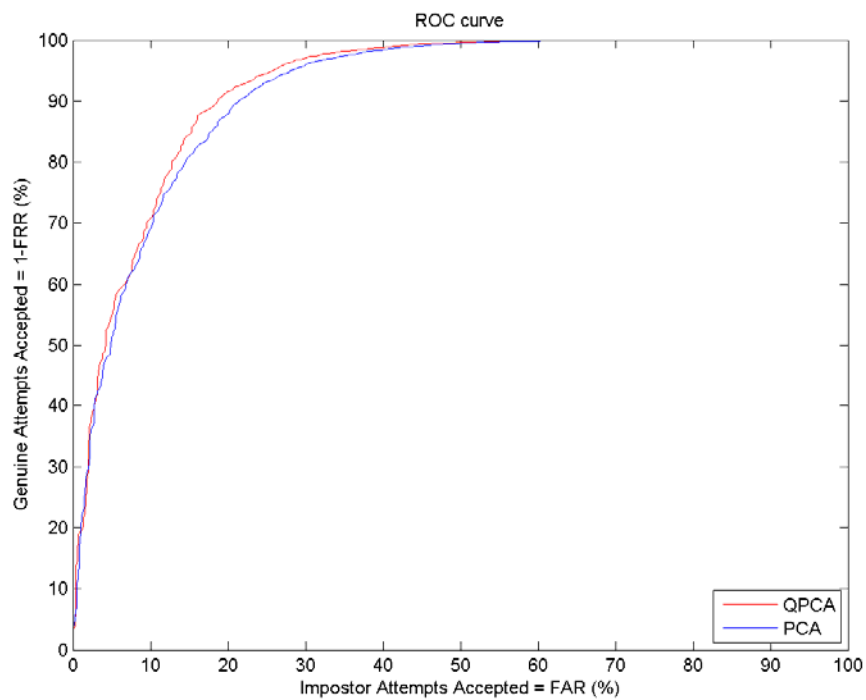


Figure 5.65: PCA and QPCA algorithms ROC curves

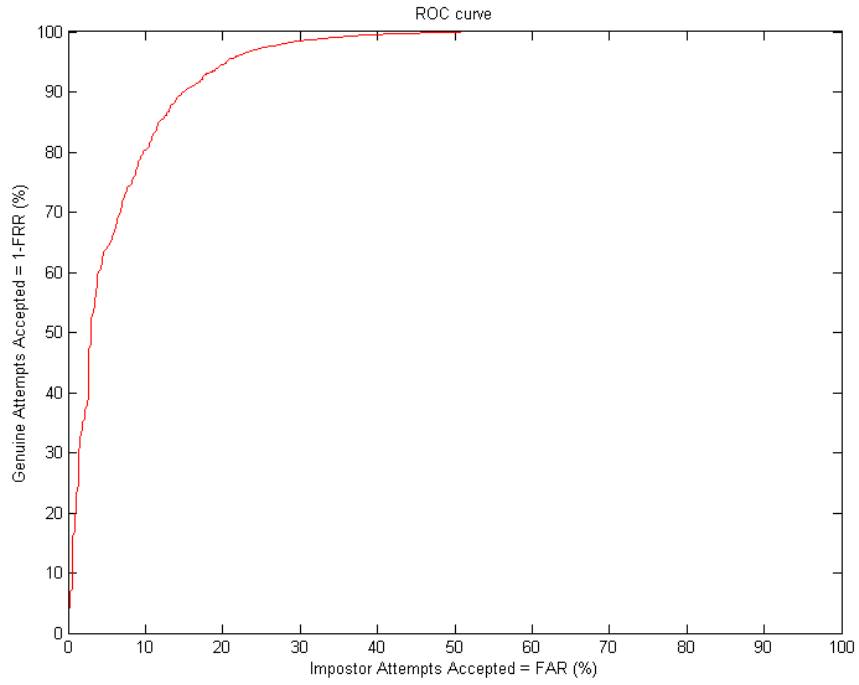


Figure 5.66: ROC curve for Red PCA algorithm

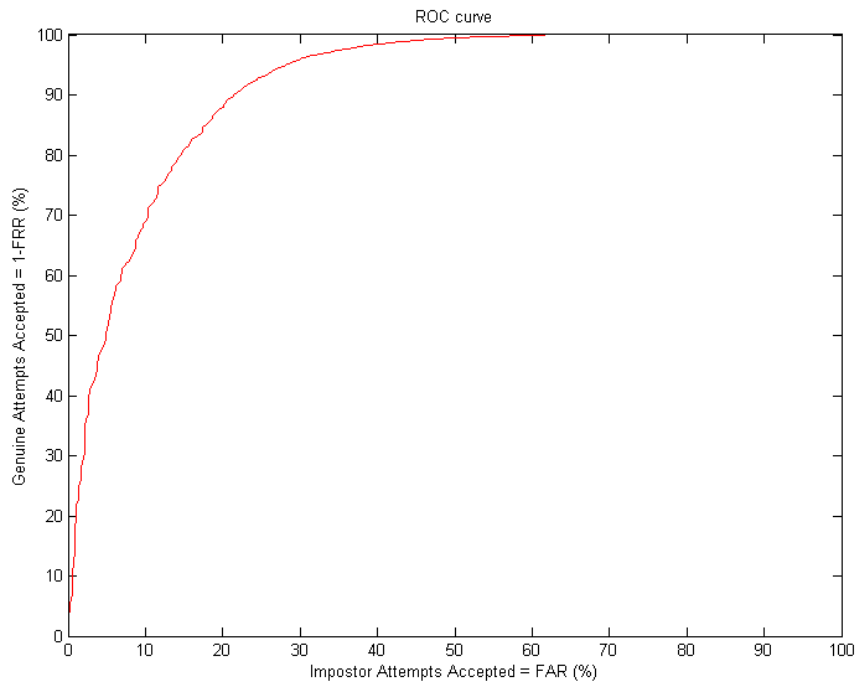


Figure 5.67: ROC curve for Green PCA algorithm

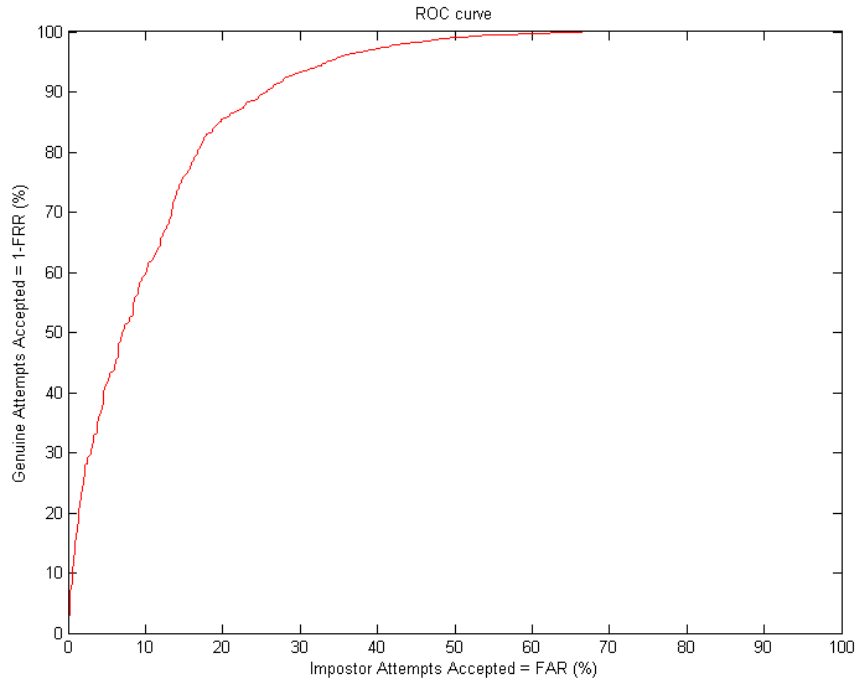


Figure 5.68: ROC curve for Blue PCA algorithm

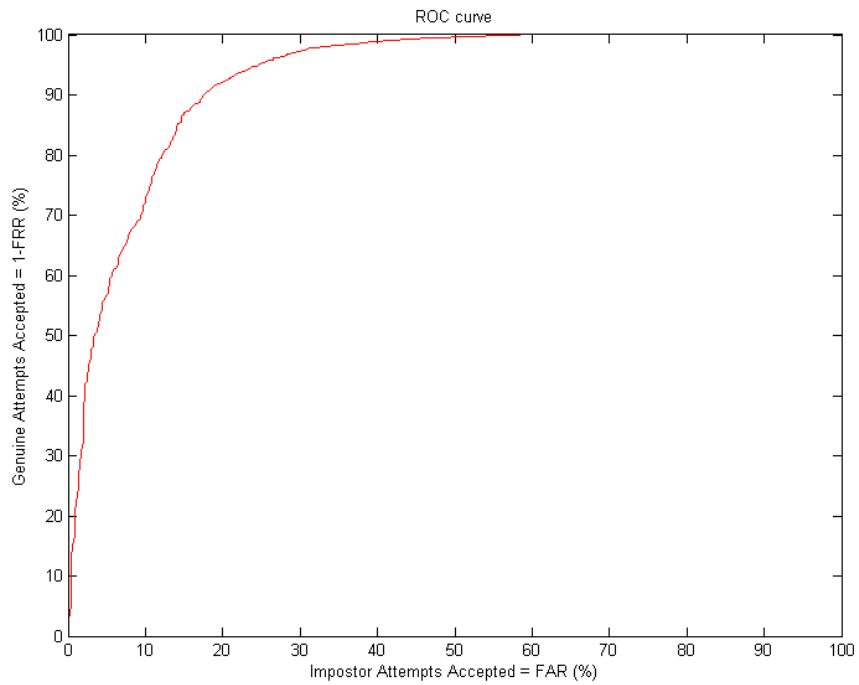


Figure 5.69: ROC curve for Avg RGB PCA algorithm

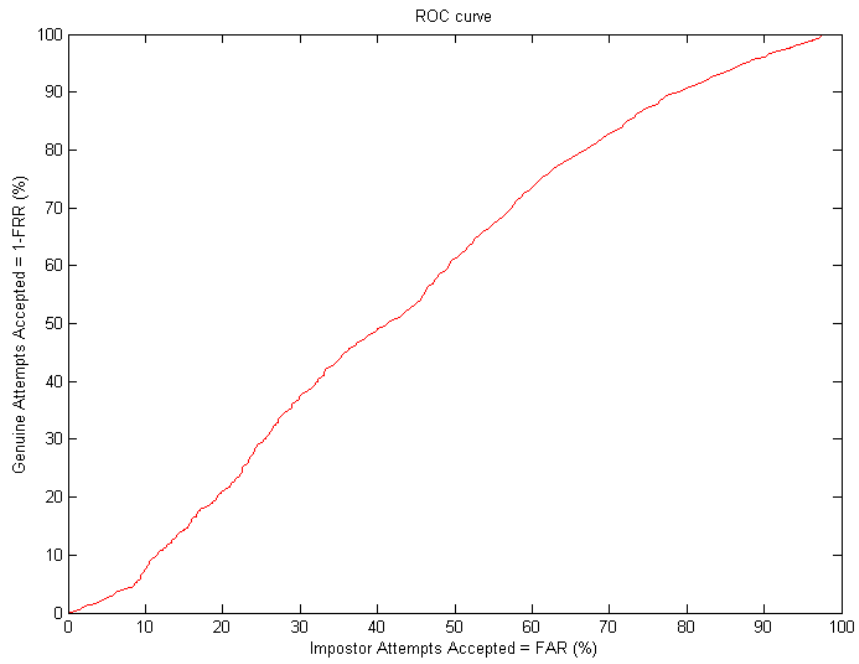


Figure 5.70: ROC curve for SCFT CPCA algorithm

CHAPTER 6

6. CONCLUSION AND FUTURE WORK

This chapter presents the conclusions of the aspects studied in this thesis along with a summary of the research and findings in light of experimental work and testing results. Furthermore, proposed directions for the extension of this work are offered as possible future work.

6.1. Summary and Findings

In this thesis, an overall background on biometric traits and systems, and on face recognition concepts, techniques and processing have been provided. Holistic quaternionic representation for color face images has been investigated. Besides, an overview of Quaternion (Hypercomplex) concepts including basic definitions, properties, and representations has been focused on. Then, the PCA and SVD concepts have been explained and further extended to the QPCA and QSVD which have been adopted and employed to design a biometric-based system for color face recognition and matching as well. After that, the design and implementation used to evaluate and compare the proposed technique with other PCA-based techniques and the testing methodology including data and experiments have been described and discussed. Within the performance evaluation, the following experimental investigation avenues have been conducted:

1. Identification performance against probe categories.

2. Performance comparison using CMC in different resolutions.
3. Variation in identification performance.
4. GD versus ID.
5. FAR versus FRR errors.
6. ROC curves.

The following are the major contributions of this research work.

- A novel scheme for efficient color face representation and processing for face-based biometric recognition system.
- The concept of the PCA and SVD are extended to the quaternionic and carried over into the hypercomplex to compactly represent color face images.
- Detailed analysis of the incorporation of color information in face recognition is provided.
- Performance improvement by using color information and the Q-PCA method.
- Extended performance evaluation is performed and comparisons from different perspectives are provided.

The following work was performed in support of these contributions:

- Development of a new algorithm for face recognition and matching based on quaternion principle component analysis (QPCA) technique and extension of the face recognition software to color images.

- Implementation of other standard PCA-based algorithms for the sake of comparison against the Q-PCA algorithm, these algorithms are the PCA, Red PCA, Green PCA, Blue, Avg RGB PCA, and SCFT PCA.
- Organization of facial data galleries and probes under different categories to be using in the conducted experiments.
- Performance testing and analysis by performing a number of stress test experiments for these different compared implementations to evaluate and compare each with the others.
- Generation of prober evaluation graphs and tables demonstrating and representing experimental outcomes.

The following are the major findings derived through this research work:

- Use of color information can increase accuracy.
- Regarding color face images, the red-channel or component is the highest effective channel of the three color channels as concluded from its high performance, the best separation overall algorithms, and the least EER over others. Hence, red is the most correlated component and the most proper one to build PCA features.
- While making use of the high-effective single color channel enhances the performance of face recognition, further making use of the entire color channels holistically and cooperatively is improving the performance more.

- Extending the standard grayscale PCA features to the Q-PCA using quaternion color representation can increase accuracy.
- The Q-PCA has good separation between genuine and imposter distributions and fewer errors than the PCA, despite of that Q-PCA has EER very similar to the PCA.
- The experimental outcomes indicate in most cases that the proposed Q-PCA achieves better performance than the other typical tested PCA-based algorithms.
- From robustness and reliability point of views, where each algorithm has been tested over special sets of facial database consists of samples represent the difficulties cases such as impose and illumination. Overall the tested algorithms the Q-PCA is to provide better robustness against such unconstrained cases.
- Using face image data with higher resolution can increase the precision of the derived PCA features and consequently can increase the identification and matching accuracy.

6.2. Future Work

Since the lack of research using Quaternion numbers to represent and process color images. Because it is a complicated task, it has not received enough attention in the research literature. Here are some of the suggested future studies to enhance the present research:

- The performance and accuracy can be improved by performing additional preprocessing operations for the purpose of preparing more normalized data images,

which can reduce the variety of face images (such variety extremely exists in current used database). Thus some preprocessing can be performed properly for example: all images can be translated, rotated, and scaled so that the center of the eyes can be placed on specific pixels, moreover faces can be masked to remove background and hair and so on. Thereby accuracy is expected to be increased.

- The current developed Q-PCA algorithm for color face recognition can be adapted, modified and applied on another biometric trait such as color iris.
- The proposed face-based biometric system can be applied using the quaternionic representation for color images in other color spaces such as XYZ, YUV or YCbCr color spaces. For example a face image in YCbCr color space can be represented as:

$$q = 0 + Y.i + Cb.j + Cr.k \quad (6.1)$$

- The proposed Q-PCA algorithm is fully automatic. Therefore it is suggested that to investigate the development of partially automatic QPCA-based algorithm for face recognition. Such partially automatic algorithm is supplied with some information as guidance such as the coordinates of the center of the eyes (this guide is already available in FERET database). These guides used to increase the precision then consequently the performance and accuracy are improved. Consequently, this new implementation approach can be compared with the current fully automatic approach.

REFERENCES

- [1] C. Jones, "Color Face Recognition using Quaternionic Gabor Filters," PhD Dissertation, Virginia Institute of Technology, 2004.
- [2] C. Wang, B. Yin, X. Bai, and Y. Sun, "Color Face Recognition Based on 2DPCA," 19th International Conference on Pattern Recognition (ICPR 2008), pp. 1-4, 8-11 Dec., 2008.
- [3] C. Wang, and X. Bai, "Color Face Recognition Based on Revised NMF Algorithm," Second International Conference on Future Information Technology and Management Engineering (FITME '09), pp. 455-458, 13-14 Dec., 2009.
- [4] F. Al-Qunaieer, "Color Iris Recognition and Matching using Quaternion Gabor Wavelets," MS Thesis, KFUPM University, 2009.
- [5] Face Recognition Homepage, <http://face-rec.org>.
- [6] J. Choi, S. Yang, Y. Ro, and K. Plataniotis, "Color Effect on the Face Recognition with Spatial Resolution Constraints," 10th IEEE International Symposium on Multimedia (ISM 2008), pp. 294-301, 15-17 Dec., 2008.
- [7] J. Choi, Y. Ro, and K. Plataniotis, "Color Face Recognition for Degraded Face Images," IEEE Transactions on Systems, Man, and Cybernetics, Part B: Cybernetics, vol. 39, no. 5, pp. 1217-1230, Oct., 2009.
- [8] J. Yang, and C. Liu, "A General Discriminant Model for Color Face Recognition," IEEE 11th International Conference on Computer Vision (ICCV 2007), pp. 1-6, 14-21 Oct., 2007.
- [9] C. Jones, and A. Abbott, "Color Face Recognition by Hypercomplex Gabor Analysis," 7th International Conference on Automatic Face and Gesture Recognition (FGR 2006), pp.6-131, 2-6 April., 2006.

- [10] N. Le Bihan, and S. Sangwine, "Quaternion Principal Component Analysis of Color Images," International Conference on Image Processing Proceedings (ICIP 2003), vol.1, pp. I- 809-12, 14-17 Sept., 2003.
- [11] L. Ding, and H. Feng, "Quaternion K-L Transform and Biomimetic Pattern Recognition Approaches for Color-face Recognition," IEEE International Conference on Intelligent Computing and Intelligent Systems (ICIS 2009), vol.1, pp. 165-169, 20-22 Nov., 2009.
- [12] H. Moon, and P. Phillips, "Computational and Performance Aspects of PCA-based Face Recognition Algorithms," Perception, vol. 30, pp. 301-321, 2001.
- [13] S. Pei, and C. Cheng, "A Novel Block Truncation Coding of Color Images by Using Quaternion-moment Preserving Principle," IEEE International Symposium on Circuits and systems, vol. 2, pp. 684-687, Atlanta, FA. 12-15 May., 1996.
- [14] S. Li, and A. Jain, Handbook of Face Recognition, Springer, New York, USA, 2005.
- [15] S. Chen, Y. Sun, and B. Yin, "A Novel Hybrid Approach Based on Sub-pattern Technique and Extended 2DPCA for Color Face Recognition," 11th IEEE International Symposium on Multimedia (ISM '09), pp. 630-634, 14-16 Dec., 2009.
- [16] P. Shih, and C. Liu, "Extracting Efficient Color Features for Face Recognition Using Evolutionary Computation," 6th International Conference on Computational Intelligence and Multimedia Applications, pp. 285- 290, 16-18 Aug., 2005.
- [17] J. Shlens, "A Tutorial on Principal Component Analysis," Unpublished, version 3.01, 2009.
- [18] L. Smith, "A Tutorial on Principal Component Analysis," Unpublished, 2002.
- [19] T. Ganapathi, and K. Plataniotis, "Color Face Recognition under Various Learning Scenarios," IEEE Canadian Conference on Electrical and Computer Engineering, 5-7 May., 2008.

- [20] T. Ganapathi, "Color Image Based Face Recognition," MS Thesis, University of Toronto, 2009.
- [21] M. Thomas, C. Kambhamettu, and S. Kumar, "Face Recognition Using a Color Subspace LDA Approach," 20th IEEE International Conference on Tools with Artificial Intelligence (ICTAI '08), vol. 1, pp. 231-235, 3-5 Nov., 2008.
- [22] M. Turk, and A. Pentland, "Eigenfaces for recognition," Journal of Cognitive Neuroscience, vol. 3, no 1, pp. 72-86, 1991.
- [23] L. Wei, X. Yi, X. Yang, and L. Song, "Local Quaternionic Gabor Binary Patterns for Color Face Recognition," IEEE International Conference on Acoustics, Speech and Signal Processing (ICASSP 2008), pp. 741-744, March 31 2008-April 4 2008.
- [24] W. Zhao, R. Chellappa, J. Phillips, and A. Rosenfeld, "Face Recognition: A Literature Survey," ACM Computing Surveys, vol. 35, no. 4, pp. 399-458, Dec., 2003.
- [25] S. Thakur, J.K. Sing, D. K. Basu, M. Nasipuri, and M. Kundu, "Face Recognition Using Principal Component Analysis and RBF Neural Networks," First International Conference on Emerging Trends in Engineering and Technology (ICETET '08), pp. 695-700, 2008.
- [26] T. Rahman, and A. Bhuiyan, "Face Recognition using Gabor Filters ," 11th International Conference on Computer and Information Technology Proceedings (ICCIT 2008), pp. 510-515, Khulna, Bangladesh, 25-27 Dec., 2008.
- [27] X. Wang, C. Huang, G. Ni, and J. Liu, "Face Recognition Based on Face Gabor Image and SVM," 2nd International Congress on Image and Signal Processing (CISP '09), pp. 1-4, Oct., 2009.
- [28] C. Liu, and D. Dai, "Face Recognition Using Dual-Tree Complex Wavelet Features," IEEE Transactions On Image Processing, vol. 18, no. 11, pp. 2593-2599, Nov., 2009.

- [29] Z. Chai, K. Ma, and Z. Liu, "Complex Wavelet-based Face Recognition Using Independent Component Analysis," 5th International Conference on Intelligent Information Hiding and Multimedia Signal Processing, pp. 832-835, 12-14 Sep., 2009.
- [30] L. Shi, "Exploration in Quaternion Colour," MS Thesis, Simon Fraser University, 2005.
- [31] S. Sangwine, and N. Le Bihan, "Computing the SVD of a quaternion matrix," 7th IMA Conference on Mathematics in Signal Processing Royaume-Uni, 2006.
- [32] P. J. Phillips, H. Moon, P. Rauss, and S. Rizvi, "The FERET Evaluation Methodology for Face-Recognition Algorithms," Tech. Rep. NISTIR 6264, National Institute of Standards and Technology, 7 Jan. 1999.
- [33] P. J. Phillips, A. Martin, C. Wilson and M. Przybocki. "An Introduction to Evaluating Biometric Systems", IEEE Computer, pp. 56-63, Feb., 2000.
- [34] F. Zhang, "Quaternions and Matrices of Quaternions," Linear algebra and its applications, vol. 251, pp. 21-57, 1997.
- [35] A. Koschan and M. Abidi, "Digital color image processing," first ed. John Wiley & Sons, New York, 2008.
- [36] W. Hamilton, "On quaternions; or on a new system of imaginaries in algebra," Edinburgh and Dublin Philosophical Magazine and Journal of Science, pp. 25-36, 1844-1850.
- [37] A. McCabe, T. Caelli, G. West and A. Reeves, "Theory of spatiochromatic image encoding and feature extraction," Journal of the Optical Society of America A: Optics, Image Science, and Vision, vol. 17, no. 10, 2000.
- [38] S.-C. Pei, J.-J. Ding and J.-H. Chang, "Efficient implementation of quaternion Fourier transform, convolution, and correlation by 2-D complex FFT," IEEE Transactions on Signal Processing, vol. 49, no. 11, 2001.

- [39] S. Westland and C. Ripamonti, "Computational Colour Science Using MATLAB," John Wiley & Sons, new york, 2004.
- [40] A. McCabe, T. Caelli, G. West and A. Reeves, " Encoding and Processing Spatio-Chromatic Image Information Using Complex Fourier Transform Methods," Technical Report, Curtin University of Technology, Perth, Western Australia, pp. 228–24, 1997.

Vita

Personal Information	<ul style="list-style-type: none">▪ Date of Birth: 1982▪ Place of Birth: Jeddah▪ Nationality: Saudi▪ Emails:<ol style="list-style-type: none">1. e_jaha@hotmail.com2. ejaha@kau.edu.sa▪ Mobile Number: 0504696694▪ Present Address: 1st street, Al-Badee District, Dammam, Saudi Arabia.▪ Permanent Address: P.O.BOX 1237, Jeddah – 21433, Saudia Arabia.▪ Languages:<ol style="list-style-type: none">1. Arabic (native language)2. English
Education	<ul style="list-style-type: none">▪ 2000 -2004: King Abdul-Aziz University Jeddah, Bachelor of Science in Computer Science▪ 2007-2010: King Fahd University of Petroleum & Minerals Dhahran, Master of Science in Computer Science
Work	<ul style="list-style-type: none">▪ 2004-2005: Developer in IT Unit in Deanship of Community Services & Continuing Education at King Abdul-Aziz University▪ 2005-Present: Graduate Assistiz in Computer Science Department in College of Education at King Abdul-Aziz University
Interests	<ul style="list-style-type: none">▪ Image processing and pattern recognition▪ Biometric Systems▪ Web development
